DAMPING OF INTER-AREA MODE OSCILLATIONS USING FACTS CONTROLLERS

Ph.D. THESIS

by

BHAVIN JAGIDHSHBHAI SHAH

DEPARTMENT OF ELECTRICAL ENGINEERING
INDIAN INSTITUTE OF TECHNOLOGY ROORKEE
ROORKEE – 247667 (INDIA)
APRIL, 2018

DAMPING OF INTER-AREA MODE OSCILLATIONS USING FACTS CONTROLLERS

A THESIS

Submitted in partial fulfilment of the requirements for the award of the degree

of

DOCTOR OF PHILOSOPHY

in

ELECTRICAL ENGINEERING

by

BHAVIN JAGDISHBHAI SHAH

DEPARTMENT OF ELECTRICAL ENGINEERING
INDIAN INSTITUTE OF TECHNOLOGY ROORKEE
ROORKEE – 247667 (INDIA)
APRIL, 2018

INDIAN INSTITUTE OF TECHNOLOGY ROORKEE
ROORKEE

CANDIDATE'S DECLARATION

I hereby certify that the work which is being presented in this thesis entitled **"DAMPING OF INTER-AREA MODE OSCILLATIONS USING FACTS CONTROLLERS "** in partial fulfillment of the requirements for the award of the Degree of Doctor of Philosophy and submitted in the Department of Electrical Engineering of Indian Institute of Technology Roorkee, Roorkee is an authentic record of my own work carried out during a period from August, 2011 to April, 2018 under the supervision of **Dr. Pramod Agarwal**, Professor and **Dr. G.N. Pillai**, Professor, Department of Electrical Engineering, Indian Institute of Technology Roorkee, Roorkee.

The matter presented in this thesis has not been submitted by me for the award of any other degree of this or any other Institute.

(BHAVIN JAGDISHBHAI SHAH)

This is to certify that the above statement made by the candidate is correct to the best of our knowledge.

(Supervisor) (Supervisor)

Date: _____

The Ph. D. Viva-Voce Examination of **Mr. BHAVIN JAGDISHBHAI SHAH**, Research Scholar, has been held on……

Chairman, SRC **Signature of External Examiner**

This to certify that the student has made all the corrections in the thesis.

Signature of Supervisors **Head of the Department**

ABSTRACT

Deregulation of electricity market across the world results in the bulk amount of power transfer over long distances. Also, the integration of renewable energy generations into existing network causes significant changes in the power flows and dynamic behavior of the system. Non- uniform utilization of facilities, unwanted loop flows, and bottlenecks are very common in transmission networks. On the other hand, the expansion of transmission networks is very restricted due to environmental issues, rights of way issues and cost-related issues. As a result, network operators are facing the challenge of efficient utilization of transmission networks. The transmission networks are forced to operate closer to stability and thermal limits. Stressed transmission lines and heavy power transfer between geographically separated areas result in poorly damped oscillations in the power system. Poorly damped electromechanical oscillations inherent in the large interconnected power system are not only dangerous to the reliability of the system but also results in poor quality of the power supply. These oscillations are mainly classified as local mode oscillations and inter-area mode oscillations. Insufficient damping or negative damping is the main reasons for electromechanical oscillations. The damping of power system mainly depends upon the topology of the system, controller parameters, operating conditions and characteristics of the load. Failing to address the issue of electromechanical oscillations leads to some serious situations in power system. Many blackouts are observed in the history of the power system due to such oscillations.

The Power System Stabilizers (PSSs) and Flexible AC Transmission (FACTS) devices are the conventional solutions to damp out these oscillations. The power system stabilizers are normally employed to damp out the local area mode oscillations due to its location in the excitation system local to the generator. However, PSSs have limited ability to damp out the inter-area mode oscillations as it requires phase lead the design and damping torque provided by the PSS is inversely proportional to the electrical length of the transmission network. Also, tuning of PSSs for inter-area mode may adversely affect the local modes. On the other hand, FACTS devices as supplementary damping control are found to be very satisfactory for damping the inter-area modes. However, for effective damping of the inter-area modes, the FACTS devices must be supplied with

suitable global feedback signal in which inter-area modes are properly observable. Also, the designed FACTS controller must address the issues like uncertainties present in the power system model, continuously changing operating points in the power system and robustness for contingencies conditions like line outages, line faults, and load shedding.

The recent advances in linear control technique based robust control theories and use of phasor measurement units (PMU) based wide area measurements makes the wide area damping controller a strong candidate for damping electromechanical oscillations. This main objective of the thesis is the damping of the inter-area mode oscillations using FACTS controllers. The design of the FACTS controllers are based on robust control theories. The multi-objective features of the Linear Matrix Inequality (LMI) based techniques are used for the design of proposed wide-area damping controllers. The pole placement objective which ensures minimum damping ratio is also included in the design of the controller. The multi-objective design ensures the robustness of the designed controller for various operating conditions in power system. The design procedure is carried out on two area four machine test system and the designed controller is tested for various objective requirements. For large power system employing multiple FACTS devices, multi-objective mixed H_2/H_∞ synthesis combined with the sequential approach is applied for designing the wide area damping controller. The adverse interactions among the control action of different FACTS controller are avoided by sequentially designing the multiple single input single output controllers. Residue analysis is carried out for deciding the best global feedback signal for the controllers. The sequential design procedure is carried out on modified New York – New England test system which includes multiple FACTS devices. The performance of the designed controller is tested for different operating conditions in power system and for various contingency conditions. The performance of the designed controller is found to be robust for such conditions.

To overcome the difficulties in the selection of weights in case of mixed sensitivity based LMI approach, H_∞ loop shaping using LMI approach is applied. The H_∞ loop shaping using LMI focusses on maximizing the robustness to co-prime factor uncertainty rather than multiplicative or additive uncertainty. This results in a very attractive design procedure which yields controller with strong robustness properties. The LMI approach to H_∞ loop shaping technique is applied to the design of WADC for 10-machine 39-bus modified New England test system employing UPFC. The designed WADC is tested for

various contingency conditions to ensure the robustness and its performance is found to be very satisfactory.

ACKNOWLEDGEMENT

I express my deepest sense of gratitude towards my supervisors Dr. Pramod Agarwal, Professor, Department of Electrical Engineering and Dr. Gopi Nath Pillai, Professor, Department of Electrical Engineering of Indian Institute of Technology Roorkee, Roorkee, for their patience, inspiring guidance, constant encouragement, moral support, and keen interest in minute details of the work. I am sincerely indebted to them for their pronounced individuality, humanistic and warm personal approach.

My deepest gratitude and sincere thanks to Dr. B. Das, Chairman SRC, Department of Electrical Engineering, Indian Institute of Technology Roorkee, Roorkee. I am heartily thankful to Dr. S. P. Gupta, Professor, Department of Electrical Engineering, Indian Institute of Technology Roorkee, Roorkee for guiding me as an internal expert in my SRC committee and Dr. M. J. Nigam, Professor, Department of Electronics and Communication Engineering, Indian Institute of Technology Roorkee, Roorkee for guiding me as an external expert in my SRC committee as well as for their invaluable direction, encouragement and support, and above all the noblest treatment extended by them during the course of my studies at Indian Institute of Technology Roorkee, Roorkee. I am also grateful to the Directorate of Technical Education, Education Department, Government of Gujarat, Gandhinagar for sponsoring me for my doctoral research work under Quality Improvement Programme and Ministry of Human Resources and Development, Government of India, AICTE, New Delhi for giving the opportunity to me under QIP programme for doctoral research work.

I extend my sincere thanks to all research scholars especially to Mr. Kunal Bhatt, Mr. Yogesh Makwana, Dr. Nagendrakumar, Dr. Shailendra Bhaskar and Dr. K. S. Sajan for supporting me during my research work. I would also like to thank all the administrative and technical staff of the Department of Electrical Engineering, Indian Institute of Technology Roorkee, Roorkee for their cooperation and necessary facility provided to me. I express my sense of gratitude to Mr. Amir Ahmed, Caretaker Workshop, Department of Electrical Engineering, Indian Institute of Technology Roorkee, Roorkee for their co-operation and assistance. I am also thankful to all the faculty members of

Electrical Engineering Department of Government Engineering Colleges of Dahod, Surat, Valsad, and Ahmedabad for supporting me during my Ph.D. tenure.

I owe a debt of gratitude to my parents, my sister and family members for their consistent encouragement, moral support, patience, and care. Heavenly blessings from my father, Late Shri Jagdishbhai M Shah and my sister Late Smt. Jayshree Shah kept me motivated for completing my thesis. No words can adequately express my deepest gratitude and love to my mother Smt. Ranjanben J Shah and my wife Smt. Hetal Shah for their unconditional support, encouragement, love, and inspiration and always being there for good and bad times. I express my deepest love to my cute daughter Harshavee and my nephew Nihar, whose smiling faces always refreshes me.

Last but not the least; I am thankful to the almighty who gave me the strength and health for completing the work.

(Bhavin J Shah)

CONTENTS

LIST OF FIGURES

LIST OF TABLES

LIST OF ABBREVIATIONS

Abbreviations	Meaning
AVR	Automatic Voltage Regulator
PSS	Power System Stabilizer
FACTS	Flexible Alternating Current Transmission System
SDC	Supplementary Damping Controller
FC	Fixed Capacitor
TCR	Thyristor Controlled Reactor
TSC	Thyristor Switched Capacitor
SVC	Static Var Compensator
TCSC	Thyristor Controlled Series Capacitor
STATCOM	Static Synchronous Compensator
SSSC	Static Synchronous Series Compensator
UPFC	Unified Power Flow Controller
MOSFET	Metal Oxide Semi-Conductor Field Effect Transistor
IGBT	Insulated Gate Bipolar Transistor
ATC	Available Transfer Capacity
PMU	Phasor Measurement Unit
WAMs	Wide Area Measurements
WAC	Wide Area Control
WADC	Wide Area Damping Controller
LMI	Linear Matrix Inequality
HVDC	High Voltage Direct Current
SISO	Single Input Single Output
MISO	Multiple Input Single Output
MIMO	Multiple Input Multiple Output
TGR	Transient Gain Reduction
LQG	Linear Quadratic Gaussian

CHAPTER 1 INTRODUCTION

1.1 Electromechanical Oscillations in Power System

Recently, due to deregulation of electrical energy markets across the world, a bulk amount of power transfer over long distance has increased. Also, power transfer became unpredictable as it is governed by market price fluctuations. The integration of renewable energy generations into existing network causes significant changes in the power flows and dynamic behavior of the system. Due to the intermittent nature of the renewable generations, the power flows in the transmission lines are unpredictable. Nonuniform utilization of facilities, unwanted loop flows, shortage of the sufficient reserve generation capacity and bottlenecks are very common in transmission networks. On the other hand, the expansion of transmission networks is very restricted due to environmental issues, rights of way issues and cost-related issues. As a result, network operators are facing the challenge of efficient utilization of transmission networks. Thus, transmission networks are forced to operate closer to stability and thermal limits [1]. Stressed transmission lines and heavy power transfer between geographically separated areas result in poorly damped electromechanical oscillations in the power system [2]. Also, the response of automatic voltage regulator (AVR) at the time of the line to ground faults and interaction among different control devices result in the electromechanical oscillations of various frequencies ranging from 0.1Hz- 46 Hz. These oscillations are mainly classified as follows [2]:

i) Local mode: When a generator (or group of generators) of a power station oscillates against the rest of the system, the resulting oscillations are known as local mode oscillations. These are mainly caused by the response of AVR units operating at high output and supplying power to weak transmission networks. The problem is further enhanced with high-speed excitation system. The typical characteristic frequency of local mode oscillations is in the range of 1-2 Hz. Power System Stabilizers (PSSs) can provide effective damping against local mode oscillations with additional control of excitation system.

ii) Inter-area mode: When a group of generators of one part of the system oscillates against the group of generators of another part of the system, resulting oscillations are known as an inter-area mode. These are mainly caused by closely coupled generators connected by weak tie-lines. The typical characteristic frequency of inter-area mode oscillations is in the range of 0.1-1.0 Hz. The characteristics of these modes are more complex and different from the local mode oscillations. The nature of the load, the strength of the tie-line, power flow in the tie-line, control devices employed in the transmission network and the dynamic behavior of the generators decide the damping of the inter-area modes.

iii) Torsional mode: These oscillations are associated with the turbine-generator rotational system. These modes are generated by a multi-stage turbine generator connected to transmission network through series compensated transmission line. Normally, the torsional mode lies in the frequency range of 10-46 Hz.

iv) Control mode: These oscillations are associated with the generator controls and other controlling devices employed in the transmission network. Poor tuning of the control of excitation system of the generators, governors and Flexible AC Transmission System (FACTS) Controllers causes the control mode oscillations.

Apart from reliability, the electrical energy supplied to the customer must possess a necessary quality which can be represented in terms of technical specifications (i.e. voltage and frequency must be within the allowable limits as mentioned in concern standards). However, poorly damped electromechanical oscillations inherent in the large interconnected power system are not only dangerous to the reliability of the system but also results in poor quality of the power supply. Insufficient damping or negative damping in the power system is the main reason for these electromechanical oscillations. The damping of power system mainly depends upon the following factors:

i) The topology of the system- When the existing generation/load areas are connected to similar areas through weak tie lines (having large line

impedances), electromechanical oscillations occurs. The frequency and damping of inter-area oscillation are inversely proportional to inter-area line impedance [3].

ii) Controller parameters- The main source of synchronizing torque is exciter but its operation may result in decreasing natural damping of the power system. The type and location of exciter affect the damping of the power system. The most effective solution for increasing the damping is by using Power System Stabilizers (PSSs). However, the parameters of the PSSs must be chosen and adjusted carefully for achieving positive contribution for damping the inter-area mode oscillations [4].

iii) Operating conditions- Power flows in the given system largely affects the damping of inter-area mode oscillations [3]. Any future expansion of the present power system may result in a reduction of the damping of inter-area mode oscillations.

iv) Characteristics of Load- Electromechanical oscillations result in voltage oscillations at various load buses and hence causes load variations. Also load variations will change the system voltages and influences the electromechanical oscillations. Hence, it forms interdependence between load and electromechanical oscillations. The type of load i.e., constant power, constant current, constant impedance and dynamic load influences the voltage profiles at various buses. Hence it may increase or decrease the damping of power system oscillations [5-6].

Failing to address the issues of electromechanical oscillations leads to some serious situations in power system. These low-frequency oscillations may result in loss of synchronism between the generators which could further turn into wide-area blackouts. Although all these oscillations can exist simultaneously, the primary focus of this thesis is on damping the inter-area mode oscillations. Some of the important incidents related to blackouts due to inter-area mode oscillations in the history of the power system are listed in Table 1.1[7].

The conventional practices to improve the damping of these oscillations are as follows [2]:

i) Improving the system topology by reinforcing the tie line capacity.

ii) Increase active and reactive power sources.

iii) Improve the performance of Automatic Voltage Regulator (AVR) in excitation systems.

iv) Installing PSSs and FACTS devices as Supplementary Damping Controllers (SDCs).

Table 1.1 Well-known blackouts due to inter-area oscillations in power system

Inter-area oscillation Incidents	**Frequency of inter-area oscillations**
U.K (1980)	0.5 Hz
Taiwan (1984,1989,1990,1991,1992)	0.78-1.05 Hz
West USA / Canadian system separation	0.22 Hz
Scandinavia (1997)	0.5 Hz
China (2003)	0.4 Hz
USA (2003)	0.17 Hz
Italy (2003)	0.55 Hz

The basic philosophy behind the first three solutions is to reduce the electrical length of the transmission network i.e. to reduce the electrical length between the synchronous generator and the load which involves large capital cost. The fourth solution i.e. PSSs and FACTS supplementary controller improves the damping by dynamic control of some interrelated electrical parameters. These parameters could be voltage, line reactance, active power, reactive power and phase angle etc. As the first three measures are related to change in system topology, they are not discussed here. Detailed attention is given to the fourth measure i.e. damping of electromechanical oscillations by using PSSs and FACTS devices.

1.2 Power System Stabilizers

Around the mid-1960s, excitation system of the generators is modified for providing the damping of rotor oscillations. Power System Stabilizers (PSSs) were added in the

excitation system with the supplementary feedback control signal [8-9]. The high-speed excitation system improves the transmission capacity and steady-state stability margins in power system. However, the damping torque produced by the synchronous generators is reduced due to fast-acting voltage regulator [10]. Auxiliary signals were introduced in the feedback control system in order to overcome the above-mentioned problem. The resulting controllers were known as power system stabilizers. The basic block diagram of PSS is as shown in Figure 1.1.

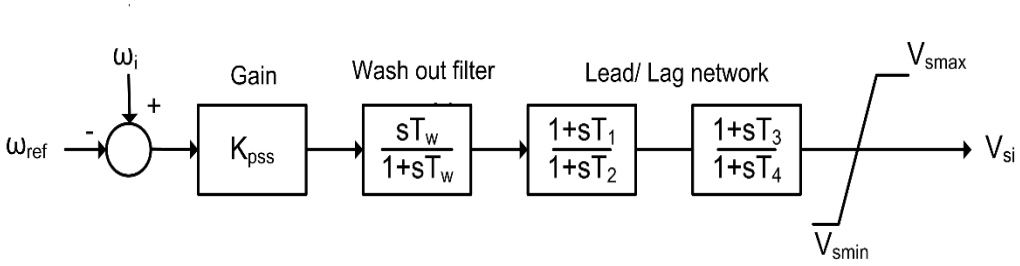

Figure 1.1 Block diagram of PSS [2]

PSSs restore the diminishing damping torque by generating additional damping torque by forming the closed loop with chosen input signal [2]. The rotor speed deviation $\Delta\omega$ is the most widely used feedback signal. However, variation in power flow ΔP, variation in rotor angle $\Delta\delta$ and change in frequency Δf are also considered as effective feedback signals for producing additional damping torque [11-12]. The structure of PSSs includes a wash out filter followed by lead-lag compensation block [13]. The main function of the lead/lag block is to provide the phase lead so as to reduce the phase lag between the excitation system input and electrical torque generated at the output. The wash-out stage functions as a band pass filter. Relatively small variation in generator terminal voltage due to very small change in rotor speed is prevented by wash-out stage. The time constant of wash-out stage is usually adjusted to 1 to 20 seconds. For damping local modes, the time constant of 1-2 seconds is considered appropriate while time constant of 10 second is preferred for damping inter-area modes [14].

Due to its local installation on the exciter of the generators, PSSs are more suitable for damping the local modes. However, with proper tuning of its parameters, PSSs can help in damping inter-area mode oscillations. The performance of PSSs is quite different for both modes with different load models and different locations [15]. Many research studies

are carried out for designing PSS over common low-frequency band [16-18]. However, the impact of PSS for damping of inter-area modes is quite limited due to the local compensating arrangement. In general, due to the following limitations, PSSs are not suitable for damping inter-area mode oscillations [15-18]:

i) Tuning of PSSs for damping the inter-area mode oscillations may adversely affect its setting for damping the local mode oscillations.
ii) PSSs requires phase lead design with reduced gain margin and hence inter-area mode oscillations are poorly controllable due to its location.
iii) Co-ordinations between various PSSs become extremely difficult in deregulated electricity markets.

However, the FACTS devices do not suffer from the above limitations as they are located in the transmission network. Although the primary function of the FACTS devices in the transmission network is to overcome the specific limitations of the given transmission network, it can be successfully employed for damping the inter-area mode oscillations.

1.3 Flexible AC Transmission System (FACTS) devices

Conventionally, the active power flow in the system is controlled through turbine governing system of the generator while voltage regulation is achieved through series and shunt connected reactive power devices and phase shifting transformers. Phase shifting transformers are also used for controlling active power flow. However, some of them are operated with fixed phase angle while in most cases, variable tappings are used. Series reactors are used to reduce the short circuit fault current and power flow. Series capacitors are used to reduce the electrical length of the transmission lines and hence increase the power flow. The conventional solutions of controlling the parameters of the transmission network worked satisfactorily until the concept of deregulation of the electricity market was introduced in the last decade of the twentieth century [1]. The continuous expansion of the power system and problem in acquiring new right of way forced power system engineers to think in the direction of introducing power electronics based high voltage, high current solid state devices, known as FACTS devices. Variable impedance based FACTS devices like Thyristor Controlled Reactor (TCR), Thyristor Controlled Series Capacitor (TCSC), Thyristor Controlled Phase Shifting Transformers

(TCPST), and Thyristor switched Capacitors (TSC) etc. were introduced in power system as first generation FACTS devices. These devices employed Thyristor for controlling the parameters of the power system and have only “ON” control. With the advancement in the technology, voltage and current source converter based FACTS devices like Static Synchronous Compensator (STATCOM), Static Synchronous Series Compensator (SSSC) and Unified Power Flow Controller (UPFC) were introduced in the power system. These devices are known as second generation FACTS devices. These devices employed Metal Oxide Semi-Conductor Field Effect Transistor (MOSFET) or Insulated Gate Bipolar Transistor (IGBT) as switching device and have both “ON” and “OFF” control. In general, the FACTS devices offer the following merits:

i) Control of active power flow as per requirement.
ii) Increase the available transfer capacity (ATC) of given transmission network.
iii) Improvement of transient stability of the power system.
iv) Act as power system damping controller.
v) Reduction in loop flow in the transmission network.
vi) Control of reactive power flow and hence increasing the active power capability.

Table 1.2 shows the suitable FACTS devices for various operating conditions.

Table 1.2 Suitable FACTS devices for various operating conditions

Operating condition	**Appropriate action**	**Suitable devices**
Voltage sag due to heavy loading condition	Supply reactive power	SVC, STATCOM
Voltage rise due to light loading condition	Absorb reactive power	TCR, SVC, STATCOM
Low voltage due to faults	Supply reactive power	SVC, STATCOM
High voltage due to faults	Absorb reactive power	TCR, SVC, STATCOM
Damping of inter-area mode	Adjust susceptance of the FACTS devices	SVC,STATCOM,TCSC, UPFC
Loop flows	Adjust reactance	TCSC,SSSC,UPFC
Reversal of power flow in line	Adjust phase angle	SSSC, UPFC

However, the operating conditions of our interest at present are the damping of the inter-area mode oscillations using FACTS devices. As discussed earlier, inter-area mode oscillations are defined as oscillations of a group of generators of one area of the system against a group of generators of another area of the system. The role of the FACTS devices in damping of the inter-area mode is more effective when they are located in particular transmission line from the viewpoint of controllability and observability indices. Therefore, in comparison of PSSs which are situated locally to generators, FACTS devices are more suitable for damping inter-area mode oscillations as they are situated in transmission networks and designed for controlling the inter-related parameters of the transmission network.

The damping provided by FACTS devices can be explained by system parameter modulation. The system parameter could be line power flow, bus voltage or line current etc. The concept of damping mechanism with line power modulation can be explained with the two machine system as shown in Figure 1.2.

The machine SM_1 supplies power P to machine SM_2 over a lossless transmission line. The speed and rotor angle of machine SM_1 is η_1 and φ_1 respectively while the same for machine SM_2 is η_2 and φ_2. The machines oscillate at relative angle $\Delta\varphi = \varphi_2 - \varphi_1$ and relative speed $\Delta\eta = \eta_2 - \eta_1$. When the speed of receiving end machine is lower than the sending end machine speed i.e. $\Delta\eta$ is negative, the FACTS device increases the power flow in the transmission line. If $\Delta\eta$ is positive, the FACTS device should decrease the power flow in the transmission line. The FACTS devices supply modulation power ΔP_{mod}. This power produces a damping torque in the opposite direction to rotor speed deviation [19].

Figure 1.3 shows the internal control system of FACTS devices with SDC. This is very much similar to excitation control with PSS. Although FACTS devices are used as supplementary damping controller, its effectiveness in damping inter-area mode oscillations is very relevant. With continuous development in FACTS technologies, for both existing and new FACTS installation, inter-area oscillation damping became essential feature [20-24].

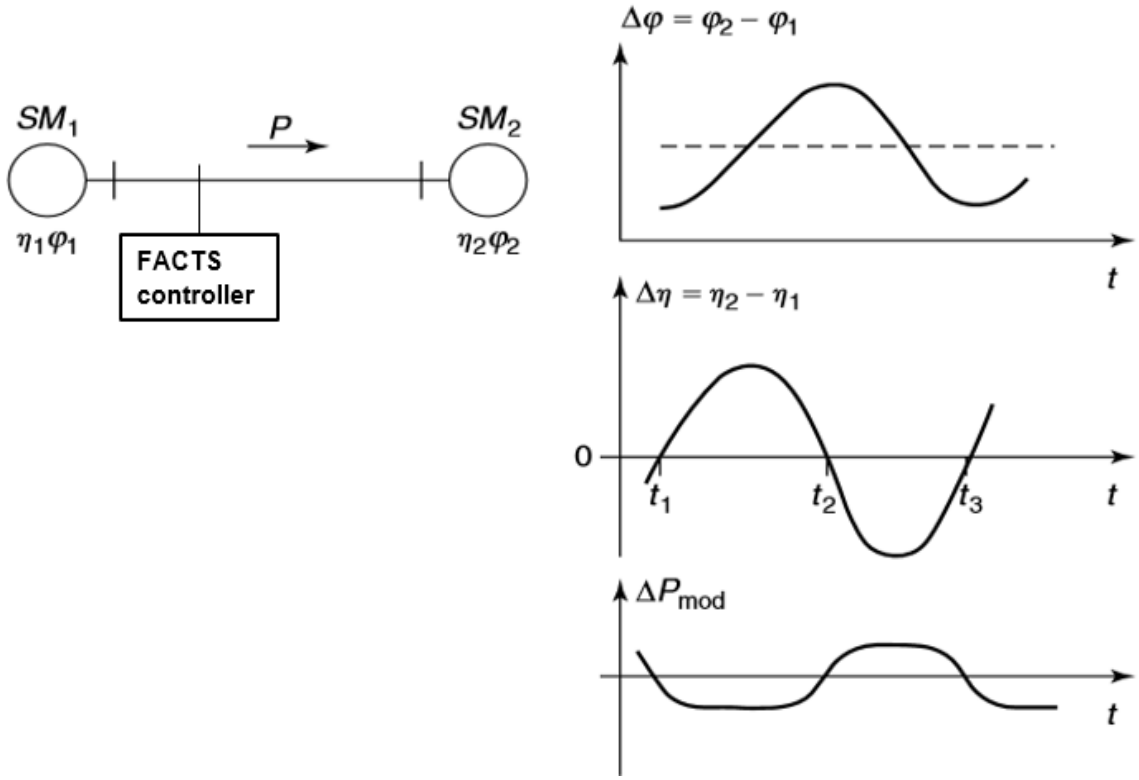

Figure 1.2 Power modulation for damping enhancement by FACTS devices [19]

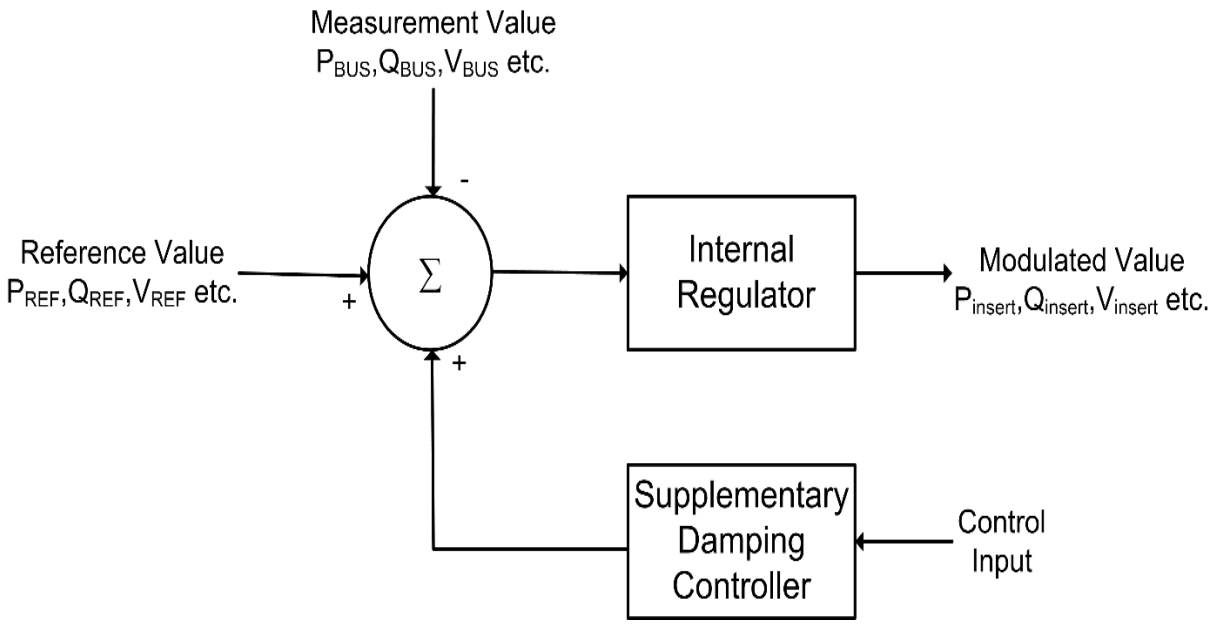

Figure 1.3 FACTS device with supplementary damping controller [19]

Conventionally the design of PSS and FACTS based on classical technique like residue based approach is for single operating point of the system. Also, both controllers are single input single output and there is no coordination between them. These controllers are designed using local inputs and hence suffer from two major drawbacks. First, as they are designed by linearization around nominal operating point, their validity is restricted around the neighboring region of this point while in actual condition, power system experiences a continuous change in operating conditions. These changes may be caused by a change in generation or load or due to changes in the transmission network. Also during normal operating conditions, a certain amount of uncertainties are present due to the approximation made in the power system modeling, neglecting high-frequency system dynamics and the invalid assumption made in modeling. Secondly, sometimes inter-area mode oscillations may not be observable by local controllers. In certain cases, inter-area mode is observable in one area but not controllable and vice-versa [25]. This may result in the ineffectiveness of the local controllers in damping inter-area mode oscillations.

The drawbacks of the local controller can be overcome by applying wide area based control technologies and using robust control theory. Robust control techniques ensure system stability with desired system performance under wide operating conditions [26-28]. Phasor Measurement Units (PMUs) based wide area measurement technologies can deliver a control signal at a high speed. The PMUs are located strategically in the multi-machine system and captures a real-time picture of given power networks by measuring voltage, current, angle, and frequency at various buses [29-30]. Positive sequence voltages and currents from different areas of the network are measured by the PMUs and these signals are delivered to Wide Area Damping Controllers (WADC) as frequently as once per cycle of system frequency. The Global Positioning System (GPS) is integrated into PMUs to assure proper time synchronization of global signals [30]. Reference [31] shows that wide area controller is more effective in preventing loss of synchronism than a local controller. Also for the same damping effect, local controllers need large gain (approximately 4 to 20 times) than wide area controllers [32].

1.4 Literature Review

The design of WADCs is carried out on linearized plant model. While linearizing the plant model, higher order dynamics are neglected. Hence these models consist of uncertainties in the plant models. The designed WADCs must work satisfactorily under these uncertainties. The inter-area mode oscillations are caused by small disturbances such as a change in load, AVR response to short circuit faults etc. This kind of unpredicted system uncertainties should not diminish the damping performance of the controllers i.e. controllers must reject such kind of disturbances. Also, after large disturbance, the system may deviate from its steady state operating point. The controller must able to function under various operating conditions. The study of the performance of controller under these conditions is known as robustness [33].

The uncertainty of the plant model was addressed in [34] to design robust controller via H_∞ approach. The largest singular gain of the frequency response of closed-loop system represents the effect of the disturbance. The basic function of the H_∞ approach is to minimize this gain. Due to this, sensitivity between the system output and disturbance can be reduced. H_∞ norm is the largest singular gain of the frequency response of the closed-loop system. Its minimization is considered as worst-case optimization [35]. This approach was then extended to state-space models [36] and resulted in new developments in robust control theories.

Robust FACTS controller using H_∞ control approach were designed in many power system studies for improving the dynamic stability of the system. The robustness problem was expressed in mixed sensitivity formulations in [37]. The robust TCSC controller based on H_∞ performance was designed by solving Riccati equations [38]. However, the unobservable modes resulted in pole-zero cancellation in case of damping controller designed via conventional Riccati approach [39]. A comparison between the centralized structure with a single TCSC device with multiple input signal and multiple FACTS devices with decentralized structure is carried out in [40]. Emphasize is given on centralized structure with the global signal. Ref. [41] discusses the coordinated damping control between multiple FACTS devices using mixed H_2/H_∞ approach. Ref. [42] shows the compatibility of H_∞ norm based method with loop shaping technique [42]. The H_∞ loop

shaping approach was applied for robust PSS design in [43]. Reference [44] proposed a two loop PSSs with decentralized/hierarchical structure. Additional damping to the local modes was provided with the wide-area signals based PSS. The global and local proposed controllers were tuned by the sequential optimization procedure. A combination of remote wide area signal and the local signal was proposed in [45] to enhance the observability and damping performance of the designed controller. With the weighted synthesis of both the signals, the PSS and the TCSC controller were successfully designed. A real-time controller to improve the dynamic stability of the power system was suggested in [46]. The designed controller initiate control actions only when oscillations with poor or negative damping were observed. The heuristic rules derived from the offline studies along with the WAMs were used for real-time application of the designed controller in the large power system. The operation of SVC is changed from natural voltage regulation mode to power system damping control (PSDC) mode whenever the oscillatory instability is detected.

A robust power system stabilizer which places the system poles in the acceptable region in the complex plane for a given set of operating and system condition was designed in [47] using Linear Matrix Inequality (LMI) technique. In reference [48], H_∞ control was used for designing a robust TCSC controller along with LMI which solves Lyapunov inequality without the weighting co-efficient. Load changes were treated as system uncertainties in LMI approach. Reference [49] discusses the placement of FACTS controller using modal controllability indices to damp out power system oscillations. Optimal control strategy using pseudo-decentralization was developed for coordination of PSSs and FACTS devices in [50]. Reference [51] discusses optimal Phasor Measurement Units (PMUs) for complete topological and numerical observability in power system. A robust SVC controller using PMU acquired bus voltage angles was developed for damping inter-area oscillations in [52]. Comparison between PSS, SVC, and STATCOM for damping power system oscillations was carried out in [53]. Oscillation problem was analyzed from the viewpoint of Hopf bifurcations as an extended eigenvalue analysis to study different controllers, their locations and use of various control signals for checking their effectiveness for damping power system oscillations. A robust decentralized fast sampling technique based PSS controller was developed in [54] using LMI approach. For different

operating conditions of the nonlinear power system, 16 linear state space models were obtained. For all these plant models, a common stabilizing feedback gain was obtained. Reference [55] discusses mixed H_2/H_∞ output feedback controller with regional pole placement using LMI approach. Two practical considerations are discussed here regarding the selection of PMU signals and PMU data reporting rate. Residue and root locus based SVC and TCSC controllers were designed in [56]. In reference [57], most effective stabilizing signals were determined by participation factor method. These signals were coordinated in wide area damping controller to achieve multi-objective collocated control. Three different methods namely, controllability/observability, residue, and Hankel singular value were used for selecting the feedback control signal and how this selection affects the performance of damping controller was discussed in [58]. A robust coordination approach for the controller design of multiple HVDC and FACTS wide-area controller using mixed H_2/H_∞ output feedback controller with regional pole placement constraint was presented in [59]. The LMI theory was then applied to solve such robust control problem. The relative gain array (RGA) based hybrid method was proposed for selection of suitable control signals for multiple HVDC and FACTS controller of large-scale interconnected power system [60]. A systematic procedure for designing decentralized wide-area damping controller for wind farms and FACTS controllers in a smart grid considering load parameter uncertainties was presented in [61].

The large multi-machine system may exhibit multiple dominant inter-area mode oscillations. The FACTS damping controller designed with the local feedback signal may exhibit poor damping performance due to the lower observability of the inter-area modes in the feedback signal. This drawback can be overcome with the help of PMU based WAMs [58-61]. The damping controller is no longer decentralized due to remote feedback signals received from the PMUs located in various areas of the multi-machine power system. For simultaneous damping of multiple inter-area oscillations mode, a TCSC controller with multiple input single output (MISO) structure was proposed in [62-63]. However, the controllability of the single FACTS controller was found to be limited in damping the multiple modes and only a few modes can be damped properly.

The effective solution for the above-mentioned problem is the coordinated damping control of multiple FACTS devices. Coordinated centralized MIMO structure is heavily

dependent on the remote input signals and hence any communication failure of the input signal jeopardize the performance of the controller as the inputs and outputs are strongly coupled. So, the direct decentralized design is preferred over the centralized structure. The optimization based robust control techniques has great performance [27, 64, 65] in the coordinated approach of decentralized fixed structure based FACTS controllers, but the problem of cross-coupling still persists with the simultaneous tuning of the parameters of the different controllers. The issue of cross-coupling can be overcome by adopting sequential approach [59]. In sequential approach, multiple controllers can be designed by the closed-loop system with previously designed controllers. The sequential approach results in independent and more reliable controllers. The following research gaps are identified from the above-mentioned literature review:

- The load models considered in above-mentioned literature review are constant impedance, constant current and constant power. However, in the practical power system, the actual composition of load model is the mixture of above load models as well as dynamic loads. So, more realistic load compositions are needed to be considered.
- The large power system employing several FACTS devices, there are chances of adverse interaction between the control actions of various controlling devices. Hence, a suitable technique for designing the multiple controllers must be applied to avoid interaction of control actions among various control devices.
- Proper selection of the FACTS devices is important. Sometimes a single FACTS device may not able to damp all the inter-area mode oscillations in the large power system. Hence, a mixture of suitable devices depending upon the network topology must be considered.

1.5 Research Objectives and Contribution

This research study presents an improvement in small signal stability of multi-machine power system using FACTS devices as supplementary damping controller. The main objective of the thesis is to improve the damping of low-frequency inter-area mode oscillations using robust control techniques. This is mainly dependent on the system configuration and control methodology applied to it. Also, the designed controllers must

be robust enough for providing sufficient damping under various contingencies arise in power systems. A linearized plant model of the power systems including FACTS devices is carried out. The mixed sensitivity based multi-objective LMI approach with pole placement is developed for the design of robust FACTS damping controller. The contribution of the thesis is as follows:

- Proposed a systematic procedure to design wide area damping controllers and to show its effectiveness for damping inter-area oscillations.
- Proposed an exclusive load composition model which covers all possible load compositions.
- The mixed H_2/H_∞ output feedback control with regional pole placement is demonstrated and applied control effort optimization simultaneously to the wide area damping controllers.
- The LMI based system sequential design approach for the coordinated design of multiple FACTS controller is demonstrated as an extension of multi-objective multi-modal system approach mentioned above. To improve the effectiveness of the design, mode-shape analysis and modal residue analysis are carried out to determine most suitable remote feedback signal for different FACTS controller.
- Extended LMI approach to loop shaping techniques.
- The designed controllers are investigated for proposed load models.
- The robustness of the controllers is investigated by evaluating its performance under various operating conditions like line faults, line outages, change in power flow and proposed load models. The response of the controllers to various disturbances using time domain simulation based on nonlinear power system models is also carried out.
- Established the effectiveness of the designed controllers under various contingencies conditions through linear and nonlinear time domain simulations.

1.6 Thesis Outline

The thesis is organized as follows:

Chapter 1- Introduction: Describes the problem statement, its conventional solutions, and limitations of the conventional solutions. A brief literature review is carried out in this chapter to outline the work done in the field of the wide area damping control for inter-area oscillations. Some research gaps are found out and proposed the methods to fill these gaps.

Chapter 2- Small-signal modeling of power system: The small signal modeling of power system components and various FACTS devices are discussed in this chapter. Also, steps for building a linearized model of the power system are discussed. Modal analysis is explained to find out the dynamic characteristics of the plant model.

Chapter 3- Design of Wide area damping controller: Describes the systematic procedure for the design of damping controllers for damping the inter-area mode oscillations. The controller synthesis includes the problem of mixed H_2/H_∞ output feedback control with regional pole placement and control effort optimization and is solved by the LMI approach and LMI approach to H_∞ loop shaping techniques.

Chapter 4- Case studies on LMI based multi-objective approach: Presents two case studies for the design of robust FACTS WADC. The steps described in chapter 3 are applied for designing the WADC. The design methodology for the controllers is mixed sensitivity based LMI approach with pole placement and LMI approach with the sequential design. The selection of global feedback signals and system model order reductions are also discussed. The controller is implemented on modified two area four machine system with TCSC and New York New England five area test system with SVC, TCSC, and UPFC. Sequential design based on mixed sensitivity formulation in LMI framework is carried out for various FACTS devices present in the modified New York New England test system. The effectiveness of the designed controller is checked for various operating points. Robustness of the controller is checked with nonlinear time domain simulations. A new composition of various types of load models is proposed in this thesis which tries to cover all possible load composition scenarios of the actual power system. A fare weight is given to all types of load models at various buses in the proposed load model compositions.

Chapter 5 – a Case study on H_∞ loop shaping techniques using LMI: Robust controller synthesis based on LMI approach to H_∞ loop shaping techniques is applied to 10-machines 39 buses modified New England test system. The performance of the designed wide area controller is checked with various proposed load composition models including dynamic load resembling actual power system loading. For validating the performance of the sequential designed FACTS controller, the nonlinear time-domain simulation was performed for various contingency conditions like line outage, line faults and load shedding on the test system.

Chapter 6- Conclusion and future scope: Summarize the findings of the research and lists several topics for the future work.

A list of references relevant to this work is given at the end.

CHAPTER 2 SMALL SIGNAL MODELING OF POWER SYSTEM

2.1 Introduction

For damping the electromechanical oscillations, two approaches are widely employed: Measurement-based approach and modal based approach. Many measurement-based techniques like prony method, wavelet transform and Hilbert-Huang transform are investigated by the researched for identifying the low frequency oscillations in power system [66, 67]. However, measurement-based technique suffers from the major disadvantage that the estimation of the stability margin of the oscillating modes cannot be derived from the calculated results. In this thesis, modal based approach is applied to identify the low frequency oscillations in the power system. For damping the low frequency inter-area oscillations in modal based approach, linearized modelling of all components of power system including FACTS devices must be carried out. This chapter presents the small signal modeling of power system components along with FACTS devices. A set of algebraic and differential equations represents the static and dynamic behavior of the systems. These equations are converted in to state space representation after carrying out linearization. Small signal analysis is then performed to identify the inter-area modes with low damping ratio. Necessary supplementary damping controllers are then designed by applying robust control theories. Different operating conditions of the power system are represented by multiple linear models. These multi-modal system is necessary for the robustness design. The power system static and dynamics equations represent the mathematical modeling of the generator (including excitation system, PSS and turbine-governing system), the power networks, the FACTS devices and the load.

2.2 Synchronous Generator Model

The demand for the electrical energy in power system is fulfilled by the synchronous generators. Driven by steam, hydro or gas turbines at synchronous speed, they convert mechanical energy into electrical energy. The field winding of the generator is situated in the rotor which is excited through direct current to produce flux. This flux induces a three-phase rotational voltages in the stator winding which is connected to the grid. The magnitude of the stator voltage is controlled by the automatic voltage regulator (AVR).

The power output of the generator is controlled by controlling the steam/water or gas input to the respective turbines through governor. The high frequency stator transients are normally neglected in the study of small signal stability. Apart from the field winding, the solid rotor body also acts a closed winding which is known as damper winding. The voltages induces and current is circulated in the damper winding when the speed of the generator is other than synchronous speed. It means that the damper winding produces the damping torque against the rotor speed variations. The nature of the study decides the number of damper windings used to represent the damping effect of the rotor. Conventionally for the small signal stability studies, the damping effect of the rotor is represented by one damper winding in the *d*-axis and two damper windings on the *q*-axis. The modeling of the synchronous machine in the rotor frame of reference is shown in Figure 2.1.

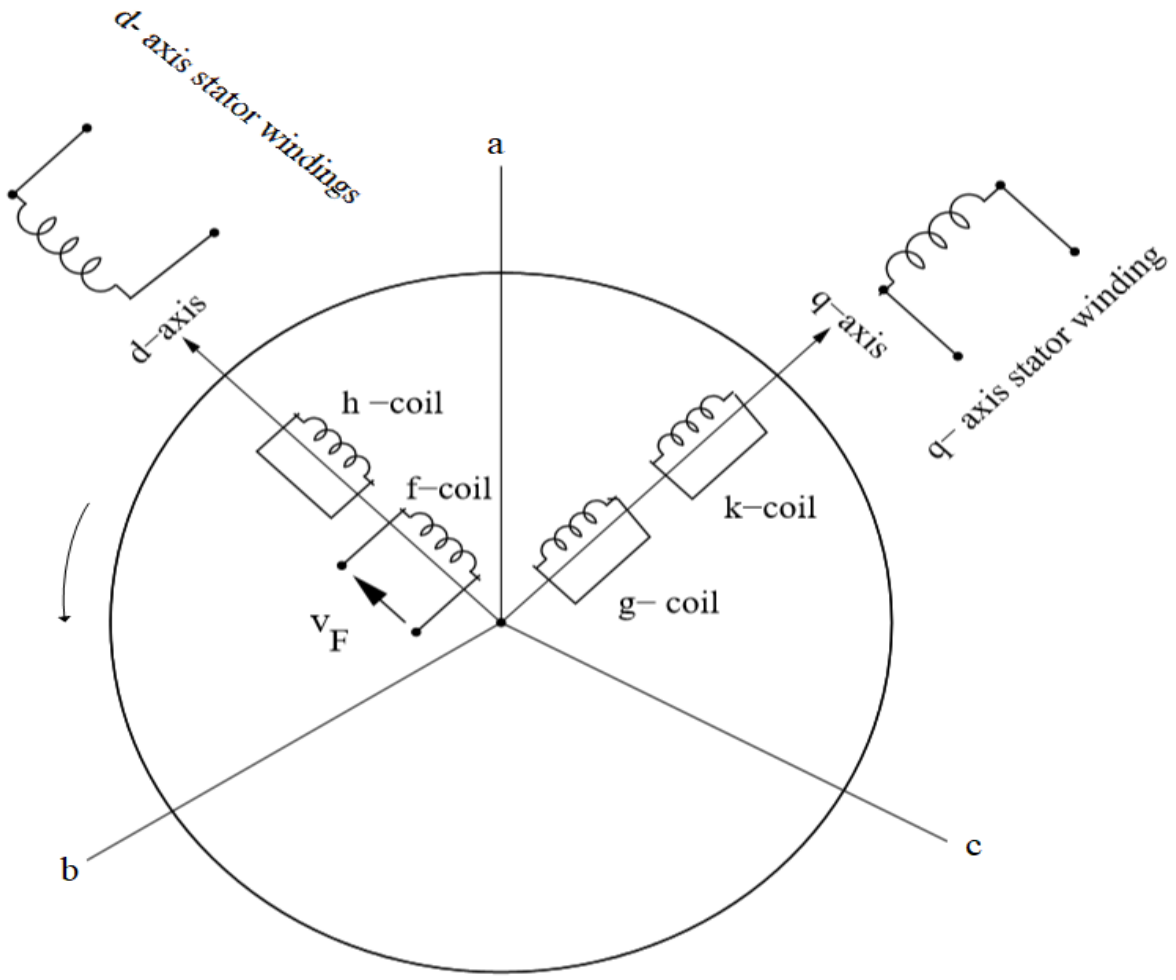

Figure 2.1 Model of a synchronous machine

Figure 2.1 shows the fictitious *d* and *q* stator windings representing the three-phase armature windings on the stator. The damping effect of the rotor is represented by two short-circuited coils ('*g*' and '*k*') on *q*-axis and one short-circuited coil ('*h*') on *d*-axis. The *d*-axis also includes the main field winding ('*f*').

In this study, cylindrical round rotor synchronous machines are used in various systems. The synchronous machine dynamics depend upon the type of machines chosen. Its order may be varied from two as in case of the classical machine to eight as in case of detailed representation. In this study sub-transient, the round rotor synchronous machine having sixth order is selected which represents necessary generator dynamics without over complicating it. The synchronous generator is represented by the six state variables as shown in Table 2.1.

Table 2.1 State variables of the synchronous generator

Name of the state variable	Description of the state variable
ω	Rotor speed
δ	Rotor angle
Ψ_f	Field winding flux linkage
Ψ_{kd}	Direct axis damper winding flux linkage
Ψ_{kq1}	First quadrature axis damper winding flux linkage
Ψ_{kq2}	second quadrature-axis damper winding flux linkage

The synchronous generator dynamic equations are as follows [2, 3]:

$$\frac{d\delta}{dt} = \omega - \omega_0 \tag{2.1}$$

$$\frac{2H}{\omega_0}\frac{d\omega}{dt} = T_m - D\,(\omega - \omega_0) - (\psi_d i_q - \psi_q i_d) \tag{2.2}$$

$$\frac{1}{\omega_0}\frac{d\psi_f}{dt} = V_f - i_f r_f \tag{2.3}$$

$$\frac{1}{\omega_0}\frac{d\psi_{kd}}{dt} = -r_{kd} i_{kd} \tag{2.4}$$

$$\frac{1}{\omega_0}\frac{d\psi_{kq1}}{dt} = -r_{kq1}i_{kq1} \tag{2.5}$$

$$\frac{1}{\omega_0}\frac{d\psi_{kq2}}{dt} = -r_{kq2}i_{kq2} \tag{2.6}$$

$$\begin{bmatrix}\psi_d\\ \psi_f\\ \psi_{kd}\end{bmatrix} = \begin{bmatrix}x_d & x_{ad} & x_{ad}\\ x_{ad} & x_f & x_{ad}\\ x_{ad} & x_{ad} & x_{kd}\end{bmatrix}\begin{bmatrix}-i_d\\ i_f\\ i_{kd}\end{bmatrix} \tag{2.7}$$

$$\begin{bmatrix}\psi_q\\ \psi_{kq1}\\ \psi_{kq2}\end{bmatrix} = \begin{bmatrix}x_q & x_{aq} & x_{aq}\\ x_{aq} & x_{kq1} & x_{aq}\\ x_{aq} & x_{aq} & x_{kq2}\end{bmatrix}\begin{bmatrix}-i_q\\ i_{kq1}\\ i_{kq2}\end{bmatrix} \tag{2.8}$$

H	Inertia constant
D	Damping coefficient
ω_0	Synchronous speed
T_m	Mechanical torque developed by the rotor
Ψ_d	Direct axis airgap flux linkage
Ψ_q	Quadrature axis airgap flux linkage
i_d	Direct axis terminal current
i_q	Quadrature axis terminal current
r_{kd}	Direct axis damper winding resistance
i_{kd}	Direct axis damper winding current
r_f	Field winding resistance
i_f	Field winding current
V_f	Field winding voltage
r_{kq1}	First quadrature axis damper winding resistance
i_{kq1}	First quadrature axis damper winding current
r_{kq2}	Second quadrature axis damper winding resistance
i_{kq2}	Second quadrature axis damper winding current
x_d	Unsaturated direct axis reactance
X_{ad}	Saturated direct axis magnetizing reactance
x_f	Field winding leakage reactance
x_{kd}	Direct axis damper winding leakage reactance

x_q	Unsaturated quadrature axis reactance
x_{aq}	Saturated quadrature axis magnetizing reactance
x_{kq1}	First quadrature axis damper winding leakage reactance
x_{kq2}	Second quadrature axis damper winding leakage reactance

The output voltage at the generator terminal can be represented by the following algebraic equations [2]:

$$0 = v_i \sin(\delta_i - \theta_i) - \frac{x_{qppi} - x_{li}}{x_{api} - x_{li}} E_{dpi} - \frac{x_{qpi} - x_{qppi}}{x_{api} - x_{li}} \psi_{qi} - r_{ai} i_{di} - x_{qpp} i_{qi} \quad (2.9)$$

$$0 = v_i \cos(\delta_i - \theta_i) - \frac{x_{dppi} - x_{li}}{x_{dpi} - x_{li}} E_{qpi} - \frac{x_{dpi} - x_{qppi}}{x_{dpi} - x_{li}} \psi_{di} - r_{ai} i_{qi} - x_{dpp} i_{di} \quad (2.10)$$

I	1,2,3…… , Generator index
v_i	i^{th} generator terminal voltage
Θ_i	Phase angle of the i^{th} generator terminal voltage
x_{dpi}	Unsaturated direct axis transient reactance of i^{th} generator
x_{dppi}	Unsaturated direct axis sub-transient reactance of i^{th} generator
x_{qpi}	Unsaturated quadrature axis transient reactance of i^{th} generator
x_{qppi}	Unsaturated quadrature axis sub-transient reactance of i^{th} generator
r_{ai}	Stator resistance of i^{th} generator
E_{dpi}	Induced transient voltages in direct axis of i^{th} generator
E_{qpi}	Induced transient voltages in quadrature axis of i^{th} generator

2.3 Excitation System Model

To produce rated terminal voltage, synchronous generators require direct current in the field winding. This direct current is provided by the excitation system. The basic block

diagram of excitation system is as shown in Figure 2.2 [2, 68]. The exciter supplies DC power to the field winding of the synchronous generator to produce necessary flux. The regulator processes and amplifies the input control signal and form control for the excitation system. Both regulating and excitation system stabilizing functions are included in it. Voltage transducers measure the terminal voltage of the generator, rectifies this voltage into DC voltage and filters this voltage. The rectified DC voltages are compared to the reference value which represents the desired terminal voltage of the generator. The additional input signal necessary to damp the power system oscillations is provided by the PSSs. Typical input signals are rotor speed variation, frequency deviation etc. Limiters and the protective circuit include a wide array of devices to ensure that the capability limits of the exciter and generator are not violated. This typically includes field current limiters, under and overexcitation limiter, terminal voltage limiter, voltage/Hz regulator and protection etc. These are normally different circuits and their output is provided at appropriate place as summing input in the excitation system. Only for simplicity of understanding, their output is grouped as shown in Figure 2.2. In this study, two types of exciters are used: Type AC4A and type ST1A. The detail description of the above exciters are as follow:

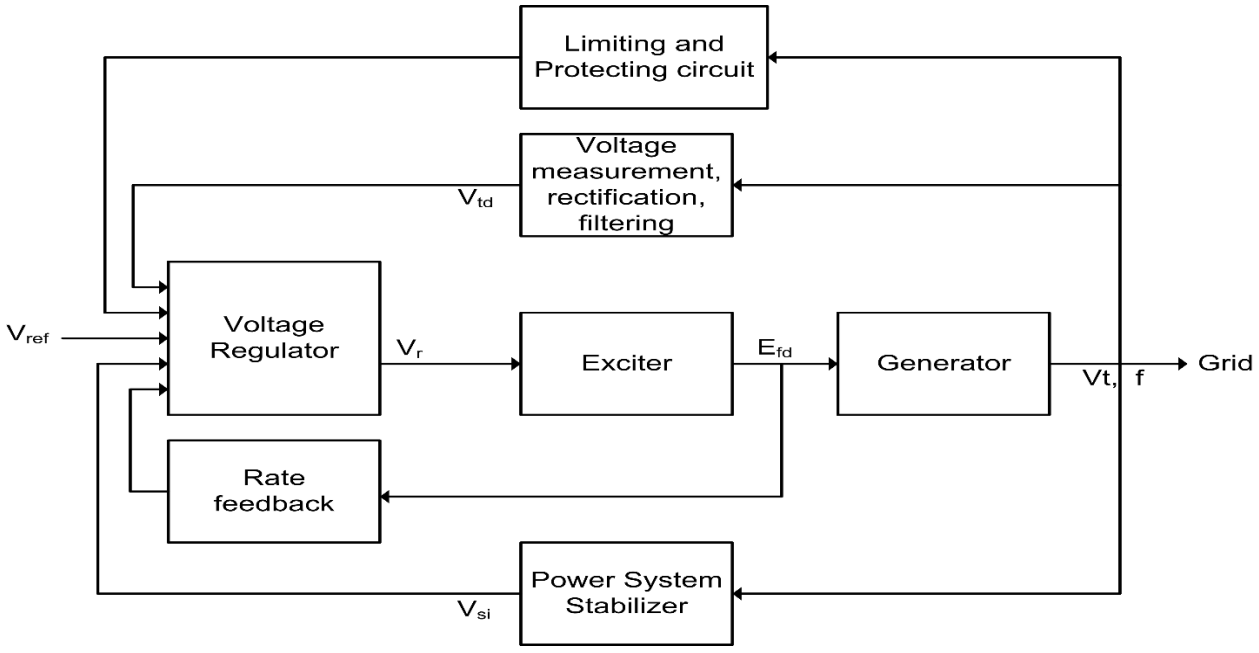

Figure 2.2 Basic block diagram of excitation system [2]

2.3.1 Type AC4A Excitation System Model

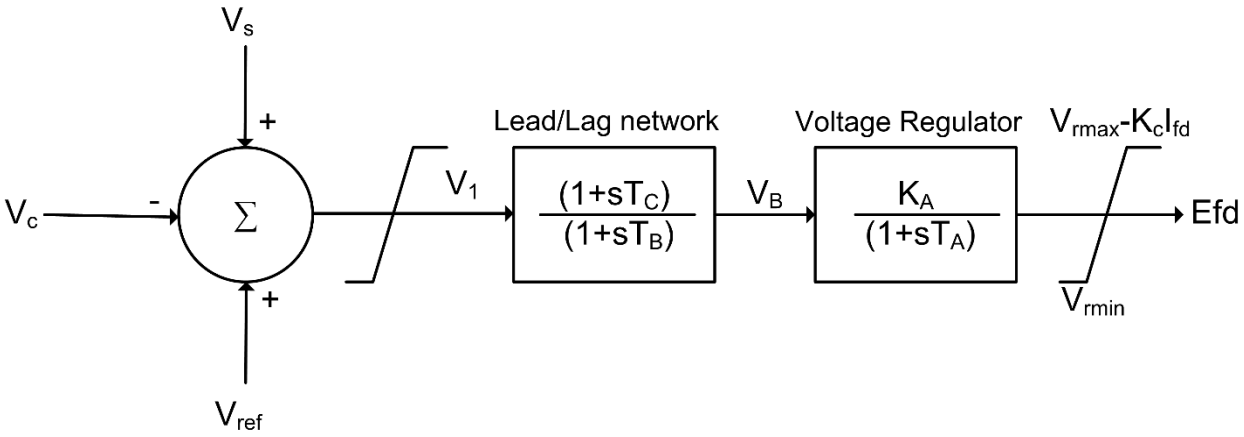

Figure 2.3 Type AC4a excitation system [68]

The type AC4a alternator supplied controlled rectifier system shown in Figure 2.3.These excitation system models a high initial response exciter with a full Thyristor bridge rectifier which supplies the generator field. The voltage regulator controls the firing of the Thyristor bridges and exciter uses an independent voltage regulator to control generator output voltage to a constant value.

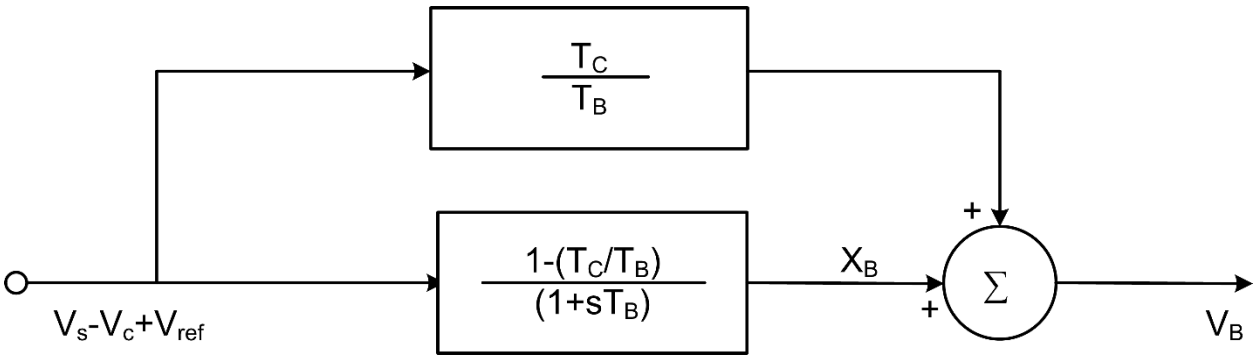

Figure 2.4 Transient gain reduction (TGR) block [68]

The excitation system simulation is accomplished by the lag-lead network. The time constants T_B and T_C allow simulation of this control function. The overall equivalent gain and the time constant associated with the regulator are simulated by K_A and T_A respectively. In certain cases, K_A is kept too large in order to have better transient stability

performance but this may result in the negative damping torque produced by the exciter. In such cases, the voltage regulator block is preceded by transient gain reduction (TGR) block. This block is shown in Figure 2.4. The differential equations for the type AC4A excitation system are given by:

$$\frac{dx_B}{dt} = \frac{1}{T_B}\left[-x_B + \left(1 - \frac{T_C}{T_B}\right)\left(V_{ref} + V_S - V_C\right)\right] \quad (2.11)$$

$$\frac{dE_{fd}}{dt} = \frac{1}{T_A}\left[-E_{fd} + K_A\left(x_B + \frac{T_C}{T_B}\left(V_{ref} + V_S - V_C\right)\right)\right] \quad (2.12)$$

2.3.2 Type ST1A Excitation System Model

In this type of excitation system, excitation power is obtained from generator terminal or stationary auxiliary bus through the transformer and regulated by a controlled rectifier. The maximum and minimum exciter output voltage are a function of generator terminal voltage magnitude and generator field current. The block diagram of ST1A excitation system is as shown in Figure 2.5. This exciter model is fast acting and hence no time constant. The exciter model is shown in Figure 2.6. The exciter output may be rate feedback to the automatic voltage regulator.

The automatic voltage regulator block (shown in Figure 2.7) comprises of two-phase lag/lead block and a rate feedback block. The exciter under generator open circuit conditions is stabilized with the help of rate feedback block. This type of exciter has high gain and fast acting amplifier. K_a and T_a represent voltage regulator gain and excitation system time constant.

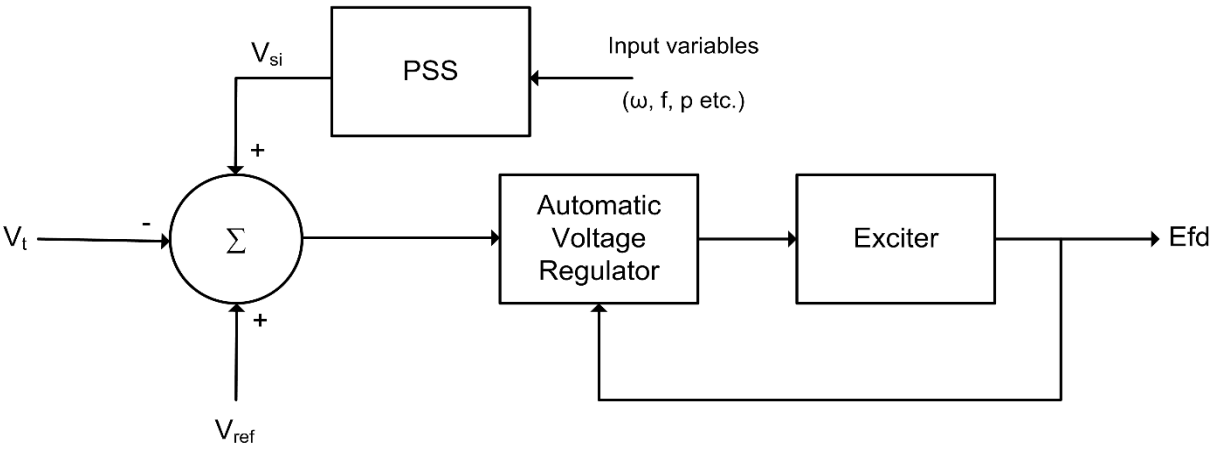

Figure 2.5 Block diagram of ST1A excitation system [68]

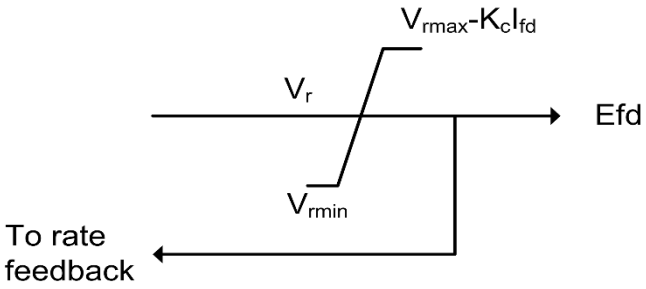

Figure 2.6 Type ST1A exciter [68]

The model shown is sufficiently versatile to reduce transient gain and hence, no separate transient gain reduction block is added. The transient gain reduction is achieved in a forward path through proper selection of time constants T_b and T_c or in a feedback path by suitable choice of rate feedback parameters K_f and T_f.

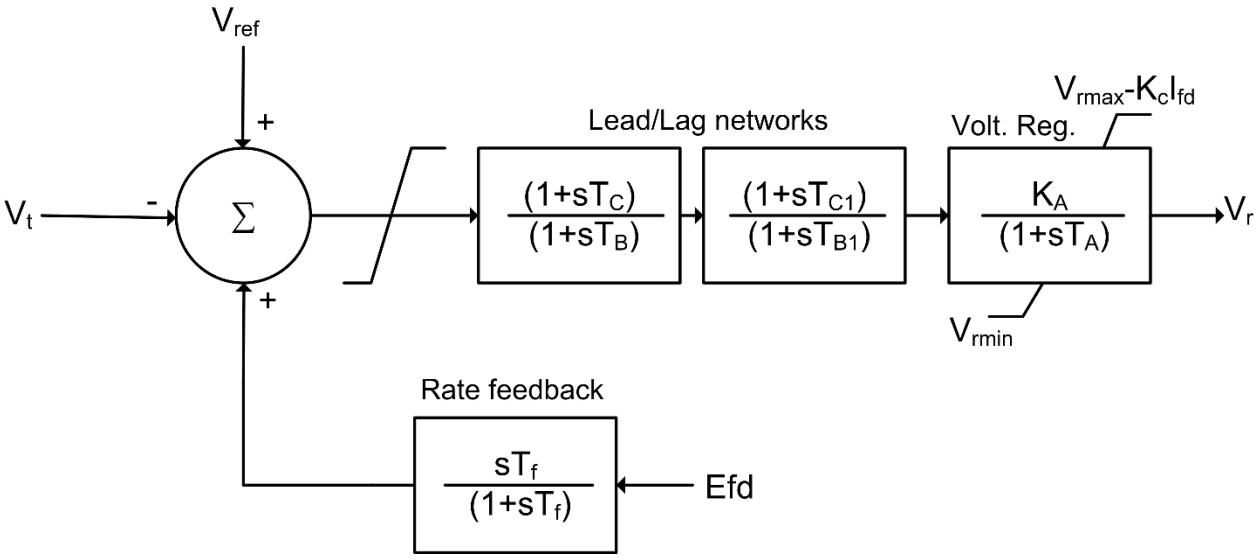

Figure 2.7 Type ST1A automatic voltage regulator [68]

2.4 Power System Stabilizer Model

The power system stabilizers can be connected to any exciter except DC3 exciter. The main controlling element of PSS is phase comparator. The output of PSS is fed to the reference summing junction of the exciter. The input to the PSS can be rotor angle deviation, rotor speed deviation (ω/ω_0), bus frequency or generator power. Most of the PSSs are fitted with the pre-compensator block. The input to the pre-compensator block

may be speed or frequency and electrical power. The function of the pre-compensator is to filter the torsional oscillation frequency so that turbine shaft instability can be eliminated. Electrical power input signal solely can achieve this function however it may cause low generator voltage when power setting is changed from one value to another. A basic block diagram of pre-compensator is as shown in Figure 2.8.

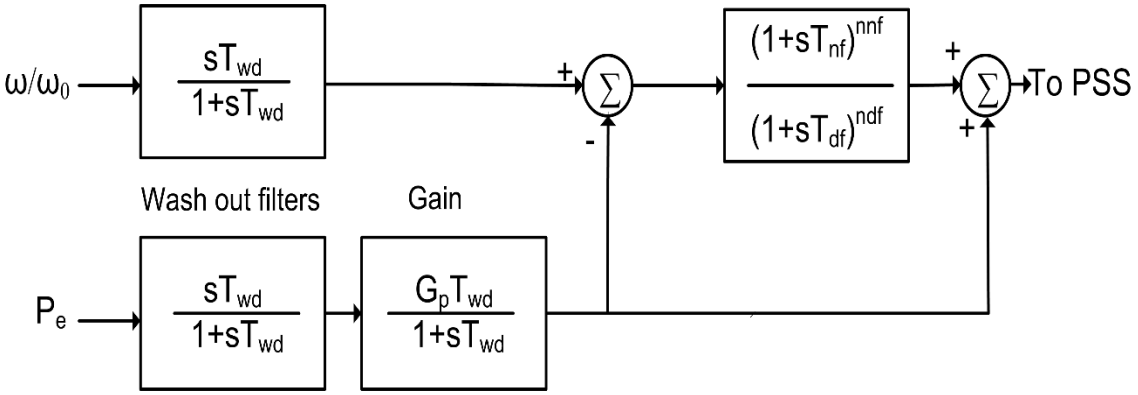

Figure 2.8 Power and speed input pre-compensator [69]

In case of synchronous generators,

$$\frac{d(\omega/\omega_0)}{dt} = \frac{1}{2H}(P_m - P_e) \quad (2.13)$$

where P_m = Mechanical input power to the turbine

P_e = Electrical output power of the generator

However, change in P_m is generally small and hence

$$\frac{d(\omega/\omega_0)}{dt} = -\frac{1}{2H}P_e \quad (2.14)$$

The pre-compensator is acting as low pass filter at low frequencies and hence eliminating the power signal from the output. At high frequencies, the output block of G_p is equivalent to generator speed change. Hence, torsional oscillation frequencies can be removed from input to the PSS at all frequency ranges.

In the present study, rotor speed deviations are used as input to the PSSs. The basic block diagram of PSSs is as shown in Figure 2.9 [69]. The description of the various blocks is already discussed in section 1.2.

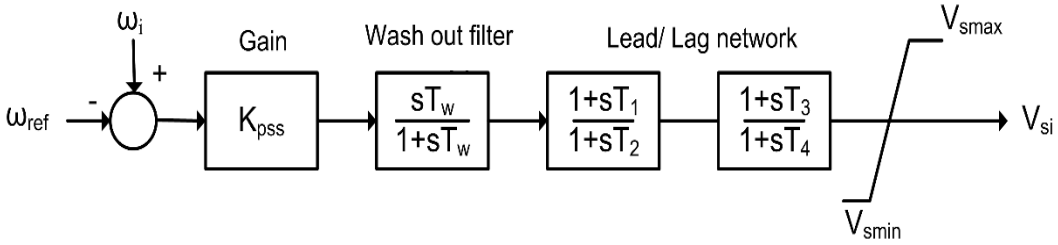

Figure 2.9 Basic block diagram of PSS [69]

2.5 Steam Turbine/Governor System Model

Synchronous generators are driven by either a steam turbine or hydro turbine. Turbines are fitted with speed governing system. In case of an isolated synchronous generator, the speed is controlled by the governor. However, in case of the interconnected power system in which the synchronous generator is synchronized with the rest of the power system generators, the speed of the generator is determined by the power system so that synchronism can be maintained. In such case, the function of the governor is to change the power output of that particular generator in accordance with the change in the system load.

Most of the governors are having droop characteristics i.e. as the load on the generator is increased from no load to full load, its speed is decreased. The decrease in speed is determined by the droop rating of the generator. If all the generators of the system have same droop characteristics, the load shared by the individual generator is according to its own rating. In the present study, all the synchronous generators are thermal. Hence the modeling of the thermal turbine and governing system are discussed.

2.5.1 Steam Turbine Model

In this turbine model, the torque required by the synchronous generator is provided by one high pressure and two low-pressure turbines. The steam from the high-pressure turbine is fed to reheat system and after reheating this steam is fed to low-pressure turbine. By controlling the opening of the control valve, the steam flow to the high-pressure turbine can be controlled. The steam flow to the low-pressure turbine is controlled through the opening/closing the intercept valve. Figure 2.10 represents the block diagram of the steam turbine.

2.5.2 Steam Governor Model

Thermal governor acts through the control valve. In case of an isolated generator, main droop r_c decides the drop in per unit speed as the load on the generator is increased from no load to full load. The intercept valve is normally kept fully open unless the maximum speed limit is reached. When the maximum speed limit is reached, the intercept valve is closed rapidly to cut-off the steam supply to low-pressure turbines. However, for small signal stability studies, the position of intercept valve is assumed to be fully open (Iv=1). Figure 2.11 represents the thermal governor model for the thermal turbine.

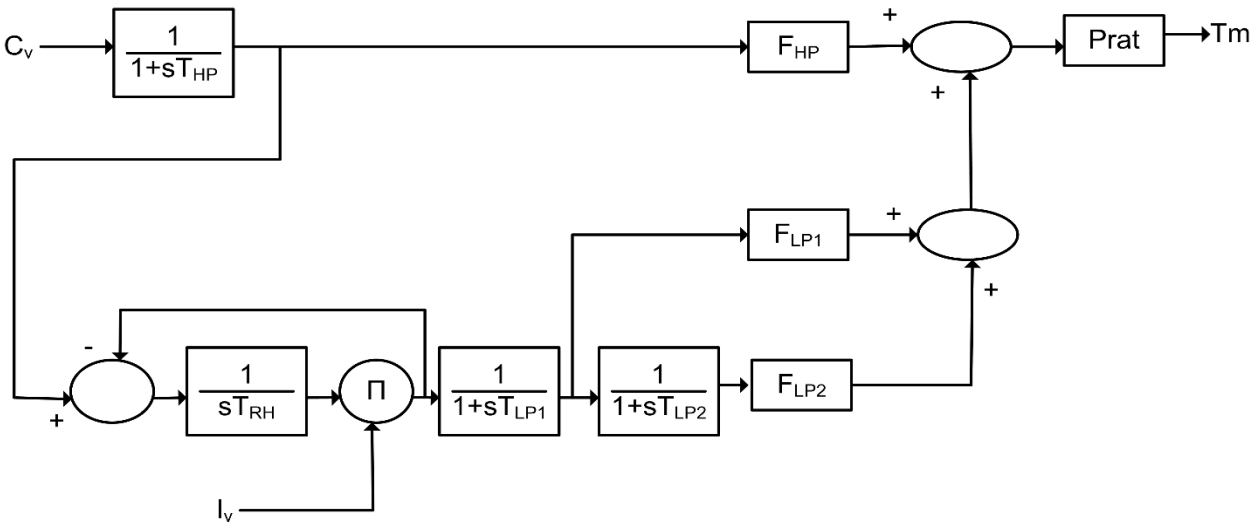

Figure 2.10 Block diagram of steam turbine

C_v	Opening of the control valve
I_v	Opening of the intercept valve
T_{HP}	Time constant of high-pressure turbine
T_{RH}	Time constant of reheat system
T_{LP1}	Time constant of first low-pressure turbine
T_{LP2}	Time constant of second low-pressure turbine
F_{HP}	Sharing of HP stage torque in final output torque
F_{LP1}	Sharing of first LP stage torque in final output torque

F_{LP2}	Sharing of second LP stage torque in final output torque
P_{rat}	Ratio of turbine rating to generator MVA rating
Tm	Output mechanical torque

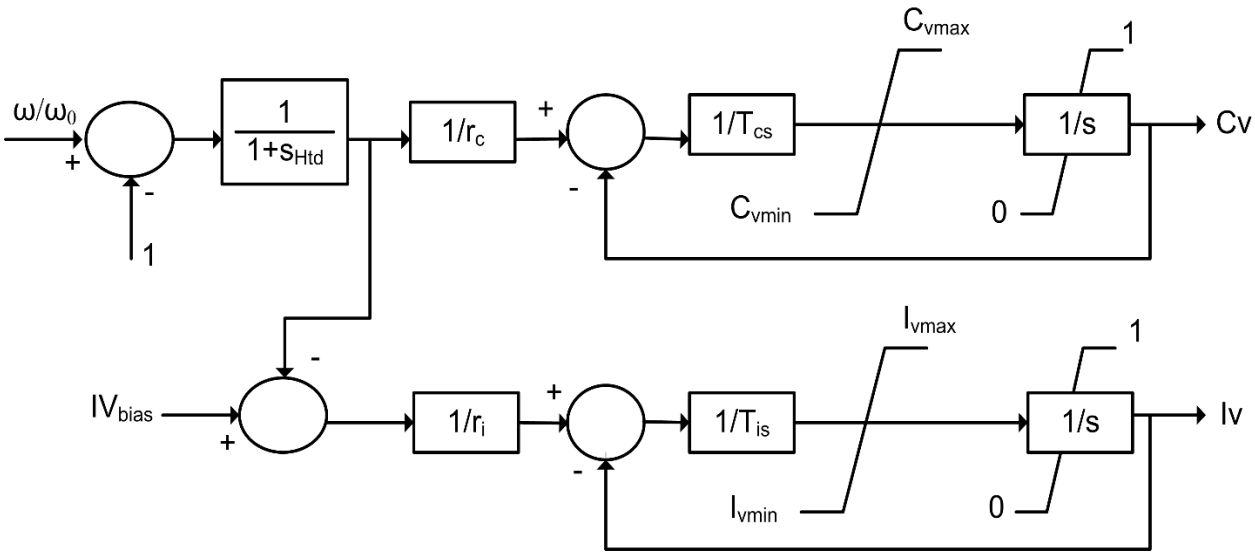

Figure 2.11 Steam governor model

r_c	Main droop
r_i	Intercept droop
T_{td}	Time constant of speed transducer
T_{cs}	Time constant of control valve servo
C_{vrmax}	Maximum opening of control valve
C_{vrmin}	Minimum opening of control valve
T_{is}	Time constant of intercept valve
P_{ref}	Reference power
i_{vrmax}	Maximum opening of intercept valve
i_{vrmin}	Minimum opening of intercept valve

2.6 Power Flow in the System

The current balance or the power balance forms are normally used to express the load flow equations in the power system. In this study power flow equations are represented in

power balance form. For the generator buses (PV buses) the algebraic equations of active and reactive power are expressed as follows [69]:

$$V_i \left(I_{qi}\cos(\delta_i - \theta_i) + I_{di}\sin(\delta_i - \theta_i)\right) + P_{Li} = \sum_{k=1}^{n} V_i V_k \left(G_{ik}\cos(\theta_i - \theta_k) + B_{ik}\sin(\theta_i - \theta_k)\right) \quad (2.15)$$

$$V_i \left(I_{di}\cos(\delta_i - \theta_i) - I_{di}\sin(\delta_i - \theta_i)\right) + Q_{Li} = \sum_{k=1}^{n} V_i V_k \left(G_{ik}\sin(\theta_i - \theta_k) + B_{ik}\cos(\theta_i - \theta_k)\right) \quad (2.16)$$

$i = 1, 2, 3, \ldots m$

m is the total number of generator buses and n is the total number of system buses. G_{ik} and B_{ik} are the conductance and susceptance between buses i and k from the node admittance matrix. For the non-generator buses (PQ buses) the active and reactive power balancing equations are [69]:

$$P_{Li} = \sum_{k=1}^{n} V_i V_k \left(G_{ik}\cos(\theta_i - \theta_k) + B_{ik}\sin(\theta_i - \theta_k)\right) \quad (2.17)$$

$$Q_{Li} = \sum_{k=1}^{n} V_i V_k \left(G_{ik}\sin(\theta_i - \theta_k) + B_{ik}\cos(\theta_i - \theta_k)\right) \quad (2.18)$$

$i = m+1, m+2 \ldots n$

P_{Li} and Q_{Li} are active and reactive loads on bus i.

2.7 Load Model

Accurate load modeling of the power system loads is an important aspect of power system dynamics and stability studies. The load modeling has critical effects on the small signal stability studies and hence it is essential to find more accurate load models than the conventionally used load models [70, 71]. Conventionally static load models are used in small signal stability studies but the idea of using the dynamic load models is also gaining momentum in last few years. Although power system load modeling has gained attention, yet it is one of the most difficult tasks to accurately represent the load models. Factors like the diversity of load components, changing load composition with a time of the day, week and seasons and uncertainties regarding characteristics of load components at the time of large voltage and frequency variations make the load modeling a difficult task. An attempt is made here to look into the various aspects of load modeling like data acquisition, load characterization, load compositions and standard load models.

2.7.1 Types of Load

The load composition of an area depends upon many factors. These may include data class, the composition of each data class and characteristic of load component. The load classes are mainly classified as industrial, agricultural, residential and commercial. The industrial load mainly comprises of the heavy motor loads (up to 90%) and heating loads. The agricultural load mainly comprises of an induction motor for pumping. The residential load comprises of lighting and mainly heating and air-conditioning during the winter and summer seasons. The commercial load mainly comprises of lighting and air-conditioning. In general, the behavior of various load component can be broadly classified into following the categories [2]:

- Loads with fast dynamic electrical and mechanical characteristics such as induction motors.
- Loads with slow dynamic electrical characteristics such as electric heating.
- Loads which are highly sensitive to under voltage such as lighting and motor.
- Loads which are insensitive to voltage variations such as incandescent lighting.

An overview of some of the important load components is as follow:

Induction motors: Induction motors are extensively used in residential, agricultural and industrial applications. In residential applications, it is mainly used for water pumping and for driving compressors of air-conditioners and refrigerators. In agricultural applications, it is mainly used for water pumping. In industrial applications, it is mainly used for driving pumps, fans, and compressors. Almost 65-70 % of total electrical energy consumption in power system is by induction motors. Hence, its dynamic characteristics are very important in small signal stability studies.

Lighting: For industrial and street lighting purposes sodium vapor, mercury vapor and compact fluorescent lamps are mainly used. Both the sodium vapor and mercury vapor lamps are much sensitive to voltage variations and their luminous output reduces significantly when the supply voltage is below 80%. Fluorescent lamps are mainly used in commercial and residential applications for lighting purposes due to its low power consumption and high luminous output.

Heating loads: In residential applications, thermal load comprises mainly for heating, electric oven, and water heating purposes while in industrial applications it mainly comprises of heating, welding and molding purposes. This kind of load behaves as constant resistance. During the low voltage situations in power system, the thermostat continuously works in 'on cycle' and hence the device behaves like a constant power load.

2.7.2 Acquisition of Data for Load Modeling

To obtain the data for composite load modeling, following approaches are used [2]:

Measurement-based approach: In this approach, the sensitivity of load to voltage and frequency is determined by direct measurement of active and reactive power at various feeders, substations etc. The data regarding the change in active and reactive power due to the change in voltage and frequency is obtained from the field measurements for various inherent system disturbances, natural system operations, and intentional system disturbances. By adjusting the field data into assumed load model, the parameters of the load models are identified. However, this technique is comparatively straightforward for static load models compared to dynamic load models. Due to the availability of the actual field measurements, this method offers the advantage of tracking the change in load parameters due to seasonal changes and behavior of the system under normal operations and for various system disturbances. However, the involvement of capital cost for measurements and monitoring of the field equipment is restricting factor for the application of this approach.

Component-based approach: In this approach, the load supplied at the distribution point is classified into several classes of load categories like industrial, commercial, agricultural, residential, air-conditioning, heating load etc. The composite load model is developed from the information on its constituent parts i.e. a mix of the classes at the substation and characteristics of each single load component. The advantage of this approach is that it does not require any field measurements. Also, it offers adaptability to different system and conditions. However, load composition varies from bus to bus and it depends upon the weather. Hence, it is necessary to update the load composition data at each bus of the system.

2.7.3 Load Composition

The load composition is largely driven by various factors like time of the day, month and seasons. In cold countries during the winter season, electric heating comprises the highest share in electrical energy consumption while in summer in these countries the air-conditioning system has little share in total electrical energy consumption. In case of warmer countries, the situations are exact opposites. Also during the working days, industrial and commercial utilities have a major share of electrical energy consumption while it changes extensively during the weekends.

2.7.4 Standard Load Models

The model of a system is represented by a set of equations relating its input to its output. Mathematical load modeling represents the measured voltage and/or frequency at a bus to the active and reactive power drawn by the load. Due to diversity in types of load, it is very difficult to represent the load model. Several attempts were made to represent the load model depending upon the purpose for which the modeling is used.

Mainly the load models are classified into two categories: Static load model and dynamic load model. The static load model does not depend upon time and hence it represents the active and reactive power drawn by the load at any time with the instantaneous value of voltage/frequency at that time. In case of dynamic load models, the active and reactive power drawn by the load depends upon the voltage/frequency at past time and normally including the present time. In most of the earlier studies, static load models were used to represent both static and dynamic load models. The dynamic load models were approximated to represents it as static loads. However, in small signal stability studies, this approximation may result in the under/overestimation of the damping capability of the design controllers [71]. The brief description of the static and dynamic load models is as follow:

Static load models: In this model, the static characteristics of various loads are divided as constant power, constant current and constant impedance type of load depending upon the relation between the power and voltage of the particulate type of load. For constant impedance load, the relation between power and voltage is quadratic. For constant current load, the relation between power and voltage is linear and for constant

power load, the power drawn by the load is independent of the voltage magnitude. This power and voltage relationship between various types of load can be mathematically expressed by equation (2.19) and equation (2.20). This load model is popularly known ZIP load model/ Polynomial load model. The equations are as follows [2]:

$$P = P_0\left[x1\left(\frac{V}{V_0}\right)^2 + x2\left(\frac{V}{V_0}\right) + x3\right] \tag{2.19}$$

$$Q = Q_0\left[y1\left(\frac{V}{V_0}\right)^2 + y2\left(\frac{V}{V_0}\right) + y3\right] \tag{2.20}$$

The first term of both the equations represents the proportion of constant impedance load, the second term represents constant current load and the third term represents constant power load. The constants *x1* to *x3* and *y1* to *y3* represent the proportion of each type of load. Also *x1+x2+x3 = y1+y2+y3 =1*.

Dynamic load models: When the conventional static load models are inefficient to represent the behavior of the load, dynamic load models are necessary. The parameters of the load model can be determined either by the field measurement based approach or by component-based approach model, first by analyzing the characteristics of the load and by combining them to represents a single load.

In a practical power system, the load is neither pure constant impedance type nor pure constant power type but a mixture of all three kinds. Apart from static loads, power system also comprises of a considerable amount of dynamic loads. Induction motors at various load buses are considered as dynamic loads. Considering these facts, different load models are considered in this study to check the robustness of the designed controller for worst-case load composition scenarios.

2.8 Models of FACTS devices

There are various types of FACTS devices developed over the years for controlling the important parameters of the transmission networks. The devices used in this study are SVC, TCSC, STATCOM, and UPFC. The modeling of the FACTS devices consists of

small signal dynamics of the device itself and its influence on the power flow in the network.

2.8.1 Static Var Compensator (SVC) Model

The main function of SVC in power system is to maintain a bus voltage to which it is connected by injecting controlled capacitive or inductive reactive power [72]. The most popular configuration of SVC is the FC-TCR as shown in Figure 2.12. The FC –TCR is basically a parallel combination of fixed capacitor and Thyristor Controlled Reactor. To reduce the voltage ratings of the device, normally coupling transformer is used to connect the device to the high voltage system. The coupling transformer steps down transformer. The TCR absorbs the reactive power while FC supplies the reactive power to the system. The rating of TCR is more than that of FC so that the capacitive reactive power can be compensated when the system voltages are within the permissible limit.

The fixed capacitor banks are usually connected in a star configuration and split into more than one three-phase group. A small inductor is connected in series with the capacitor so as to form a tuned filter to filter out specific order harmonic. The net susceptance of FC-TCR SVC is given by

$$B_{SVC} = \frac{B_\sigma (B_C + B_{TCR})}{B_\sigma + B_C + B_{TCR}} \tag{2.21}$$

where B_C is the susceptance of the capacitors, B_{TCR} is the susceptance of the TCR and B_σ is the susceptance of the transformer.

Even if the system voltages are normal, to compensate the reactive power output of the Fixed Capacitors, TCR needs to be operated simultaneously to compensate the reactive power output of the capacitors. This results in large steady-state losses of the order of 0.5% to 0.7% of the MVA rating. This drawback can be overcome by replacing the Fixed Capacitors by Thyristor Switched Capacitors (TSC) resulting in the new device TSC-TCR as shown in Figure 2.13. This device usually consists of ‘n’ TSC banks and a single TCR connected in parallel. The rating of the TCR is normally (1/n) of the total SVC rating.

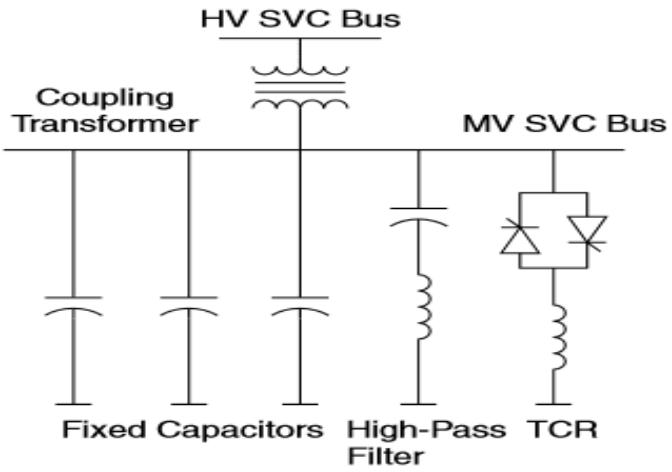

Figure 2.12 FC-TCR SVC [19]

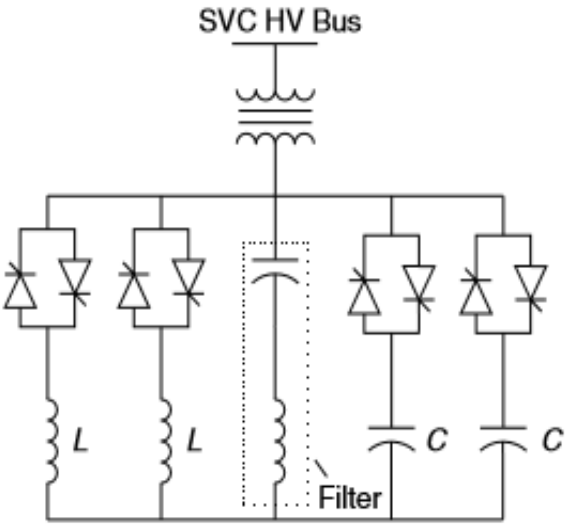

Figure 2.13 TSC-TCR SVC [19]

The TSC operates in discrete steps whereas the continuous control in each step is achieved with the help of TCR. The main advantages offered by the TSC-TCR are flexibility in the operation of the device and reduction in the steady-state losses. The basic SVC structure with voltage control is as shown in Figure 2.14. The comparator compares the reference voltage and the actual voltage of the system and generates an error signal which is fed to the controller. Depending upon the magnitude of the error signal, firing angles of the anti-parallel connected Thyristors are decided and Thyristors are fired accordingly to maintain system voltages to the desired value.

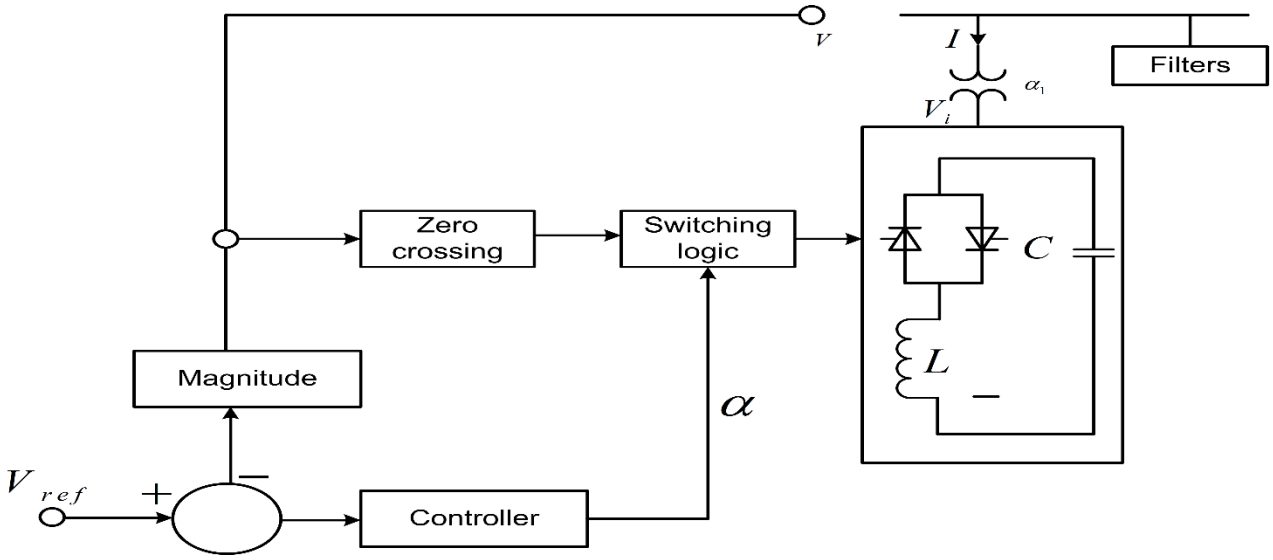

Figure 2.14 Basic SVC structure with voltage control [1]

By appropriate control of the firing angle of the Thyristors, the SVC can be operated either to supply the reactive power or to absorb the reactive power from the power system. Figure 2.15 shows typical steady state voltage control characteristic of SVC.

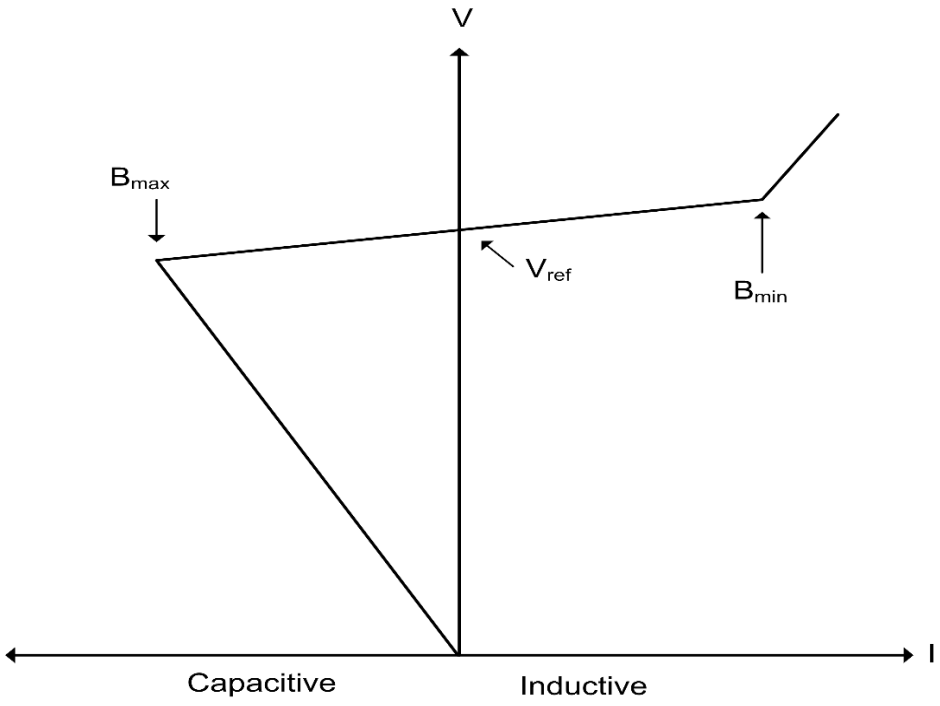

Figure 2.15 Steady-state voltage control characteristic of SVC [19]

In small signal modeling of SVC, it is represented as variable reactance with maximum capacitive and inductive limits which correspondence to firing angle of Thyristors. In steady state conditions, SVC is used for voltage control while for damping of oscillations its reactance is varied as per requirement as shown in Figure 2.16 by SVC-sig [73].

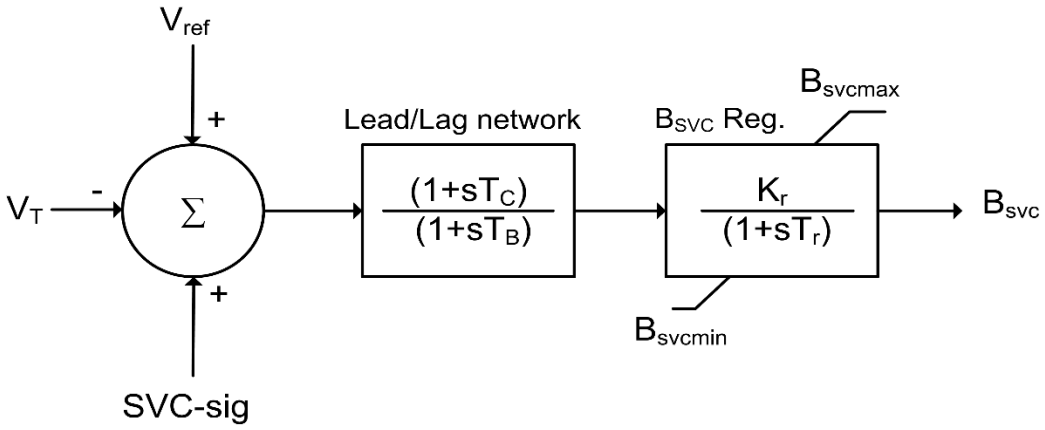

Figure 2.16 Small-signal modeling of SVC [73]

B_{svcmx}	Maximum output susceptance of SVC
B_{svcmn}	Minimum output susceptance of SVC
T_c	Lead time constant
T_b	Lag time constant
K_r	Regulator gain
T_r	Regulator time constant

2.8.2 Thyristor Controlled Series Capacitor (TCSC) Model

The basic TCSC module consists of a Fixed Capacitor in parallel with Thyristor Controlled Reactor as shown in Figure 2.17. The device operates as a variable inductor or capacitor by changing the firing angle of the Thyristors in TCR. In most of the configurations, TCSC is operated in a capacitive mode to reduce the reactance of the transmission line in which it is connected. By reducing the net inductive reactance of the transmission line, it increases the steady state power transfer capability of the transmission network.

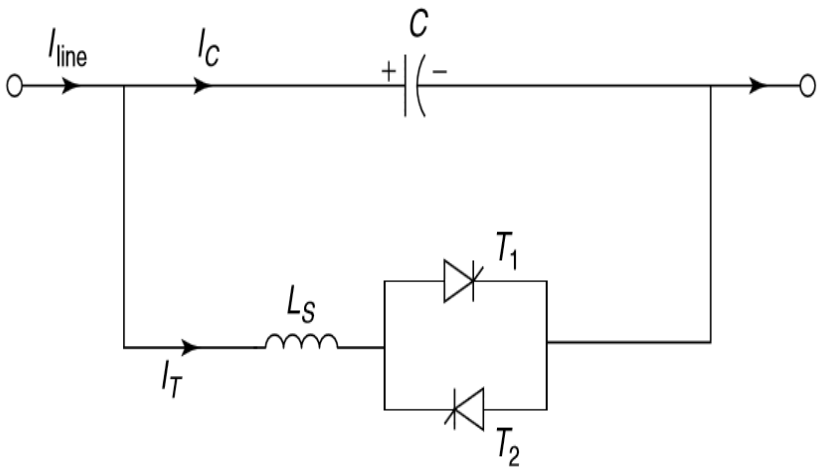

Figure 2.17 Basic TCSC Module [19]

The firing angle α of the Thyristors decides the reactance of TCSC module. The variation of TCSC reactance with firing angle α is as shown in Figure 2.18. At some particular value of firing angle α, the reactance of the parallel connected fixed capacitor and Thyristor Controlled Reactor becomes equal and the TCSC module acts as an open circuit. The operation of the TCSC module in this firing angle range is avoided by inserting limiters in the firing circuit.

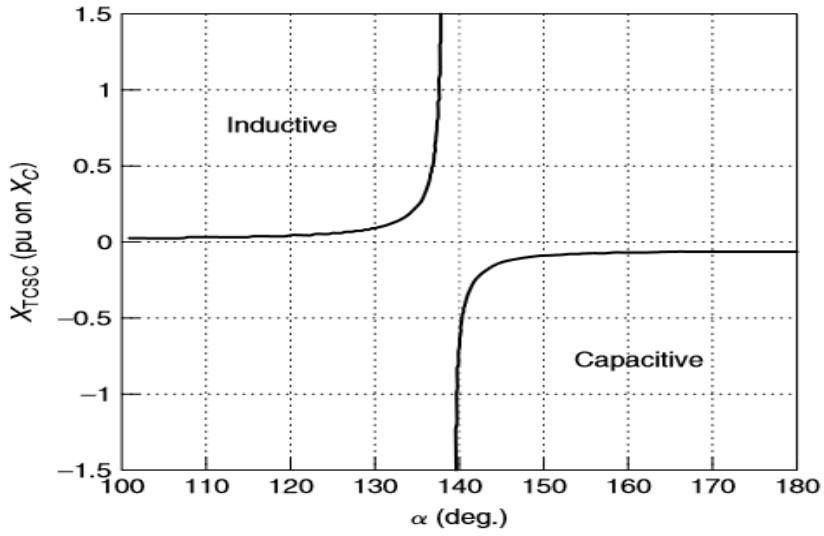

Figure 2.18 Variation of the TCSC reactance with firing angle α [19]

The capability characteristics of TCSC is as shown in Figure 2.19. These capability characteristics are drawn for continuous time operation, short duration operation (30

minutes) and for 1-10 second operation. In both capacitive and inductive zone, the operation is normally between the maximum and minimum reactance limits.

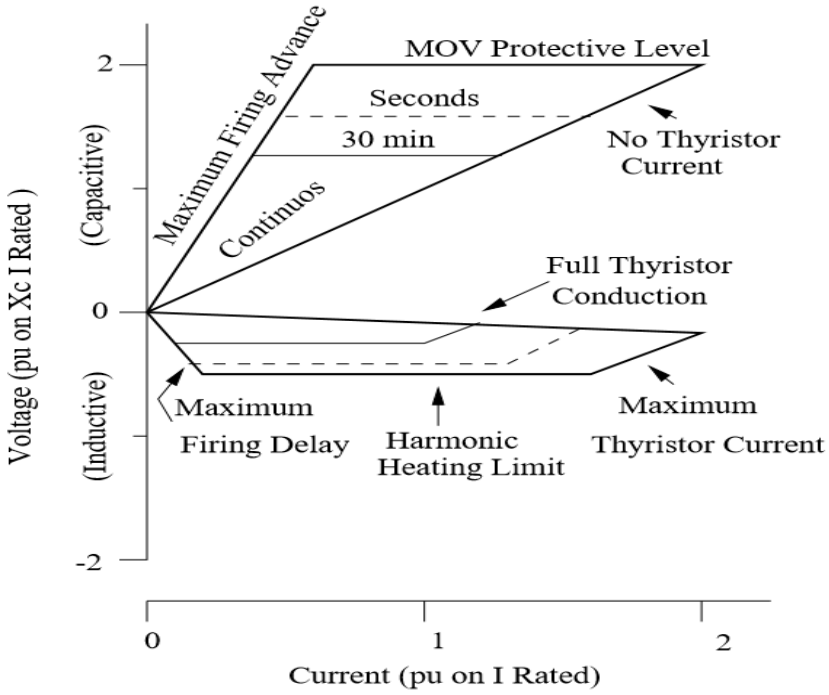

Figure 2.19 V-I capability characteristics of TCSC [19]

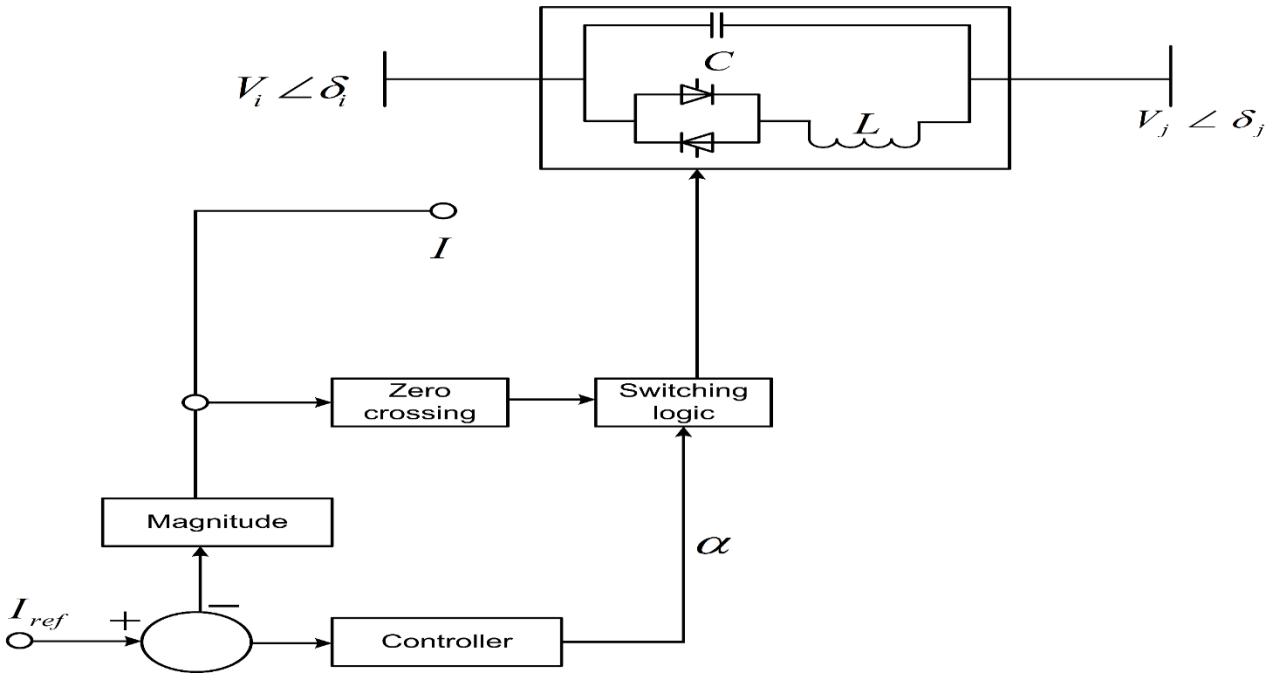

Figure 2.20 Basic TCSC structure with current control

TCSC can be controlled through various control strategies like voltage control, current control and reactance control. The current control strategy is extensively used in field applications. The basic TCSC structure with current control is as shown in Figure 2.20. As discussed in section 2.8.1, the firing angle of the Thyristors is decided by the error signal obtained by comparing the reference value and actual value of current I.

The small signal modeling TCSC involves a lead/lag network followed by a susceptance regulator. The small signal modeling of TCSC is as shown in Figure 2.21.

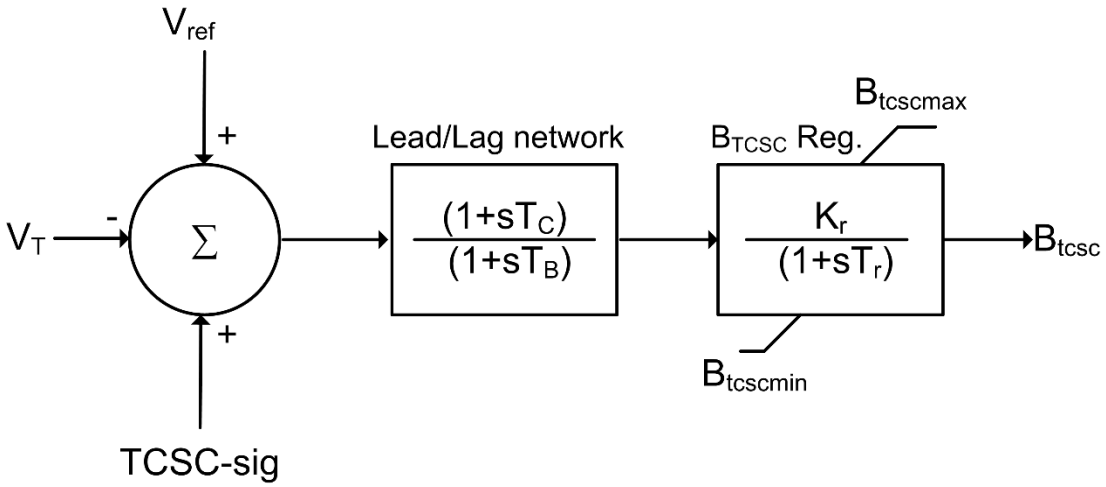

Figure 2.21 Small-signal modeling of TCSC [73]

B_{tcscmx}	Maximum output susceptance of TCSC
B_{tcscmn}	Minimum output susceptance of TCSC
T_c	Lead time constant
T_b	Lag time constant
K_r	Regulator gain
T_r	Regulator time constant

2.8.3 Unified Power Flow Controller (UPFC) /STATCOM/SSSC Model

UPFC is one of the most powerful FACTS devices which can perform the functions of voltage regulations, series compensation, and phase shift. The basic structure of UPFC is shown in Figure 2.22. The UPFC can independently control active and reactive power

simultaneously. It consists of two voltage source converters connected back to back and operated from a common DC link provided by a DC storage capacitor [1]. Due to this arrangement, the UPFC can generate/absorb active/reactive power at its ac terminals. Capacitor bank supplies DC voltages to both converters necessary for their operation. The series converter injects voltage V_{pq} in series with the transmission line. The shunt converter is used mainly to supply the active power demand of converter 2 which it draws from transmission line itself. Also, it maintains a constant voltage at DC common link. The shunt converter regulates the voltage at the connecting bus by supplying/absorbing the reactive power and hence functions as a Static Compensator (STATCOM) while the series converter acts as Static Synchronous Series Capacitor (SSSC). In this study, UPFC can be operated for voltage control, series active power control and series reactive power control. The dynamic modeling blocks for the same are shown in Figure 2.23-Figure 2.26 [73].

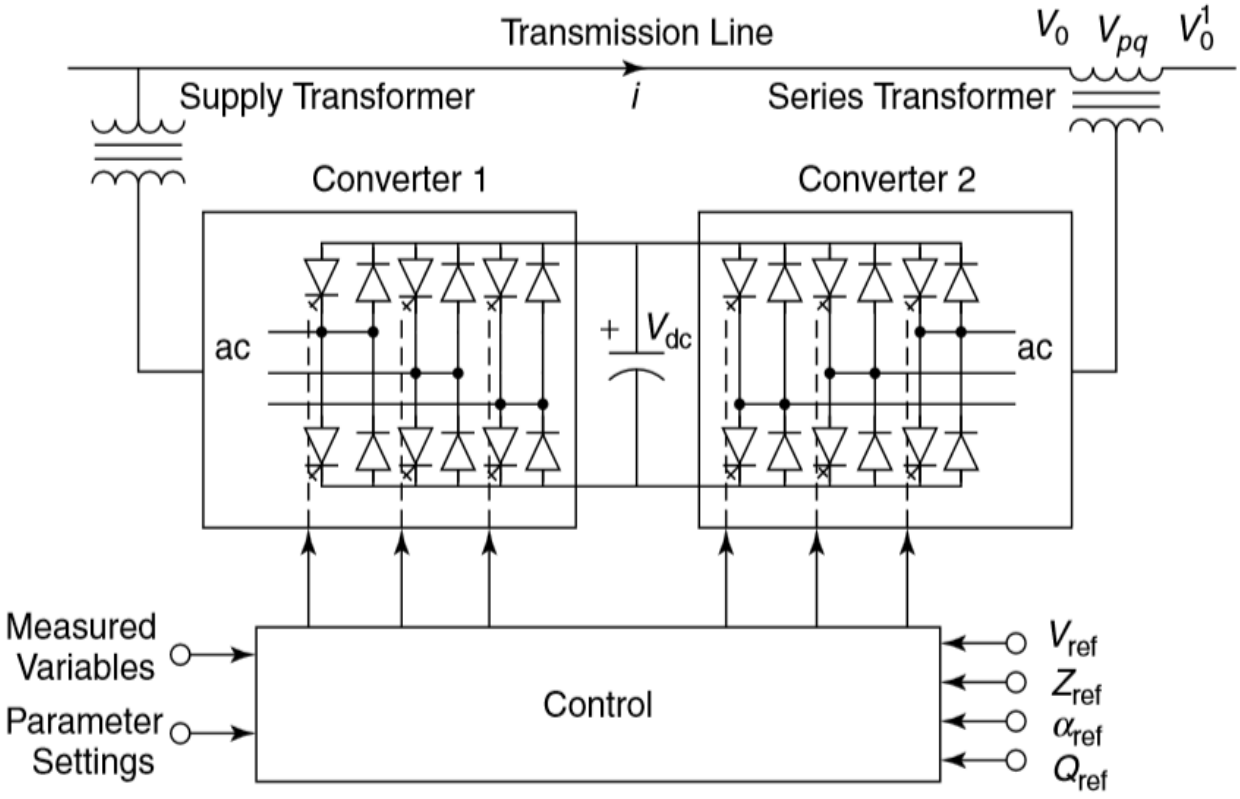

Figure 2.22 Basic UPFC structure [19]

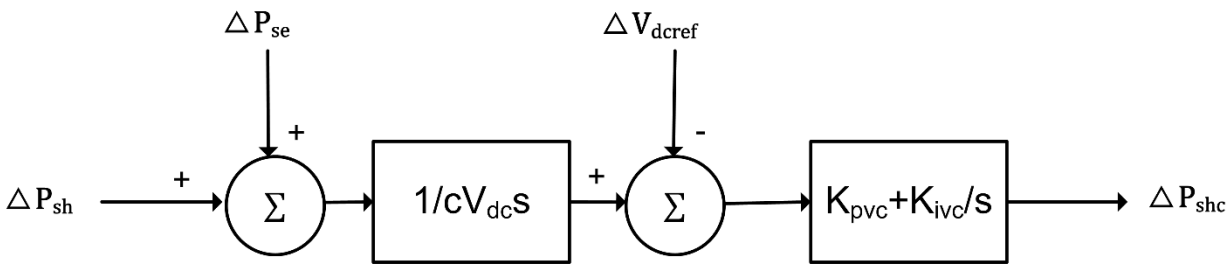

Figure 2.23 Common converter DC Voltage control of UPFC

By providing the bus voltage magnitude as an input signal, the same UPFC device can be operated as Static Compensators (STATCOM) [73] and by providing series active power as input signal UPFC can be operated as Static Synchronous Series Compensators (SSSC) [73].

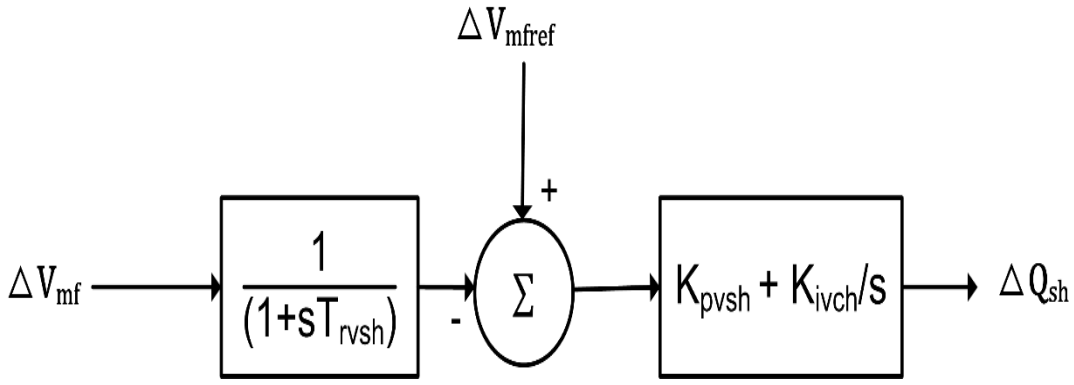

Figure 2.24 Bus Voltage magnitude control of UPFC (STATCOM)

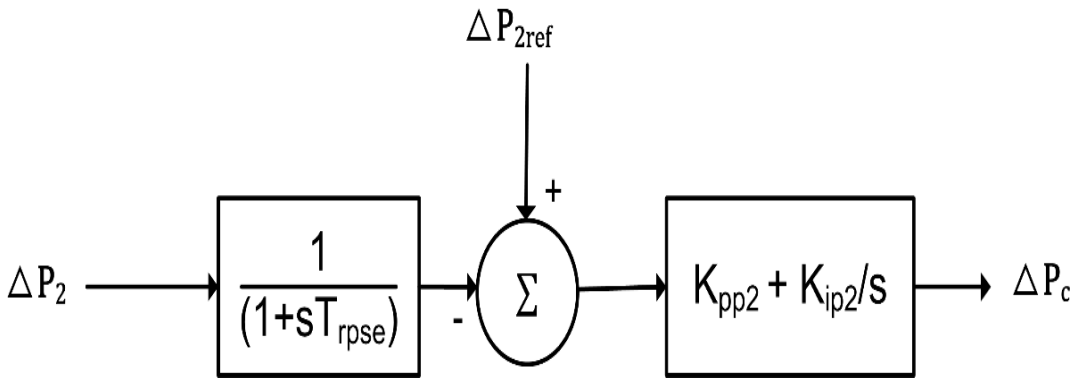

Figure 2.25 Series active power control of UPFC (SSSC)

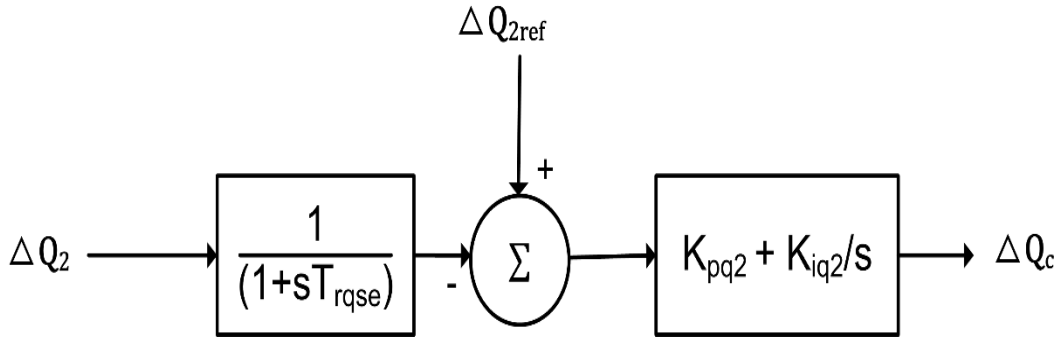

Figure 2.26 Series reactive power control of UPFC

2.9 Linearized State Space Model of Power System

The dynamic behavior of the power system can be represented by a set of *n* first order nonlinear differential equations of the following form [2]:

$$\dot{x_d} = f(x_d, x_a, u) \tag{2.22}$$

$$0 = g(x_d, x_a, u) \tag{2.23}$$

$$y = h(x_d, x_a, u) \tag{2.24}$$

where, x_d is a vector of state variables which includes variables of generators, exciters and PSSs and FACTS devices, x_a is a vector of algebraic variables, u is a vector of input variables and y is a vector of output variables. Equation (2.22) describes the dynamics of the power system, equation (2.23) describes the power flow equations and the equation (2.24) describes the output variable in terms of input variables and state variables. In small signal stability studies, the dynamic characteristics of the system are interpreted around an equilibrium point with a nonlinear model linearized around the equilibrium point. When subjected to a disturbance, the equilibrium point changes. The validation of the linearized model depends upon the response of the linearized model to the disturbance. If the disturbance is very small, the resulting response can be linearized for analytical purposes and hence, the model is valid and vice versa. Let the equilibrium point of the system is (x_d^0, x_a^0, y^0, u^0), then the small deviations from the linearized point are:

$$\Delta x_d = x_d - x_d^0 \tag{2.25}$$

$$\Delta x_a = x_a - x_a^0 \tag{2.26}$$

$$\Delta y = y - y^0 \quad (2.27)$$

$$\Delta u = u - u^0 \quad (2.28)$$

The partial differentiation of nonlinear functions *f, g* and *h* yields the linear Differential Algebraic Equations (DAE) model which is as follows:

$$\Delta \dot{x_d} = A_1 \Delta x_d + A_2 \Delta x_a + B_1 \Delta u \quad (2.29)$$

$$0 = A_3 \Delta x_d + A_4 \Delta x_a + B_2 \Delta u \quad (2.30)$$

$$y = C_1 \Delta x_d + C_2 \Delta x_a + D_1 \Delta u \quad (2.31)$$

Where the Jacobian matrices are:

$$A_1 = \left[\frac{\partial f}{\partial x_d}\right], A_2 = \left[\frac{\partial f}{\partial x_a}\right], A_3 = \left[\frac{\partial g}{\partial x_d}\right], A_4 = \left[\frac{\partial g}{\partial x_a}\right] \quad (2.32)$$

$$B_1 = \left[\frac{\partial f}{\partial u}\right], B_2 = \left[\frac{\partial g}{\partial u}\right] \quad (2.33)$$

$$C_1 = \left[\frac{\partial h}{\partial x_d}\right], C_2 = \left[\frac{\partial h}{\partial x_a}\right] \quad (2.34)$$

$$D_1 = \left[\frac{\partial h}{\partial u}\right] \quad (2.35)$$

Assuming A_4 is invertible, the algebraic variables can be determined from

$$x_a = -A_4^{-1}(A_3 \Delta x_d + B_2 \Delta u) \quad (2.36)$$

Thus the algebraic variables can be eliminated. The conventional form of the linearized state-space model of the power system can be achieved by eliminating the algebraic variables. This form can be represented by following Ordinary Differential Equation (ODE).

$$\dot{x} = Ax + Bu \quad (2.37)$$

$$y = Cx + Du \quad (2.38)$$

Where, *x* is the vector of state variables, *y* is the vector of output variables and *u* is the vector of input variables. *A* is state matrix or plant matrix, *B* is input matrix, *C* is output matrix and *D* is feedforward matrix. These matrices are given by:

$$A = A_1 - A_2 A_4^{-1} A_3 \quad (2.39)$$

$$B = B_1 - A_2 A_4^{-1} B_2 \quad (2.40)$$

$$C = C_1 - C_2 A_4^{-1} A_3 \quad (2.41)$$

$$D = D_1 - C_2 A_4^{-1} B_2 \quad (2.42)$$

The above state space matrices can also be represented by the frequency domain methods based on transfer functions. Equation 2.37 and 2.38 alternatively can be represented in the frequency domain by corresponding transfer function by:

$$G(s) = \frac{Y(s)}{U(s)} = \mathrm{C}\,(\mathrm{sI} - \mathrm{A})^{-1}B + D \quad (2.43)$$

where *s* is the Laplace operator. As the transfer function is the ratio of input to output, it is very acceptable method when a model is based on measurements.

2.10 Modal Analysis and Small Signal Stability

After achieving the state space matrices of the system matrices by solving equations (2.39-2.42), the dynamic characteristics of the system can be derived and analyzed. The eigenvalues λ_i of the dynamic system are non-trivial solutions of the equation (2.44), where *A* is the state matrix.

$$A\,\phi = \lambda\,\phi \quad (2.44)$$

where ϕ is *n×1* vector. λ can be derived by readjusting the equation (2.44).

$$\det(A - \lambda\, I) = 0 \quad (2.45)$$

The solution of equation (2.45) are the eigenvalues of the *n×n* matrix A. Conventionally, the eigenvalues are of the form $\sigma \pm j\omega$. The eigenvalues decide whether the operating point is stable or not. If the real part of the eigenvalues exists on the left side of the imaginary axis of the complex plane, the system is stable and when it exists on the right side, the system is unstable. The stability is confirmed by looking at the time-dependent characteristics of the oscillatory mode corresponding to each eigenvalue λ_i given by $e^{t\lambda i}$. Real eigenvalue corresponds to non-oscillatory mode. If the real eigenvalue is negative, the mode decays over time. The magnitude is related to the time of decay, larger the magnitude quicker the decay. If the real eigenvalue is positive, the mode is said to have aperiodic instability.

The conjugate pair of complex eigenvalues ($\pm j\omega$) represents an oscillatory mode. A pair with a positive σ represents an unstable oscillatory mode since the time response of this eigenvalues is of increasing magnitude and represents the unstable system. A pair with a negative σ indicates stable oscillatory mode. The time response of the system is dominated by the dominant modes which basically represents poorly damped or unstable modes. The locations of the eigenvalues on the left-hand side of the imaginary axis ensure the stale operation of the system. From eigenvalues, two important characteristics of the states are derived from the following equations:

$$f = \frac{\omega}{2\pi} \quad (2.46)$$

$$\delta = \frac{\sigma}{\sqrt{\sigma^2 + \omega^2}} \quad (2.47)$$

where *f* is the frequency of oscillation (Hz) and δ is the damping ratio.

The dynamics of the linear system can be expressed as a collection of modes. Activity pattern of the system state, frequency and damping ratio are the essential features of the mode. The modes with poor damping ratio can be considered as undamped oscillations. The mode concept is based on a change of coordinates by diagonalization. The intension is to decouple the complex relation with an adequate choice of coordinates as executed in many engineering areas.

With the square right modal matrix ϕ, the matrix A can be arranged as:

$$\phi^{-1} A \, \phi = \Lambda \tag{2.48}$$

The right eigenvectors are the columns of ϕ. Eigenvalues are the diagonal elements of matrix Λ. Similarly, the left eigenvectors are the rows of modal matrix ψ given by:

$$\psi^{-1} A \, \psi = \Lambda \tag{2.49}$$

From equation (2.48) and equation (2.49), ψ is the inverse of ϕ. However, if any eigenvalue of the system is zero, ϕ cannot be inverted. The product of ψ_i and ϕ_i in such cases is zero. However, in practice instead of zero value, a small value of eigenvalues are taken to avoid ill-conditioning of the matrix. Provided that ψ and ϕ are available, the ODE system can be transformed into modal coordinates *z* through a transformation $x = \phi z$.

$$\dot{z} = \Lambda \mathrm{z} + \psi \mathrm{Bu} \tag{2.50}$$

$$y = C\phi z + Du \tag{2.51}$$

The equations (2.50) and (2.51) represents the uncoupled first order differential equations. This equations which are known as the modes govern the dynamics after transformation. After decoupling the state equations through equations (2.50) and (2.51), the behavior of particular oscillatory mode can be derived through mode shape. Mode shape is the response of a particular state variable, say Δx_k, examined in each i^{th} mode in the right eigenvector ϕ. Occasionally the importance of the dynamic state to the particular modes needs to be quantified i.e. expressed mathematically. This is achieved by calculating the participation factors [74]. Participation matrix provides a relation between the state variables and the oscillatory modes. It is defined as:

$$P = [p_1 \quad p_2 \quad p_3 \quad \ldots\ldots \quad p_n] \tag{2.52}$$

$$p_i = \begin{bmatrix} p_{1i} \\ : \\ p_{ni} \end{bmatrix} = \begin{bmatrix} \phi_{1i}\psi_{i1} \\ : \\ \phi_{ni}\psi_{in} \end{bmatrix} \tag{2.53}$$

The element $p_{ki} = \phi_{ki}\,\psi_{ik}$ is called the participation factor and gives a measure of the participation of the *k*th state variable in the i^{th} mode [75].

The controllability of mode k from the i^{th} input is given by:

$$cont_{ki} = \psi_k B_i \tag{2.54}$$

The observability of mode *k* from the j^{th} output is given by:

$$obs_{kj} = C_j B \phi_k \tag{2.55}$$

The *D* matrix described in (2.43) is usually a zero matrix. Thus, equation (2.43) can be modified as follows:

$$G(s) = \frac{Y(s)}{U(s)} = \mathrm{C}\,(\mathrm{sI} - \mathrm{A})^{-1} B \tag{2.56}$$

G(s) can be expanded in partial fraction as:

$$G(s) = \frac{Y(s)}{U(s)} = \sum_{k=1}^{n} \frac{R_k}{s-\lambda_k} \tag{2.57}$$

where R_k is the residue of the *G(s)* at eigenvalue λ_k mode *k*.

Combining equations (2.56) and (2.57) and expanding it in the partial fraction form yields the following result:

$$G(s) = \sum_{k=1}^{n} \frac{R_k}{s-\lambda_k} = \sum_{k=1}^{n} \frac{C\phi(:,k)\psi(k,:)B}{(s-\lambda_k)} \tag{2.58}$$

Equations (2.58) gives the relation between input and output matrices and left and right eigenvectors. The participation of any particular mode in the system dynamics can be derived from residue analysis. Also, from equation (2.58) it clear that the residue R_k is the product of mode's observability and controllability [76] and can be expressed mathematically as:

$$R_k = C\phi_k\psi_k B \tag{2.59}$$

2.11 Summary

This chapter presented the small signal modeling of various components of the power system. The dynamic behavior of the power system was considered at electromechanical transient level. The system dynamics were represented by differential and algebraic equations. Redundant variables were removed by replacing linearized algebraic equations into differential equations. The system small signal dynamics were represented in state space form. This representation can further be utilized for designing the necessary controllers in the next chapters.

CHAPTER 3 DESIGN OF WIDE AREA DAMPING CONTROLLER

3.1 Introduction

This chapter describes the general procedure for designing the wide area measurement based damping controller. This procedure mainly involves various steps like forming the linearized model of the test system, selection of suitable global signal for the controller, small signal analysis of the linearized model, model order reduction, selection of proper weights and controller synthesis. For controller synthesis, the theory of robust control techniques like standard H_∞ optimization, mixed H_2/H_∞ output feedback control, LMI approach to H_∞ control with a pole-placement objective and LMI approach to H_∞ loop shaping techniques for the linear model are discussed. The basic structure of wide area measurements is also discussed. Robust control toolbox in MATLAB is used for designing the controller [77].

3.2 General Procedure for Designing the WAM based Damping Controller

The design of wide area measurements based damping controller for inter-area oscillation damping normally comprises of following steps:

1) Modeling of the test system: The first step in the design is to achieve the full order nonlinear model of the given test system. This model consists of all components of power system i.e. synchronous generators, thermal turbines, exciters, PSSs, FACTS devices and the loads. The static and dynamic behavior of all these devices is represented by a set of algebraic and differential equations as per the modeling of these devices discussed in chapter 2. The nonlinear model of the test system is prepared with the help of [73].
2) Modal analysis of the test system: To evaluate the small signal stability of the test system, the nonlinearized model of the test system obtained in step 1 must be linearized around an equilibrium point. Normally, a stressed loading condition in which there is a large amount of exchange of power through tie-line between geographically separated areas are chosen as equilibrium point and the controller is designed for that operating condition. From the linearized model of the test

system, various state-space matrices are derived. Eigenvalues and eigenvectors are calculated from state matrix A. The information regarding the frequency of various modes, the damping ratio of various modes and mode shapes can be derived from the eigenvalues and eigenvectors [2]. Poorly damped local and inter-area modes are identified for further action. Mode shape shows oscillations of generator/s or area/s against the other generator/s or area/s of the test system.

3) Selection of location of FACTS device and the input signal to the FACTS controllers: To decide the location of the FACTS device and input signal to the FACTS controllers, controllability/observability analysis of the power system model is carried out [78]. The controllability refers to the ability of the actuator to control the states of the dynamic system while observability refers to the sensor's ability to observe the states of the system. Both the controllability and observability are important criteria while designing the controller because the behavior of the system mode cannot be modified unless it is both controllable and observable. However, the primary purpose of the FACTS devices in the power system is to facilitate the control of various power system parameters and to overcome the specifically designated limitation of the given power network. This fixes the location of the FACTS device in the given power networks. For input signal to the FACTS controller, observability analysis needs to be carried out. The possible candidates are bus voltage, line current, line power and rotor angle etc. However, care should be taken that the input signal can be easily available and highly observable in the critical inter-area modes. Residue analysis is carried out to decide the best suitable signal as input to the controller.
4) Model order reduction: The H_∞ and other modern linear control techniques result in the controller of the order of at least the plant order or normally higher considering the inclusion of weights [79, 80]. A large size system has usually few hundred states. To design such large size controller is neither practical nor necessary. Also, the design of such a large order controller results in tremendous computational efforts. Thus for simplification of the design procedure, model order reduction is required. The reduced order plant must closely approximate the original full order plant. Schur balanced model reduction procedure is used for reducing the order of the plant using robust control toolbox in MATLAB [77].

5) Controller synthesis: The mixed sensitivity based Linear Matrix Inequality (LMI) approach using H_∞ control technique is used to design the various FACTS controllers. LMI approach is further extended to H_∞ loop shaping technique for damping inter-area oscillations. Various design requirements like robustness in the performance, faster transient response etc. must be met by the designed controller.
6) Evaluation of robust performance and verification of nonlinear time-domain simulation: The designed controller must be able to provide sufficient damping to inter-area mode oscillations at various operating points. For various contingency conditions occur in power system like transient fault, line outage, load shedding etc., the performance of the designed controller is assessed via nonlinear time domain simulations. The designed controller must able to provide necessary damping in such contingency conditions.

3.3 Basic Structure of Wide Area Measurements

In general, the designed controller has two possible structure: centralized and decentralized. The decentralized structure is based on local measurements and hence, the need for communication equipment is eliminated but sometimes interarea modes are not properly observable in the local measurements and hence its effectiveness for damping the interarea mode is doubtful. On the contrary, the centralized approach uses the PMU based measurements which involves comparatively higher cost but it is more effective in damping the interarea mode as large system dynamic data is available and hence interarea modes are more observable. The remote signal in which interarea mode are more observable is found more effective for damping interarea modes [25, 40, 55].

In a large practical power system, the numbers of critical inter-area mode oscillations are more and they may act together endangering the stability of power networks. Hence coordinated approach of various FACTS devices along with wide area measurements through phasor measurement units (PMUs) is necessary for the stable and secure operations of power system [44]. Recent advances in wide area measurement technologies using PMUs can deliver a control signal at a high speed. The PMUs are located strategically in the multi-machine system and captures a real-time picture of given power networks. The PMUs measure positive sequence currents and voltages in different

areas of the grid and can deliver as frequently as once per cycle of power frequency. The latest PMUs are incorporated with Global Positioning System technology which ensures proper time synchronization of global signals [30].

The basic structure of wide area measurements system is as shown in Figure 3.1. The wide area damping framework includes wide area measurements, control devices, wide area damping controllers and power system. Global signals from the geographically separated areas of the power system are collected through phasor measurement units which is a part of wide area measurements.

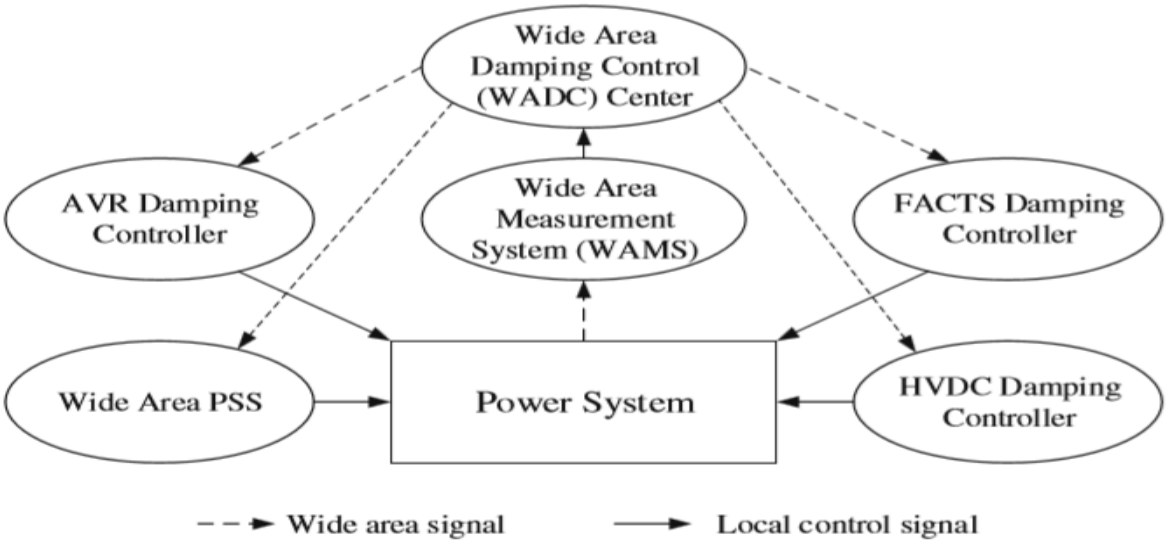

Figure 3.1 Basic structure of wide area measurements using FACTS controller [59]

These variables are processed and sent to the wide area damping control center (WADC). The WADC center selects the suitable control signals and sends these feedback control signals to local control devices through the centralized wide-area damping controller. The local devices, such as AVR, PSSs, FACTS devices and HVDC, receives these feedback signals and actuate the separate supplementary damping control. The WADC plays an important role mainly in the selection of global input signals and generation of wide area output signals.

3.4 Robust Controller Design based on H_∞ Technique

3.4.1 Introduction

The FACTS devices damp the inter-area mode oscillations by adjusting its reactance. The conventional approach to the design of FACTS controller is a residue based method. The FACTS controller in such cases has single input single output (SISO) structure. However, residue-based SISO controller has certain drawbacks. Conventionally, in the design of controller based on classical linear control techniques, the controller is designed around equilibrium point which represents particular loading condition of the test system. So the validity of this model is restricted nearer to this operating point [81]. However, in actual power system the loading conditions are continuously changing and hence the operating points are also changing. A FACTS device tuned for the specific operating condition may have deteriorated performance when operating condition changes. Also, while modeling the test system, high-frequency dynamics of the test system are normally neglected. The parameters of the plant model also change with time due to aging effects of the various elements. Hence, the plant model also contains uncertainties. The performance of the designed controller gets affected due to these uncertainties. The designed controller must be able to overcome these drawbacks.

Various linear control technique based robust control theories like LQ, LQG, H_2/H_∞ were applied for designing the controller in the last decade. The controller designed based on these robust control techniques must be able to handle the modeling errors in the plant model. Also, the designed controller must have robust behavior as far as various operating points of the test system are concerned. The designed controller must be able to overcome these two concerns. In control system terminology, these two concerns are called robust stability (able to handle the errors in the plant model) and robust performance (satisfactory performance for various operating points). H_∞ based optimization technique is very popular among various multivariable control methods [82]. H_∞ is a space of functions on the complex plane that is analytic and bounded in the right half plane. Ref. [83] suggested the application of H_∞ theory to robust stabilization. Unlike the time domain performance criterion in LQ and H_2 theories, the H_∞ based optimization technique provides flexibility to formulate the performance criteria in the frequency domain using weighting functions. The concerns mentioned above are ensured through optimization of H_∞ norm of the cost function. Different published literature shows various applications of H_∞ based controllers like servo control, flight control applications and for

various process controls. The H_∞ design methodology is extended for power system control applications in [84-85], but the designed controller has limitations due to the complexity involved in the design process.

3.4.2 Definition of Norms

The maximum singular value of a transfer function of the system over whole frequency range is known as H_∞ norm. For a SISO system, it is the peak value of bode magnitude plot. Robust stability and robust performance in controller design by H_∞ control method are ensured by minimizing the H_∞ norm. The measure of performance of the system can be expressed by this norm.

The ratio of output signal vector *y(s)* and input signal vector *u(s)* in 's' domain is known as transfer function matrix *G(s),u(s)* and *y(s)* are the Laplace transforms of signals *u(t)* and *y(t)* respectively. The size of the signal *u(t)* and *y(t)* in the time domain, size of the transfer function *G(s)* in the 's' domain and the uncertainty present in the plant model gives the measure of the performance of this system. In mathematical terms, these are expressed as 'norms'. In control system applications, the L_2 and L_∞ norms have greater significance. The L_2 norm is given as

$$\|u(t)\|_2 = \sqrt{\int_{-\infty}^{\infty} u^T(t)u(t)dt} \qquad (3.1)$$

The L_∞ norm, which is the least upper bound on the signal absolute value is given as

$$\|u(t)\|_\infty = \sup \max|u_r(t)| \qquad (3.2)$$

$t \geq 0$, $r = 1,2,3\ldots..n$

$u(t) = [u_1(t), u_2(t), \ldots.., u_n(t)]$

The change in the open loop gain with frequency greatly affects the performance of SISO systems with feedback. The disturbance rejection and accuracy of tracking are greatly affected by the open loop gain of the system. 'Principal gains' replaces the concept of gain in the case of the multivariable system. It is defined as the singular values of the transfer function matrix. These singular values are represented with respect to frequencies in this case. A non-negative number using H_2 norm and H_∞ norm are used to

express the characteristics of the transfer function matrix *G(s)*. Singular values need to be defined before defining these norms.

The size of the matrix is appropriately expressed by singular values. The strong/weak input or output direction are identified by corresponding singular vectors [86].

For a matrix $A \in F^{m\times n}$, there exists unitary matrix $U= [u_1, u_2, \ldots. u_n] \in F^{m\times m}$ and $V= [v_1, v_2, \ldots v_n] \in F^{n\times n}$ such that

$$A = U\sum V^{*},\ \sum = \begin{bmatrix} \sum_1 & 0 \\ 0 & 0 \end{bmatrix} \tag{3.3}$$

$$\sum_1 = \begin{bmatrix} \sigma_1 & \cdots & 0 \\ \vdots & \ddots & \vdots \\ 0 & \cdots & \sigma_p \end{bmatrix}, \sigma_1 \geq \sigma_2 \geq \ldots \sigma_p \geq 0\ , p = \min\{m, n\} \tag{3.4}$$

Then σ_i is the i^{th} singular value of A and the vectors u_i and v_j are, respectively, the i^{th} left singular vector and the j^{th} right singular vector.

The H_2 norm is a measure of the overall energy of the system relating input disturbance to the output response. When the system is subjected to impulse response, the total output energy of the system is same as the squared H_2 norm of the system transfer function. When the system is subjected to white noise, the H_2 norm has an interpretation in terms of the asymptotic output variance of the system. Due to this properties, H_2 performance found very suitable in stochastic aspect. The system may be subjected to various stochastics aspects like noise attenuation and random disturbances. H_2 norm is given as:

$$\|G(j\omega)\|_2 = \sqrt{\frac{1}{2\pi}\int_{-\infty}^{\infty} tr\{G(j\omega)G^T(-j\omega)\}d\omega} = \sqrt{\frac{1}{2\pi}\int_{-\infty}^{\infty} \sum_{r=1}^{n} \sigma_r^2\ \{G(j\omega)\}d\omega} \tag{3.5}$$

where *tr{.}* denotes the trace of the matrix. $\sigma_1(.)$, $\sigma_2(.)$…..,$\sigma_n(.)$ denotes the singular values.The worst case system gain is expressed by H_∞ norm. For a stable SISO linear system, the H_∞ norm is defined as

$$\|G(s)\|_\infty = sup\frac{\|y(t)\|_2}{\|u(t)\|_2}\ ,\ u(t) \neq 0 \tag{3.6}$$

where *y(t)* are the output signals and *u(t)* are the input signals to the system. From equation (3.6), the stability of the system can be expressed in the following form:

$$\|G(j\omega)\|_\infty = \sup|G(j\omega)| \quad (3.7)$$

H_∞ norm corresponds to the peak on the magnitude Bode plot for the system. H_∞ norm for a MIMO system is defined as:

$$\|G(j\omega)\|_\infty = \sup\ \sigma|G(j\omega)| \quad (3.8)$$

From equations (3.7) and (3.8), it is clear that H_∞ norm is a simple largest multiplying factor by which a sinusoid is magnified by the system.

3.4.3 Performance and Stability Requirement

The designed controller *K(s)* must ensure stabilization of nominal plant model *G(s)* against all kind of uncertainties and ensure to satisfy all performance specification. Then the closed loop system is said to have robust stability and robust performance. Figure 3.2 explains this concept for multivariable closed loop system.

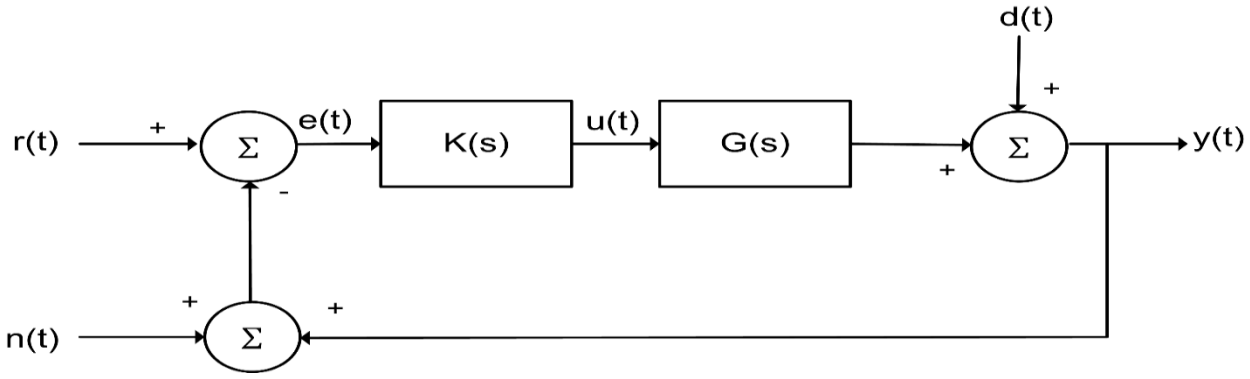

Figure 3.2 Multivariable closed loop

G(s)	Plant transfer function
K(s)	Controller transfer function
r(t)	Reference signal vector
n(t)	Measurement noise signal vector
e(t)	Tracking error signal vector
u(t)	Input signal to the plant vector
d(t)	Disturbance signal vector
y(t)	Output signal vector

Using Laplace transforms,

$$Y = (I + GK)^{-1} GK\,[r-n] + (I + GK)^{-1} d \quad (3.9)$$

The closed loop transfer function $(I + GK)^{-1}GK$ is identified as the complementary sensitivity function, T.

The closed-loop transfer function $(I + GK)^{-1}$ is identified as the sensitivity function, S. Principal gains are used to the express the closed loop performance requirements of the multivariable feedback system.

• By keeping sensitivity function $\sigma(S(jw))$ as low as possible over the frequency spectrum of the disturbances, the effect of disturbances on the output signal can be minimized.

• By keeping complimentary sensitivity function $\sigma(T(jw))$ as low as possible over the frequency spectrum of the measurement noise, the effect of measurement noise on the output signal can be minimized.

The frequency dependent bounds are used on the sensitivity and complementary sensitivity functions, and norms to redevelop the above-mentioned control objectives. Weighting functions $W_1(s)$ and $W_3(s)$ are used to represent the bounds. The weighting functions are chosen arbitrarily. Both S and T can be expressed as:

$$\sigma\,(W_1(jw)\,S(jw)) \leq 1 \quad (3.10)$$

$$\sigma\,(W_3(jw)\,T(jw)) \leq 1 \quad (3.11)$$

Matrices $W_1(s)$ and $W_3(s)$ are used to represent frequency dependent bounds in case of a multivariable system. A multivariable version of small gain theorem helps us to derive conditions for robust stability. Nyquist stability criteria is modified to derive small gain theorem. As per this theorem, the stability of the closed-loop system depends upon the product of gain of all transfer function forming the feedback path. If this product is less than unity, the system will be stable [86].

For handling the uncertainties in the plant model, the knowledge of causes of uncertainties is essential. The primary function of the feedback control system is to reduce the effect of some uncertainties while at the same it has to ensure that other

dominant factors (sensor noise, model uncertainty) do not increase beyond limits. The uncertainty may have several origins [87].

1) Some parameters in the plant model are known approximately. This may cause parametric errors in the linear model.

2) Due to aging effect and change in operating conditions of the plant, the value of the parameters changes in the plant model.

3) The inaccuracy of the measuring devices causes errors.

4) High-frequency dynamics of plant model are neglected while simplifying the plant model.

5) Inaccuracy in the model order reduction from full order to reduced order may sometimes result in an inappropriate representation of the plant model.

The uncertainty can be broadly classified in two dominant forms: Uncertainty in parameters and frequency domain uncertainty. The parametric uncertainty affects the model represented by differential equations of the plant while uncertainty in frequency domain affects the frequency response of the process. The plant model uncertainty can be taken care by designing high gain feedback controllers if the magnitude of this uncertainty is not too big. High gain larger than one in magnitude reduces the effect of plant model uncertainty and also reduces the overall sensitivity of the system to plant noise. However, it is not possible to use large feedback gain if plant model certainty is too large. In such cases, large feedback gain may result in the unstable system. Thus the plant model uncertainty is the most critical consideration while designing the controller. So modeling and bounding the uncertainty in an appropriate way is the first step in robust control design. Designing a controller which is insensitive to the error caused due to the difference between the actual system and model of the system is the second step in robust control design.

3.4.4 Standard H_∞ Optimization Problem

The H_∞ control problem is basically represented as disturbance rejection problem in its standard formulation. It can be represented by two port block diagram as shown in Figure 3.3. The objective here is to minimize the gain from w to z i.e. reducing the effect of

disturbance *w* on output *z*. In Figure 3.3, *G(s)* is the modified plant *G(s)* which includes the weighting functions and *K(s)* is the controller to be obtained by H_∞ optimization.

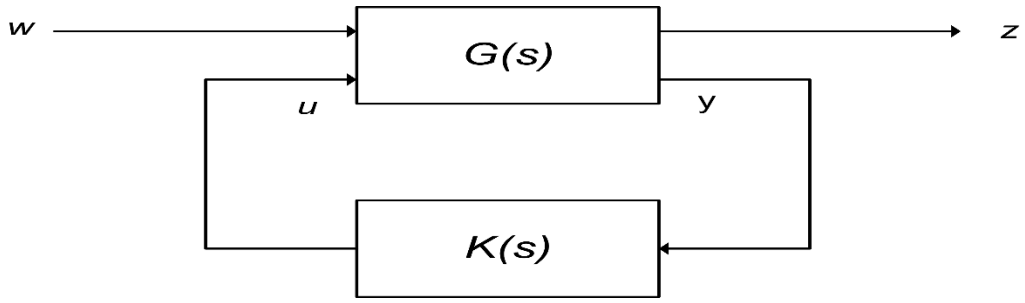

Figure 3.3 Two port block diagram of the control

The input to the plants are:

• *u*, control input signals vector;

• *w*, exogenous input signals vector;

The plant outputs are:

• *y*, the output vector which is feedback to the controller to produce control signal u

• *z*, the system performance vector

The modified plant *G(s)* may be portioned as

$$G(s) = \begin{bmatrix} G_{11}(s) & G_{12}(s) \\ G_{21}(s) & G_{22}(s) \end{bmatrix} \tag{3.12}$$

So, the two port system equations are given as

$$Z(s) = G_{11}(s)W(s) + G_{12}(s)U(s) \tag{3.13}$$

$$Y(s) = G_{21}(s)W(s) + G_{22}(s)U(s) \tag{3.14}$$

$$U(s) = K(s)Y(s) \tag{3.15}$$

From equations (3.13-3.15), the relation can be established between *Z(s)* and *W(s)* and it is as follows:

$$Z(s) = \left[F_L\left(G(s), K(s)\right)\right]W(s) \tag{3.16}$$

$$F_L\big(G(s),K(s)\big) = G_{11}(s) + G_{12}(s)K(s)\big(I - G_{22}(s)K(s)\big)^{-1}G_{21}(s) \quad (3.17)$$

A suitable definition of the signals *w(t)* and *z(t)* helps in representing the various control system problems into two port representations. The state space representation of the plant *G(s)* is as follows:

$$\dot{x}(t) = Ax(t) + B_1 w(t) + B_2 U(t) \quad (3.18)$$

$$z(t) = C_1 x(t) + D_{11} w(t) + D_{12} U(t) \quad (3.19)$$

$$y(t) = C_2 x(t) + D_{21} w(t) + D_{22} U(t) \quad (3.20)$$

resulting in the packed form notation of,

$$G(s) = \begin{bmatrix} A & B_1 & B_2 \\ C_1 & D_{11} & D_{12} \\ C_2 & D_{21} & D_{22} \end{bmatrix} \quad (3.21)$$

So the H_∞ control problem can be expressed as: “For the given plant G(s), find a stable and reliable controller K(s) such that H_∞ norm of the linear fractional transformation matrix $F_L(G(s), K(s))$, is below a given level γ” , i.e.

$$\left\|F_L\big(G(s),K(s)\big)\right\|_\infty < \square, \square \in \mathrm{r}, \square > 0 \quad (3.22)$$

3.4.5 Formulation of Weighted Mixed Sensitivity Problem

For the closed-loop system shown in Figure 3.2, various ‘closed-loop’ transfer functions can be defined as follows:

• The sensitivity $S = (I+GK)^{-1}$.

• The complementary sensitivity $T = (I+GK)^{-1} GK = I - S$.

• The control sensitivity $R = (I+GK)^{-1} K = SK$.

For achieving better tracking of reference signal *r*, the error signal *e = r-y* must be small i.e. the sensitivity function *S* must be small. For suppressing the measurement noise *n,* complementary sensitivity function *T* needs to be small. Also to optimize the control efforts i.e. to avoid saturation of the actuator, control sensitivity function *R* must be small. However, due to the complementary nature of *S* and *T*, both cannot be optimized

simultaneously. Hence a trade-off is necessary between the reference signal error tracking and reduction in measurement noise. Fortunately, the frequencies range of tracking signal *r* and measurement noise signal *n* is quite different. Tracking signal *r* is usually of very low frequencies range while measurement noise signal *n* is usually having very high frequencies range. So the controller is designed such that it has both good tracking properties (at low frequencies) and noise suppression properties (at high frequencies). 'Weighted mixed sensitivity problem' is formulated in [88] to have a trade-off between these properties. As this configuration includes various practical and physical features and indicates different performance and robustness specifications, it is widely applied in control system applications.

The cost function $F_L(G(s), K(s))$, whose H_∞ norm is to be minimized, is given by

$$\left\| \begin{matrix} W_1 S \\ W_3 T \\ W_2 SK \end{matrix} \right\|_\infty$$

where *G(s)* is the plant, *K* is the controller to be designed. W_1 is the weighting on tracking error, W_2 is the weighting on the control signal and W_3 is the weighting on the plant output as shown in Figure 3.4.

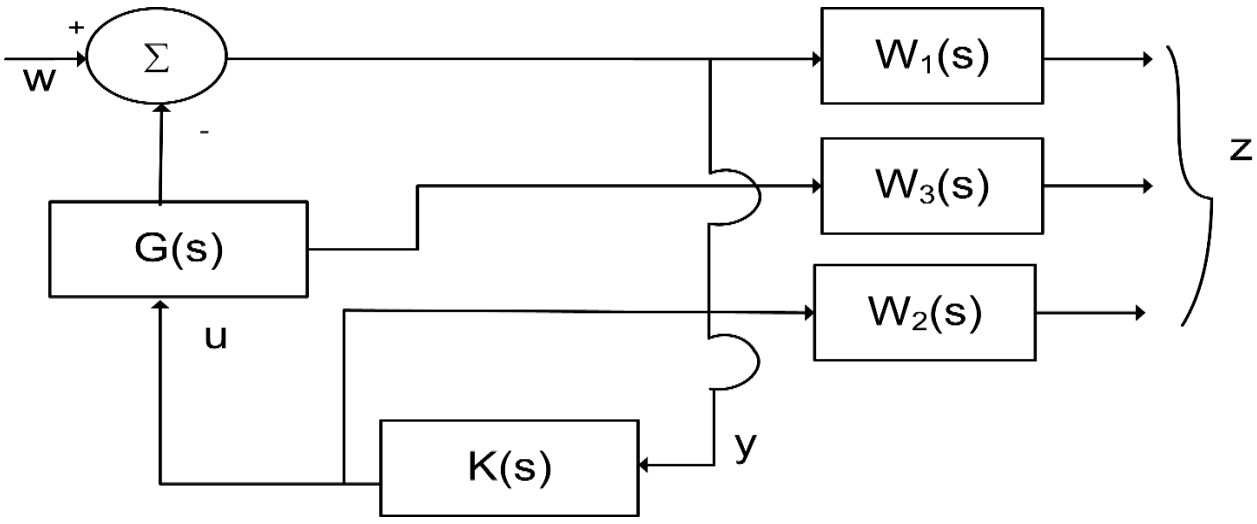

Figure 3.4 Weighted mixed sensitivity problem [88]

Figure 3.4 indicates that the weighted mixed sensitivity problem has the same form as that of the standard problem. Hence, for the given cost function, the plant model can be modified as:

$$G(s) = \begin{bmatrix} W_1(S) & -W_1(s)G_0(s) \\ 0 & W_3(s)G_0(s) \\ 0 & W_2(s) \\ I & -G_0(s) \end{bmatrix} \tag{3.23}$$

where *I* imply identity matrix.

It is not required to simultaneously optimize all three functions. Hence all three weights need not be specified. Here in this thesis, attention is given to optimizing the following objective:

$$\left\| \begin{matrix} W_1 S \\ W_2 R \end{matrix} \right\|_\infty \leq \gamma \tag{3.24}$$

where γ is the bound on H_∞ norm.

This design would result in optimization of sensitivity function S which ensures disturbance rejection and optimization of control sensitivity function R which ensures robust performance and control effort minimization. Selection of the weighting matrices is the key to the successful design of the controller. Knowledge of the plant behavior and design constrain is most important for choosing the weighting functions. The selection of the weighting functions is on trial and error bases. However, for an experienced designer, it is not a difficult task. Normally, the weighing filter needs to have a large gain in the frequencies range when it is important to constrain the magnitudes of the associated closed-loop transfer functions. Otherwise, it should have the small gain at other frequencies. A low-pass filter, a high-pass filter or band-pass filters are used as a weighting function to realize desired closed loop performance.

3.4.6 Mixed H_2 / H_∞ Output Feedback Control

Handling the modeling errors and uncertainties are the main purposes of introducing the robust control techniques for designing of damping controller in power system. The conventional practice is to define a single objective formulation which combines all control requirements. But in practical applications, the standard H_∞ synthesis cannot fulfill all

control requirements. For example, attenuation of noise and random disturbances regulations are more conveniently expressed in LQG terms (H_2 norm). Additionally, H_∞ synthesis ensures closed-loop stability but specific requirements like pole placement in the left-hand plane of the imaginary axis to ensure minimum damping of the critical modes cannot be ensured. As closed loop poles also govern the time response and transient behavior of the system, it is sometimes necessary to place the pole in a specific region. This enforces multi-objective synthesis requirements in control system applications. Each robust control technique is mainly suitable to achieve the specific objective of control system requirement [89]. For example, H_∞ control provides good robust performance when plant model uncertainties are more, but it does not ensure good transient response for the closed-loop system. On the other hand, H_2 control ensures good performance on system transient behaviors.

To serve all design requirement by a single norm, adjustment between various conflicting requirements has to be carried out. However, in such cases, the designed controller is very hidebound and its effectiveness in improving the performance specification of the closed-loop system is restricted. Also, the selection of weighting functions to meet the adjustment of the conflicting requirement is difficult and time-consuming.

The drawbacks of the single objective structure can remove with the help of multi-objective structure. The multi-objective structures easily incorporate various design specifications. The multi-objective control addresses both time and frequency domain specification requirements as well as it can address the pole placement requirements. The multi-objective structure combines the H_∞ performance and H_2 performance i.e. it ensures the good performance against plant model uncertainties, ensures good transient behavior of the system and can place the poles into the specific region to ensure sufficient damping ratio.

Figure 3.5 shows the configuration of the multi-objective robust controller synthesis. The output channel z_∞ is related to the H_∞ performance and the channel z_2 is related to H_2 performance. $W_1(s)$ is a low-pass filter in the H_∞ performance channel for output disturbance rejection. $W_2(s)$ is a high-pass filter for providing robustness against model

uncertainties. $W_3(s)$ is a high-pass filter or some constant placed in the H_2 performance channel to reduce the control efforts.

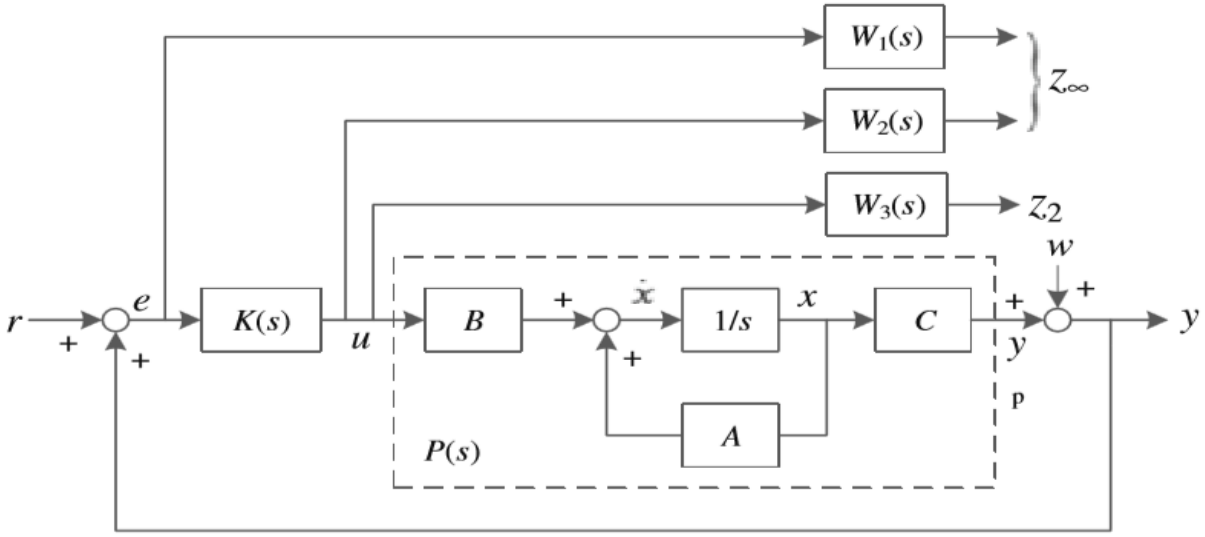

Figure 3.5 Configuration of the multi-objective robust controller synthesis [59]

3.5 LMI approach to H_∞ Controller Design

Many researchers tried to solve the H_∞ control problem analytically. Ref. [36] developed the state space approach to solving the H_∞ control problem. The characterization involves the solution of two algebraic Riccati equations, of the same order as the modified plant. Ref. [90] applied Riccati based approach for the solution to the H_∞ control design problem. However, it concluded that Riccati based approach suffers from two major drawbacks: First, it results in the design of a controller which suffers from pole-zero cancellation between the controller and the plant. Also, some time domain specifications such as settling time, peak overshoot cannot be computed easily. The selection of proper weights is the key criteria in Riccati-based design. However, the selection of weights is not straightforward and it is time-consuming.

In recent times, H_∞ synthesis problem is solved by LMI techniques. These LMIs are identical to the inequality equivalent of the conventional H_∞ Riccati equations. The solution of Riccati equations through LMI formulation offers certain benefits. The resulting controller, in this case, does not suffer from pole-zero cancellation [91]. As LMI's essentially reflect constraints rather than optimality, it provides better flexibility for

combining several constraints on the closed-loop system even when the analytical solution is impossible [92-93]. LMI solution by default if exists is robust and optimal. In case of power system applications, for deciding the robustness of the designed controller, many time-consuming simulations need to be carried out. The LMI approach helps to overcome this problem. The LMI approach was applied in [55, 57, 59, 94] for the design of H_∞ control technique based controlled for different power system applications. LMI approach with pole placement is discussed in detail in [89].

3.5.1 Introduction to LMI

A LMI is any constraint of the form

$$A(x) = A_0 + x_1 A_1 + .. + x_N A_N < 0 \tag{3.25}$$

- $x = (x_1, x_{2,\ldots\ldots,} x_n)$ is a vector of unknown scalars (the decision or optimization variables)
- $A_0, A_1, \ldots A_n$ are given symmetric matrices
- < 0 stands for "negative definite," i.e., the largest eigenvalue of $A(x)$ is negative

The LMI in equation (3.25) is a convex constraint on x. Finding a solution for x in equation (3.25), if exist, is a convex optimization problem.

LMI techniques can simultaneously solve three problems of control system: feasibility as expressed in equation (3.26), linear objective minimization as expressed in equation (3.27) and generalized eigenvalue minimization as expressed in equation (3.28). These problems are respectively expressed as follows:

Finding a solution x subject to $A(x) < 0$ (3.26)

Minimizing $C^T x$ subject to $A(x) < 0$ (3.27)

Minimizing λ subject to $\begin{cases} A(x) < \lambda B(x) \\ B(x) > 0 \\ C(x) < 0 \end{cases}$ (3.28)

The LMI problem for a linear time-invariant system can be expressed with following state space representation:

$$E\frac{dx}{dt} = Ax(t) + Bu(t)$$

$$y(t) = Cx(t) + Du(t) \tag{3.29}$$

Where, *A, B, C, D,* and *E* are real matrices and *E* is invertible. Parameter-dependent systems are normally specified by the above formulation. For power system applications, LMIs are derived in the same way.

3.5.2 LMI Formulation for Multi-Objective Synthesis

Figure 3.6 represents multi-objective H_∞ synthesis problem. The control problem is sketched in Figure. 3.6. The H_∞ performance is related to output channel z_∞. The H_2 performance (LQG aspects) is related to output channel z_2. By expressing $T_\infty(s)$ as the closed loop transfer function from *w* to z_∞ and $T_2(s)$ as the closed-loop transfer functions from *w* to z_2, respectively, the multi-objective problem is synthesized as follow:

Design a dynamic output-feedback controller $u = Ky$ that

• Maintains the H_∞ norm of $T_\infty(s)$ (RMS gain) below some prescribed value $\gamma_0 > 0$.

• Maintains the H_2 norm of $T_2(s)$ (LQG cost) below some prescribed value $v > 0$.

• Minimizes a trade-off criterion of the form

$$\alpha \|T_\infty\|_\infty^2 + \beta \|T_2\|_2^2 \ , \alpha > 0, \beta > 0 \tag{3.30}$$

• Places the closed-loop poles in some prescribed LMI region D.

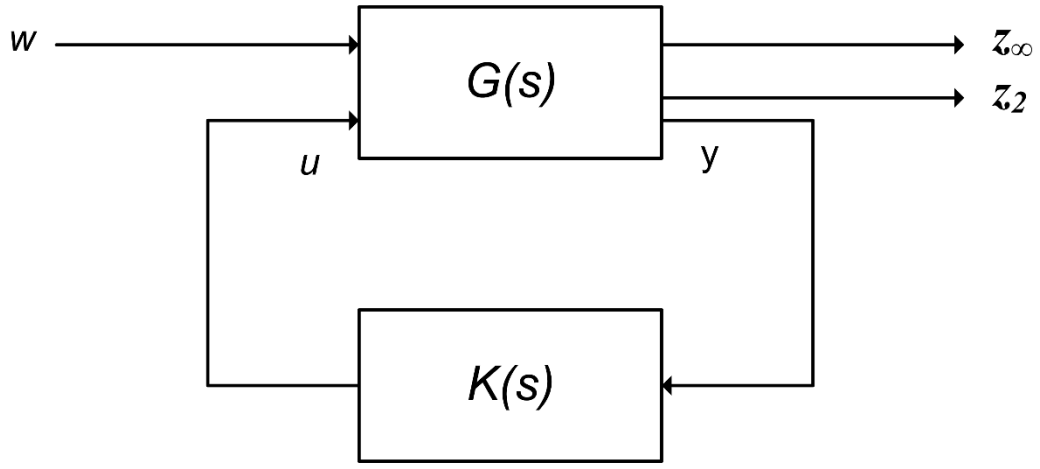

Figure 3.6 Multi-objective H_∞ synthesis problem [94]

Let,

$$\dot{x} = Ax + B_1 w + B_2 u \tag{3.31a}$$

$$z_\infty = C_\infty x + D_{\infty 1} w + D_{\infty 2} u \tag{3.31b}$$

$$z_2 = C_2 x + D_{21} w + D_{22} u \tag{3.31b}$$

$$y = C_y x + D_{y1} w \tag{3.31d}$$

and

$$\dot{x} = A_k x_k + B_k y \tag{3.32a}$$

$$u = C_k x_k + D_k y \tag{3.32b}$$

be the state space realizations of the plant *G(s)* and controller *K(s)* respectively and let

$$\dot{x} = A_{cl} x_{cl} + B_{cl} w \tag{3.33a}$$

$$z_\infty = C_{cl1} x_{cl} + D_{cl1} w \tag{3.33b}$$

$$z_2 = C_{cl2} x_{cl} + D_{cl2} w \tag{3.33c}$$

be the corresponding closed-loop state space equations.

The three design objectives can be expressed as follows:

• H_∞ performance: the closed-loop RMS gain from *w* to z_∞ does not exceed γ if and only if there exist a positive definite symmetric matrix χ_∞ such that

$$\begin{pmatrix} A_{cl} x_\infty + x_\infty A_{cl}^T & B_{cl} & x_\infty C_{cl1}^T \\ B_{cl}^T & -I & D_{cl1}^T \\ C_{cl1} x_\infty & D_{cl1} & -\gamma^2 I \end{pmatrix} < 0 \tag{3.34}$$

• H_2 performance: the H_2 norm of the closed-loop transfer function from *w* to z_2 does not exceed v if and only if $D_{cl2} = 0$ and there exist two symmetric matrices χ_2 and *Q* such that

$$\begin{pmatrix} A_{cl} x_2 + x_2 A_{cl}^T & B_{cl} \\ B_{cl}^T & -I \end{pmatrix} < 0 \tag{3.35}$$

$$\begin{pmatrix} Q & C_{cl2}\, x_2 \\ x_2 C_{cl2}^T & x_2 \end{pmatrix} > 0 \tag{3.36}$$

Trace (Q) < v^2 (3.37)

• Pole placement: the closed-loop poles lie in the LMI region

$$D = \{ z \in C: L + Mz + M_z^{T-} < 0\} \quad (3.38)$$

with $L = L^T = \{\lambda_{ij}\}_{1\le i,j\le m}$ and $M = [\mu_{ij}]_{1\le i,j\le m}$ if and only if there exists a positive definite symmetric matrix χ_{pol} satisfying

$$\left[\lambda_{ij}x_{pol} + \mu_{ij}A_{cl}x_{pol} + \mu_{ij}x_{pol}A_{cl}^T\right]_{1\le i,j\le m} < 0 \quad (3.39)$$

For traceability in the LMI framework, we must seek a single Lyapunov matrix

$x \coloneqq x_\infty = x_2 = x_{pol}$ that enforces all three sets of constraints. Find matrices *M*, *N*, $R = R^T$ and $S = S^T$ to factorize χ as $x = x_1 x_2^{-1}, x_1 = \begin{pmatrix} R & I \\ M^T & 0 \end{pmatrix}, x_2 = \begin{pmatrix} 0 & S \\ I & N^T \end{pmatrix}$ and introducing the change of controller variables [95]:

$$B_K \coloneqq NB_K + SB_2D_K \quad (3.40)$$

$$C_K \coloneqq C_KM^T + D_kC_yR \quad (3.41)$$

$$A_K \coloneqq NA_KM^T + NB_KC_yR + SB_2C_KM^T + S(A + B_2D_KC_y)R \quad (3.42)$$

The inequality constraints on χ are readily turned into LMI constraints in the variable *R, S, Q, K, A_K, B_K, C_K,* and D_K. These results in following LMI formulation in multi-objective synthesis problem:

Minimize $\alpha\gamma^2 + \beta$Trace (Q) over *R, S, Q, K, A_K, B_K, C_K*, D_K and γ^2 satisfying:

$$\begin{pmatrix} AR + RA^T + B_2C_K + C_K^TB_2^T & A_K^T + A + B_2D_KC_Y & B_1 + B_2D_KD_{Y1} & (C_\infty R + D_{\infty 2}C_K)^T \\ A_K + (A + B_2D_KC_Y)^T & A^TS + SA + B_K + C_Y^TB_K^T & SB_1 + B_KD_{Y1} & C_\infty^T + C_Y^TD_K^TD_{\infty 2}^T \\ (B_1 + B_2D_KD_{Y1})^T & SB_1 + B_KD_{Y1} & -I & (D_{\infty 1} + D_{\infty 2}D_KD_{Y1})^T \\ C_\infty R + D_{\infty 2}C_K & C_\infty + D_{\infty 2}D_KC_Y & D_{\infty 1} + D_{\infty 2}D_KD_{Y1} & -\gamma^2 I \end{pmatrix} < 0 \quad (3.43)$$

$$\begin{pmatrix} Q & C_2R + D_{22}C_K & C_2 + D_{22}D_KC_Y \\ (C_2R + D_{22}C_K)^T & R & I \\ (C_2 + D_{22}D_KC_Y)^T & I & S \end{pmatrix} > 0 \quad (3.44)$$

$$\left[\lambda_{ij}\begin{pmatrix} R & I \\ I & S \end{pmatrix} + \mu_{ij}\begin{pmatrix} AR + B_2C_K & A + B_2D_KC_2 \\ A_K & SA + B_KC_2 \end{pmatrix} + \right.$$
$$\left. \mu_{ji}\begin{pmatrix} RA^T + C_K^T B_2^T & A_K^T \\ (A + B_2D_KC_2)^T & (SA + B_KC_2)^T \end{pmatrix}\right]_{1\le i,j\le m} < 0 \quad (3.45)$$

$$Trace\ (Q) < v_0^2 \quad (3.46)$$

$$\gamma^2 < \gamma_0^2 \quad (3.47)$$

$$D_{21} + D_{22}D_KD_{y1} = 0 \quad (3.48)$$

Given optimal solutions γ^*, Q^* of this LMI problem, the closed loop H_∞ and H_2 performances are bounded by

$$\|T_\infty\|_\infty \le \gamma^* \quad (3.49)$$

$$\|T_2\|_2 \le \sqrt{Trace(Q^*)} \quad (3.50)$$

3.5.3 LMI Region for Pole Placement Objective

The location of the poles decides the transient response of the liner system. By placing all the poles in the prescribed region, the better transient response can be achieved. Minimizing the decay rate or improving the closed loop damping are the major objectives in pole placement. Also, fast dynamics and high-frequency gain can be restricted with pole placement which facilitates the digital operation of the controller [47]. Excessive controller gain should be avoided as it may result in saturation of the controller output and poor response to the disturbance rejection although it achieves the good damping ratio and acceptable decay rate. So, as large shift of the system poles on left half plane results into a large gain of the controller, this should be avoided unless it is necessary.

The development of pole placement objective in LMI terms, the concept of LMI region is effective. LMI regions are defined as convex subsets D of the complex plane and characterized by

$$D = \{z \in C: f_D(z) < 0\} \quad (3.51)$$

where,

$$f_D(z) = \alpha + \beta z + \beta^T \bar{z} = [\alpha_{kl} + \beta_{kl} z + \beta_{kl} \bar{z}]_{1 \le k,l \le m} \quad (3.52)$$

is called the characteristic function of *D*. $\alpha = [\alpha_{kl}] \in R^{m*m}$, $\beta = [\beta_{kl}] \in R^{m*m}$ are symmetric matrix.

$\dot{x} = Ax$ is called D-stable if all its poles lie in *D*. The matrix is *D*-stable if and only if there exist a symmetric matrix *X* such that

$$M_D(A, X) < 0, X > 0 \quad (3.53)$$

where $M_D(A, X) \coloneqq \alpha \otimes X + \beta \otimes (AX) + \beta^T (AX)^T$ and $\otimes$ denotes Kronecker production of matrices.

LMI regions can be expressed as convex regions in the complex plane which is symmetric with respect to the real axis. This includes horizontal strips, circles, conic sectors etc. The intersection of LMI regions also results in LMI region. Some typical LMI regions are:

1) Half-plane $R_e(z) < -\alpha : f_D(z) = z + \bar{z} + 2\alpha < 0$
2) Conic sector with the apex at the origin and inner angle 2θ (S(0,0, θ)):

$$f_D(z) = \begin{bmatrix} sin\theta(z + \bar{z}) & -cos\theta(z - \bar{z}) \\ cos\theta(z - \bar{z}) & sin\theta(z + \bar{z}) \end{bmatrix} < 0$$

From the above mentioned LMI regions, conic sector region is shown in Figure 3.7. Region D in Figure 3.7 is the pole placement region. The pole placement in region D guarantees minimum damping ratio ξ = cos θ. It also ensures other performance requirements like the minimum rate of decay σ, a maximum undamped natural frequency ω, and adequate controller gains. This consecutively results in a reduction in maximum overshoot, rise time, decay time, settling time and peak gain.

3.6 Normalized H_∞ Loop Shaping using LMI

While designing the controller based on mixed sensitivity based LMI approach, the designer needs to specify the performance requirements in terms of the weighted closed-loop transfer functions. Thereafter, the designed controller satisfies the performance criteria. However, the common difficulty in this approach is the proper selection of weights. Also, the dynamic properties of the plant model are not taken into consideration

while specifying the performance criteria. This shortcoming of the mixed sensitivity based LMI approach can be overcome by H_∞ loop shaping using LMI.

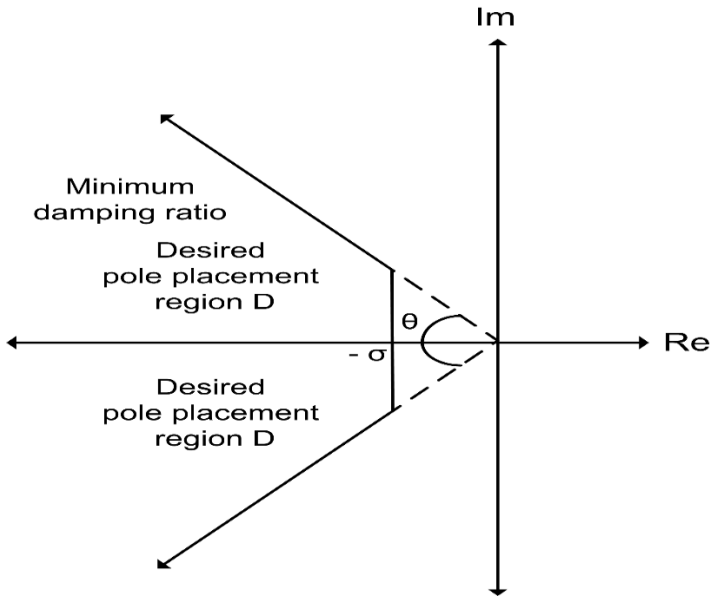

Figure 3.7 LMI region for pole placement

The H_∞ loop-shaping design combines the characteristics of both classical open-loop shaping and H_∞ optimization. References [28, 96] have applied this technique to design of damping controllers in power system applications. A solution to the problem sought analytically using a standard normalized coprime factorization approach. However, performance specification like minimum damping ration was not considered explicitly while designing.

Ref. [42, 97] suggested a normalized coprime factorization approach for loop-shaping design. The H_∞ loop shaping technique combines H_∞ robust stabilization with classical loop-shaping. The design procedure comprises of two stages. In first stage, the open loop system model is shaped i.e. with the help of pre and post compensator, the frequency response of the open loop plant is shaped as per requirement. In the second stage, the resulting shaped system model is robustly stabilized with respect to coprime factor uncertainties by solving the H_∞ optimization problem [89, 98].

3.6.1 Loop Shaping

The loop shaping design procedure is shown in Figure 3.8.The basic principle of H_∞ loop-shaping design is to shape the open-loop frequency response with the help of pre and post-compensators. The idea is to specify the performance requirements prior to robust stabilization [42]. If W_1 and W_2 are the pre and post-compensators respectively, then the shaped system model G_s is given by

$$G_S = W_2 * G * W_1 \tag{3.54}$$

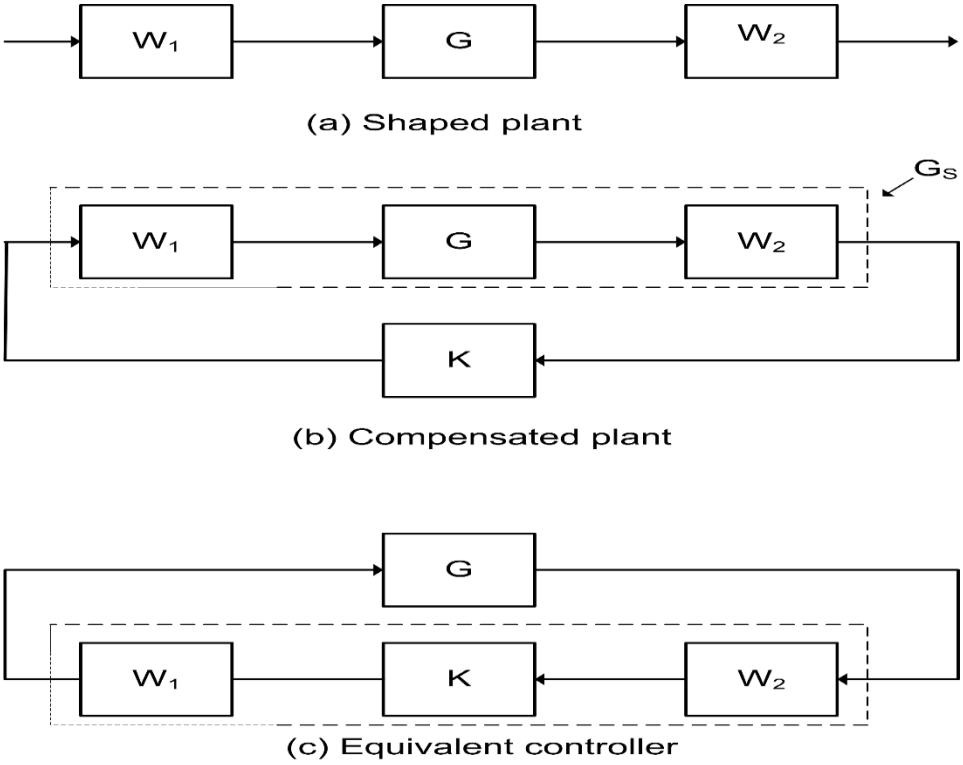

Figure 3.8 Loop shaping design procedure [98]

where G is the nominal plant model. The controller K is designed by solving the robust stabilization problem for the shaped system model G_s as described later. The equivalent feedback controller for the original system model G is obtained by augmenting the designed controller K with the compensators i.e. $K_{eq} = W_2 * K * W_1$ as shown in Figure 3.8.

The appropriate selection of the pre and post compensator weights is the main task in loop shaping design procedure. However, following guidelines are available for the selection of weights [42, 98]:

- Proper scaling needs to be applied to input and output to ease out the design problem.
- The selection of compensator weights which results in singular values of the shaped plant model is very essential.
- At low frequencies, integral action needs to be added.

However, some trial and error are involved in the selection of weights, but experienced design person can quickly overcome this limitation. The maximum stability margin ε_{max} provides an indication as to whether the choice of the compensators is appropriate or not. If the margin is too small, $\varepsilon_{max} < 0.25$, then the compensators need to be modified following the above guidelines. When $\varepsilon_{max} > 0.25$, the choice is considered to be acceptable.

3.6.2 Robust Stabilization

Suppose, the plant G has normalized left coprime factorization $G = M^{-1}N$, then perturbed plant model *Gp* can be given by

$$G_p = (M + \Delta_M)^{-1}(N + \Delta_N)^{-1} \tag{3.55}$$

Where, Δ_M and Δ_N are stable unknown transfer functions which represents the uncertainty in the nominal plant model *G*. Now the main objective is to stabilize both nominal plant model G and perturbed plants as given in (3.56).

$$Gp = \{M + \Delta_M\}^{-1}\{N + \Delta_N\}^{-1} : \|\Delta_M \quad \Delta_N\| \leq \varepsilon \tag{3.56}$$

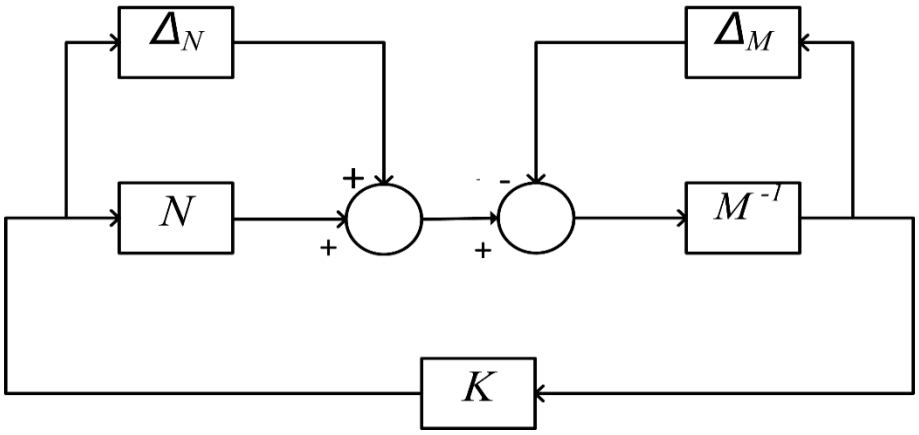

Figure 3.9 Robust stabilization problem [98]

Where, ε> 0 is known as the stability margin. The robust stabilization problem is as shown in Figure 3.9. H_∞ controller is given by the equation (3.57) for a specified $\gamma > \gamma_{\min}$.

$$\left\| \begin{bmatrix} K \\ I \end{bmatrix} (I - GK)^{-1} M^{-1} \right\|_\infty \leq \gamma \tag{3.57}$$

3.7 Summary

This chapter discusses the various steps involved in the design of the damping controller which mainly includes test system modeling, linearization of the nonlinear model, modal analysis, model order reduction, selection of input signal for the controller, controller synthesis and testing of the designed controller for robustness. The theoretical aspects of mixed sensitivity formulation in LMI and extension of LMI technique for H_∞ loop shaping technique were discussed. Application of these control techniques to various test systems is discussed in next chapters.

CHAPTER 4 CASE STUDIES ON LMI BASED MULTI-OBJECTIVE APPROACH

4.1 Introduction

This chapter discusses the design of wide-area damping controller based on mixed H_2/H_∞ output feedback control with pole placement in LMI framework. The procedure described in chapter 3 is applied to the design of wide-area damping controller. The controllers are designed for two test systems: Two area four machine test system and modified New York- New England test system. Both systems employ various FACTS devices. The designed controller is checked for robustness under various operating conditions and various contingency conditions.

4.2 Case Study I: Two Area Four Machine Test System

The two-area four-machine system was specially designed to study low-frequency oscillations in power system. This system shows both local and inter-area mode oscillations that occurs in both small and large interconnected power system. Figure 4.1 shows the single line diagram of a two-area four machine test system. All the synchronous generators are sub-transient round rotor synchronous machines and are represented by six variables as discussed in chapter 2. All the synchronous generators employ Type ST1A excitation system with the thermal governor and speed input PSSs with two lead-lag compensation blocks. Each generator is rated at 900 MVA. Area 1 (comprises of Generators 1, 2) and area 2 (comprises of Generators 3, 4) are connected by a tie line. A detailed description of the test system is given Appendix A [81]. Load in area 2 is more than area 1. Hence power is transferred from area 1 to area 2 through tie-line. To facilitate the power transfer in the tie-line, Thyristor Controlled Series Capacitor (TCSC) is employed in the tie-line. The power flow P_{tie} from area 1 to area 2 through the tie line is 376 MW (3.76 p.u.) and is chosen as a nominal operating point. The power flow in the tie-line can be varied by varying the loads and generation in each area. Figure 4.2 gives a basic idea of wide area measurement system. The global signals are acquired with the phasor measurement units located at important buses in the two area test system. The PMUs capture important dynamic data of the power system and transmit it to the wide area control (WAC) centers.

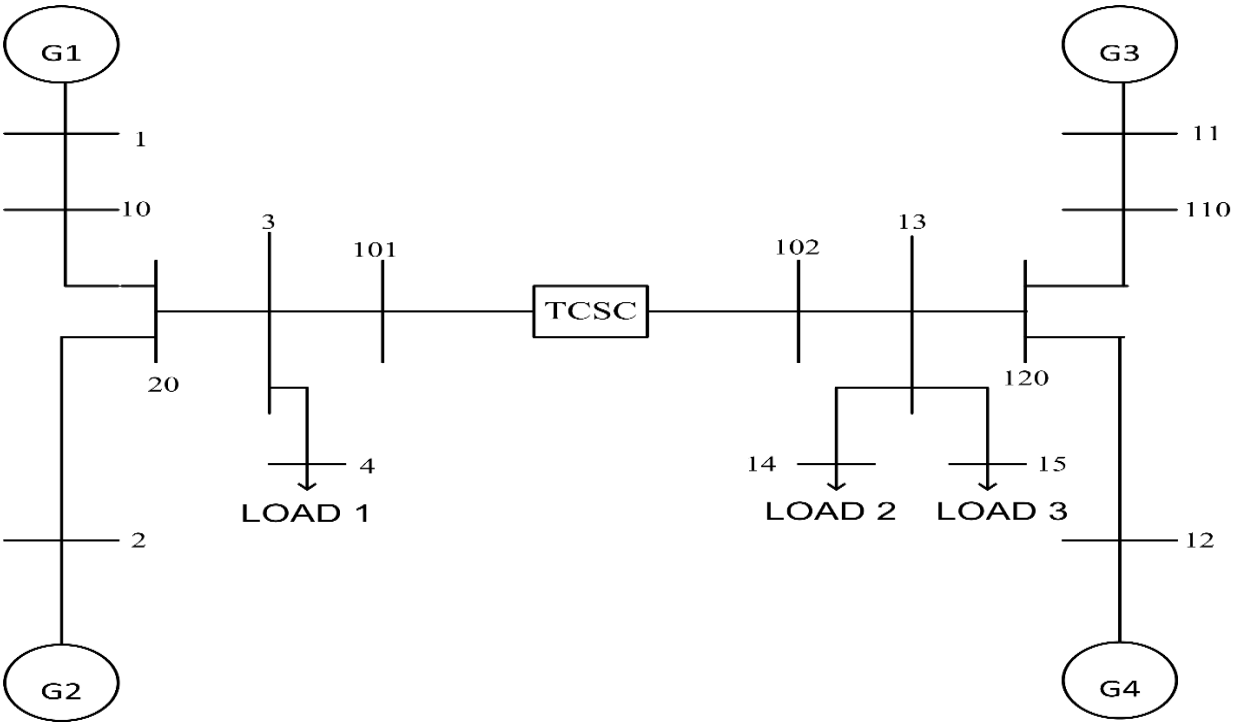

Figure 4.1 Two area four machine test system

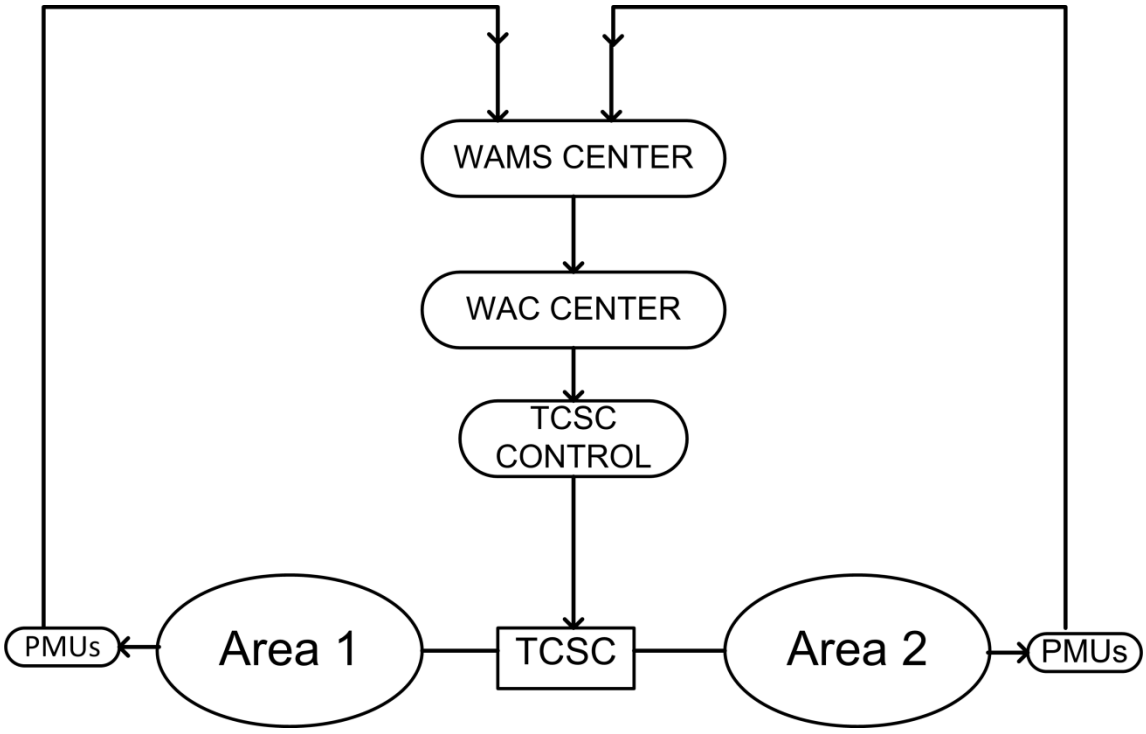

Figure 4.2 Basic structure of wide area damping control (WADC)

The wide area damping control includes the wide area measurements (WAM), wide area control center (WAC) and power system. The WAMs are used to synchronously measure and process the global signals and send it to WAC center. The WAC center is used to select the suitable input signal and send it to the local controlling devices (FACTS devices). The FACTS devices act as supplementary damping controller. The WAC center plays an important role, which includes the selection of wide area control input signals and generation of wide area control output signals.

4.3 Design of TCSC Wide-Area Damping Controller

The steps discussed in section 3.2 for designing the wide area damping controller are applied for designing the TCSC wide-area damping controller for two area four machine test system which is as described below:

4.3.1 Full Order Model and Small Signal Analysis

The detailed modeling of all the devices (i.e. generators, exciters, turbines, PSSs and TCSC) is carried out as discussed in chapter 2 and a nonlinear model of two area four machine test system is developed. The order of the nonlinear model is 59. The generation and load condition at which the power flow in tie-line is 376 MW (from Area 1 to Area 2) is selected as a nominal operating point. The modal analysis shows that this system has four local mode oscillations and one lightly damped inter-area mode oscillation. However, local mode oscillations are very well damped with the PSSs (with a minimum damping ratio of 14.67%) and hence the focus is only on lightly damped inter-area mode. The characteristic of the local and inter-area mode is as shown in Table 4.1. To find out which generators are oscillating against each other for critically damped inter-area mode, compass chart is drawn for speed component of the right eigenvector of critical mode. The mode shape of the critical inter-area mode is as shown in Figure 4.3. The compass chart clearly shows that Generators G1, G2 are oscillating against Generators G3, G4. The motive of designing the WADC is to improve damping ratio of this mode.

Table 4.1 Local and inter-area modes oscillation of two area test system

Mode Index	Eigenvalue	*f* (Hz)	Damping ratio ζ	Mode Shape
1	-0.161 ±3.604i	0.573	0.0447	G1-G2 Vs.G3-G4 (Area 1 Vs Area2)
2	-1.04 ± 7.04i	1.12	0.1467	G3 Vs. G4
3	-1.15 ± 7.04i	1.12	0.1611	G1 Vs. G2

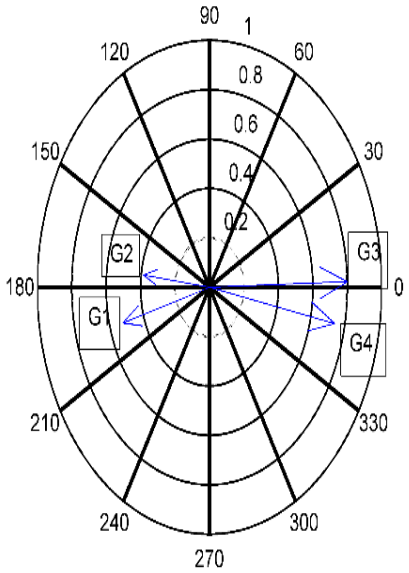

Figure 4.3 Speed component of right Eigenvector for inter-area mode

4.3.2 Selection of Suitable Global Signal

Selection of suitable input signal is of the prime importance for the effective design of the damping controller. Line current, line power, the voltage at the bus, generator rotor speeds etc. are the probable candidate as input signals. The signal with the highest controllability/observability measures is the best candidate for the critical mode. As the main purpose of the TCSC in two area test system is to improve the transmission capacity of the tie-line, the best location for TCSC, in this case, is the tie-line. Hence, only observability is to be checked i.e. the inter-area mode must be observable in the input

signal selected. The bus voltage angle difference or generator rotor speed signals may contain some spurious signals (ex. measurement noises etc.) Hence, they are not selected as input signals. The line active power is found to be free from above-mentioned eventuality. Hence, line active power is selected as an input signal. A model residue analysis suggested in [99] is carried out to identify most stabilizing global signals. The inter-area mode is found to be highly observable in the active power flow in the various transmission lines. The absolute values of the residue of various lines for concerned inter-area mode are as shown in Figure 4.4. Residue analysis clearly shows that active power in the line connecting bus 3-bus 20 has the highest residue for the inter-area mode. So, it is selected as an input signal.

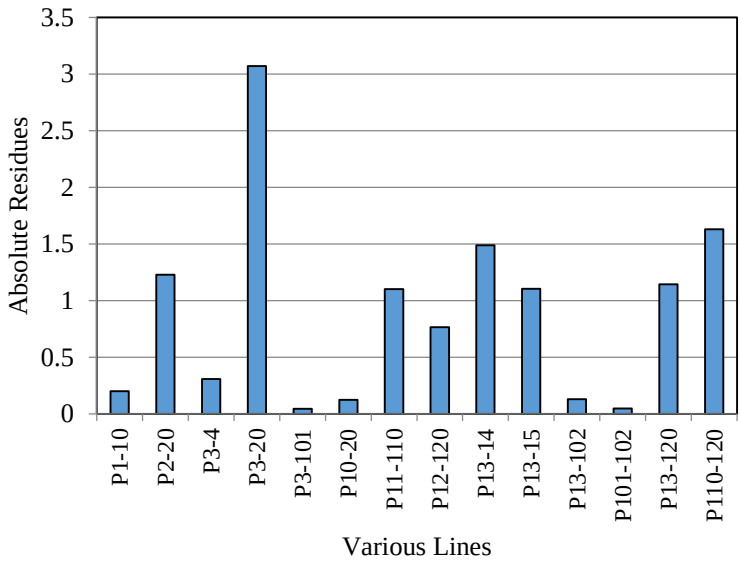

Figure 4.4 Residue analysis for a critical mode with line power as an input signal

4.3.3 Reduction of Order of Linear Model

The linearized model obtained as described in section 4.3.1 is of 59^{th} order. The time required by the LMI approach for solving such large system is quite large. Also, only a few states of the linear model are dominant and affect the inter-area mode. These dominant states contain the characteristics of the system. Therefore, it is necessary to reduce the order of the original system such that the characteristics of the system (represented by the frequency response of the system) in the interested range of frequencies are closely

matching. In the present case, balanced reduction function of MATLAB is used to reduce the order of the system from 59th to 10th order. The frequency responses of the full-order model and reduced-order model are shown in Figure 4.5. From the frequency response, it is quite clear that in the interested frequency range (i.e. less than 10 rad/sec), the full and reduced-order model is closely matching. Hence, the reduced order system is reliable for robust controller design.

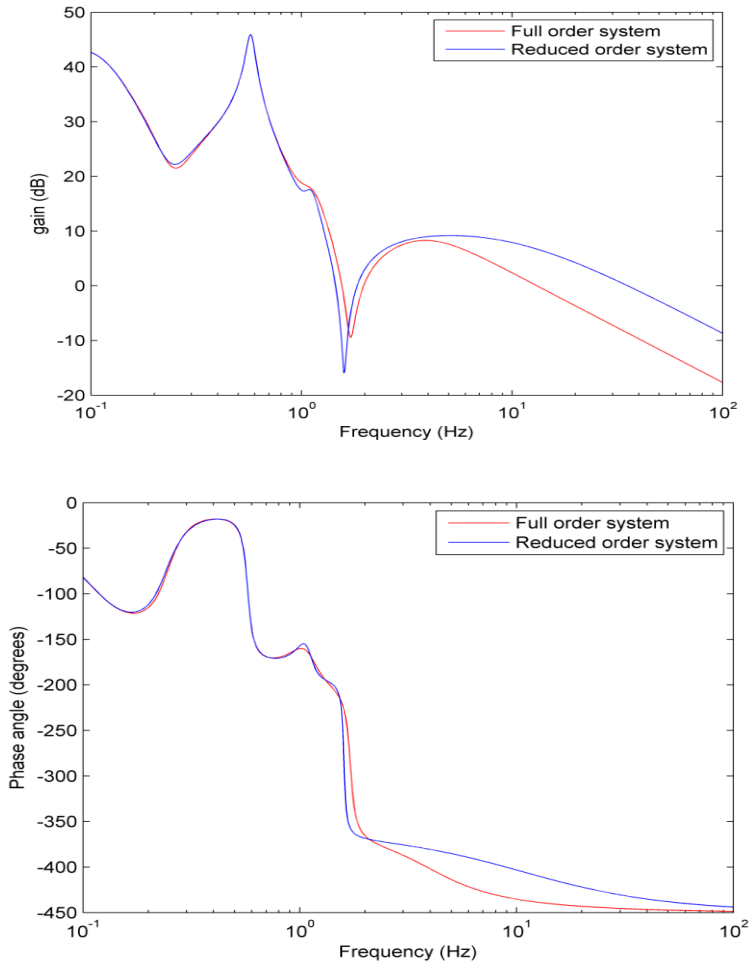

Figure 4.5 Frequency response of full order and reduced order system

4.3.4 Proposed Load Models

As discussed in chapter 2, the performance of the designed controller is greatly affected by the types of loads. In the literature review, conventionally the load is represented by constant impedance load, constant current load and constant power load separately but

in the practical power system, it is not possible to have a single kind of load at various buses. The load on various buses is a composition of the above-mentioned load models. Also, dynamic loads greatly affect the stability of the power system and therefore also needed to be considered in the modeling. The performance of the controller must be assessed for all possible kind of load model compositions so that the robustness of the designed controller can be ensured. Considering these facts, a new composition of various types of load models are proposed in this thesis which tries to cover all possible load composition scenarios of the actual power system. A fare weight is given to all types of load models at various buses in the proposed load model compositions. Also, dynamic load model is considered separately to study its indigenous effect on power system stability. These load compositions are shown in Table 4.2. The details information regarding the load modeling is discussed in section 2.7.

Table 4.2 Proposed load model compositions

Load Model	Fraction of Constant Impedance load	Fraction of Constant Power load	Fraction of Constant current load	Dynamic load
I	1.0	0	0	0
II	0	1.0	0	0
III	0	0	1.0	0
IV	0.5	0.25	0.25	0
V	0.25	0.5	0.25	0
VI	0.25	0.25	0.5	0
VIII	0.5	0	0	0.5

4.3.5 Controller Synthesis

For the reduced order model obtained in section 4.3.3, a multi-objective TCSC wide-area damping controller is designed in this section. For achieving robust controller, the mixed H_2 /H_∞ output feedback control with pole placement in LMI framework is developed. As discussed in section 3.4 the weight functions $W_1(s)$ and $W_2(s)$ which act as a low-pass filter and high-pass filter are respectively placed in H_∞ performance channel and ensures the output disturbance rejection and robustness against model uncertainties. To reduce

the control effort, weight $W_3(s)$ which is acting as a high-pass filter or some small constant, is placed in the H_2 performance. As the frequency of an inter-area mode of interest is less than 10 rad/sec, $W_1(s)$ and $W_2(s)$ are selected such that they intersect around 10 rad/sec. A small constant is also selected for the $W_3(s)$ in the H_2 performance channel. The selection of the weights are as follows:

$$W_1(s) = 10/(s+10) \quad (4.1)$$

$$W_2(s) = s/(s+10) \quad (4.2)$$

$$W_3(s) = 1 \quad (4.3)$$

The frequency response of weights $W_1(s)$ and $W_2(s)$ is as shown in Figure 4.6. From the Figure 4.6, it is clear that both frequency response intersects at 10 rad/sec. Also, $W_1(s)$ is acting as a low-pass filter while $W_2(s)$ is acting as a high-pass filter.

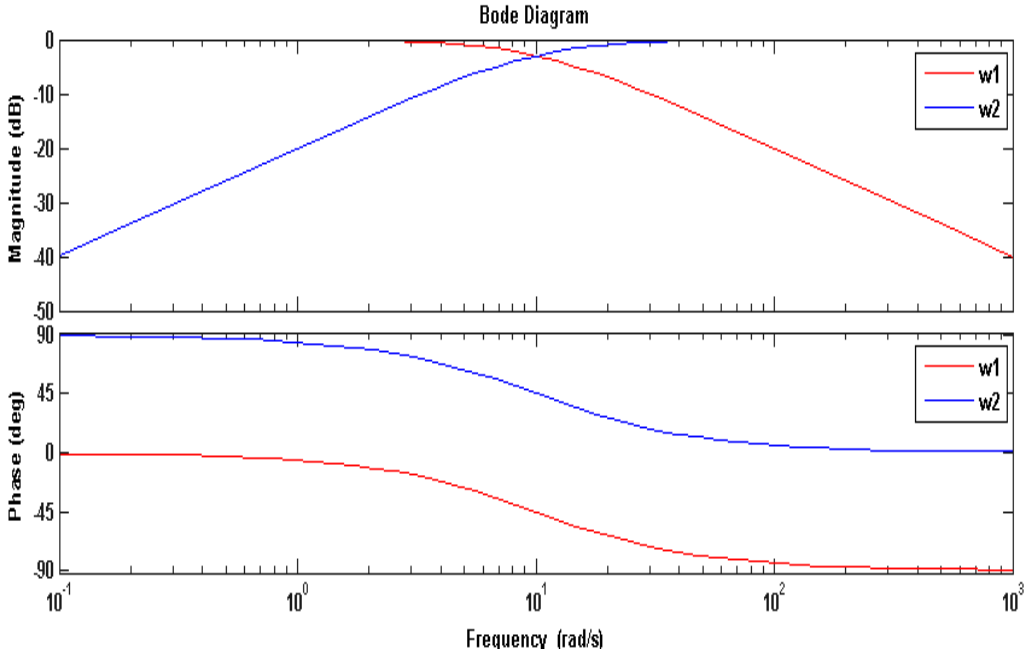

Figure 4.6 Frequency response of weights $W_1(s)$ and $W_2(s)$

As described in section 3.4, for achieving the faster response and to avoid fast dynamics and high-frequency gain in the controller, the closed loop poles of the system must be located in the D region of the left half plane (Figure 3.7). The placement of the poles in the D region ensures minimum damping (10%). The inner angle θ is set at 84° for this purpose. The design problem is solved by defining the objectives in the argument of the

function *hinfmix*, which is available in the LMI control toolbox of MATLAB [100].

By combining the weights with the reduced order plant, the controller design is carried out in LMI framework with pole placement. However, the order of the controller obtained is relatively high and it is difficult to implement practically. So, the order of the controller is further reduced. The finally obtained controller is of 9^{th} order. The controller matrices are shown in Appendix A7.

4.3.6 Robustness Evaluation of the Controller

To prove the robustness of the controller, the designed controller must be tested for various operating conditions of power system i.e. various loading conditions and various composition of load models. The closed loop performance of the designed TCSC WADC is as shown in Table 4.3. This result is for base case i.e. power flow in the tie-line is 376 MW and load compositions are purely constant impedance load. Table 4.3 clearly shows improvement in damping ratio of inter-area mode from 4.47% to 13.26%.

Table 4.3 Closed-loop performance of TCSC WADC

System	*f* (Hz)	Damping ratio ζ
Open loop	0.573	0.0447
TCSC WAD controller	0.57	0.1326

The performance of the controller is now assessed for the various load composition models proposed in Table 4.2. The results are shown in Table 4.4. Table 4.4 indicates considerable improvement in the damping ratio of critical mode for proposed load models. It has been observed that improvement in damping in case of load model II and V is less as compared to other cases. However, in these cases also the value of damping ratio is more than the specified value in the literature (minimum 10%).

The robustness of the designed TCSC WAD controller is also tested for various tie-line power flows. Tie-line power flow is increased from 100MW to 500 MW in steps. The results are shown in Table 4.5. The results show the robustness of the designed controller for various operating conditions.

The performance of the controller is also evaluated for tie-line power flow of 450 MW for proposed load models. Results are shown in Table 4.6. Results indicate the robustness of the designed TCSC WAD controller**.** Thus it can be concluded that the designed TCSC

WAD controller is robust enough for varying operating conditions and proposed load models. The robustness of the designed controller can be further accessed via nonlinear time domain simulations.

Table 4.4 Performance of TCSC WADC with proposed load models

Proposed load models	Open-loop system		Closed-loop system with TCSC WADC	
	Damping ratio (ζ)	Frequency (Hz)	Damping ratio (ζ)	Frequency (Hz)
I	0.0447	0.573	0.1326	0.570
II	0.0422	0.558	0.1079	0.551
III	0.0441	0.563	0.1208	0.559
IV	0.0440	0.566	0.1225	0.550
V	0.0431	0.559	0.1104	0.548
VI	0.0435	0.562	0.1182	0.545
VII	0.0432	0.560	0.1287	0.548

Table 4.5 Performance of TCSC WADC for various tie-line power flows

Tie line power flows (MW)	Open-loop system		Closed-loop system with TCSC WADC	
	Damping ratio (ζ)	Frequency (Hz)	Damping ratio (ζ)	Frequency (Hz)
100	0.0512	0.558	0.1705	0.588
200	0.0476	0.546	0.1557	0.576
300	0.0451	0.540	0.1412	0.559
400	0.0437	0.533	0.1215	0.544
500	0.0428	0.517	0.1166	0.527

From Table 4.3, 4.4 and 4.5, it is very clear that the closed loop performance of the designed TCSC WADC is robust for all operating conditions and various load composition models. The damping ratio in all tested conditions is more than 10% which is considered

to be the acceptable limit. However, improvement in constant power dominated load is less as compared to other cases.

Table 4.6 Performance of TCSC WADC for tie-line power flow of 450 MW

Proposed load models	Open loop system		Closed loop system with TCSC WADC	
	Damping ratio (ζ)	Frequency (Hz)	Damping ratio (ζ)	Frequency (Hz)
I	0.0435	0.527	0.1190	0.535
II	0.0410	0.510	0.1012	0.516
III	0.0429	0.515	0.1105	0.524
IV	0.0428	0.516	0.1121	0.516
V	0.0419	0.511	0.1065	0.513
VI	0.0423	0.514	0.1092	0.512
VII	0.0442	0.512	0.1171	0.520

4.3.7 Nonlinear Time-Domain Simulations

In a practical power system, the inter-area modes are excited by different contingency conditions emerging in power system. Such typical condition includes line faults, load shedding etc. The designed controller must be able to damp the oscillations produced in the power system due to these contingency conditions. Nonlinear time domain simulations are performed to prove the robustness of the designed controller under the influence of these conditions. Two such contingency conditions are simulated here:

1) Line fault: In this case, a transient line to ground fault near bus 20 in the line connecting bus 20 and bus 3 is simulated to check the performance of the designed controller. The dynamic response of the controller where the variations of the relative angle between generator 1 and generator 3 located in different areas are as shown in Figure 4.7. It can be seen that transient faults excite the oscillation in the test system. It can be seen that the TCSC WADC damped the oscillations within 15 seconds. Figure 4.8 shows the change in percentage compensation of TCSC for the same case.

2) Load shedding: For observing the performance of the TCSC WADC, the load on bus 15 is reduced from 1000 MW to 900 MW (i.e. 10.00 p.u. to 9.0 p.u.). The resulting change in the power flow in tie-line is as shown in Figure 4.9. The oscillations produced due to load shedding are clearly damped within 15 seconds.

Hence, we can conclude that the performance of the designed TCSC WADC is satisfactory for various operating conditions in the test system and for various contingency conditions.

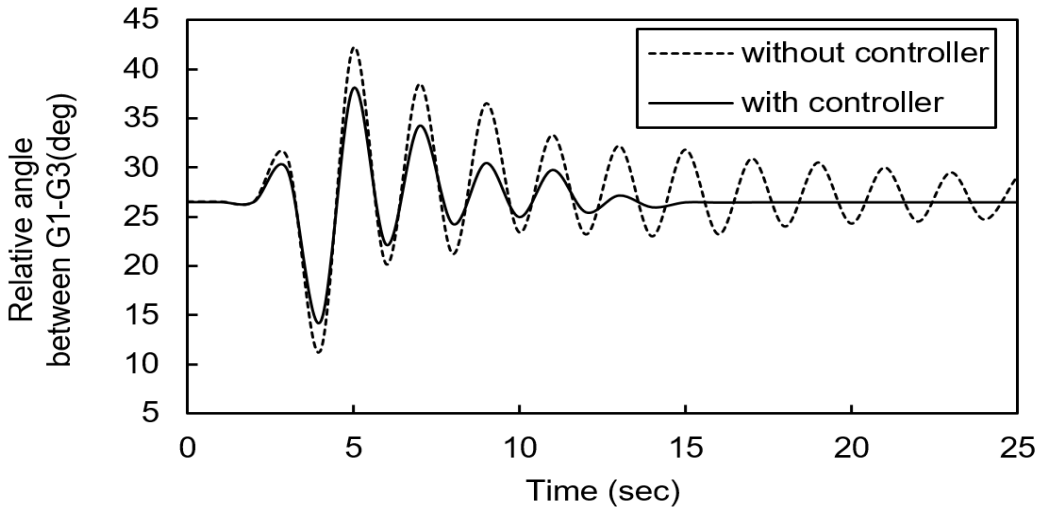

Figure 4.7 Dynamic response of TCSC WADC during line fault at bus 20 (Relative angle between G1-G3)

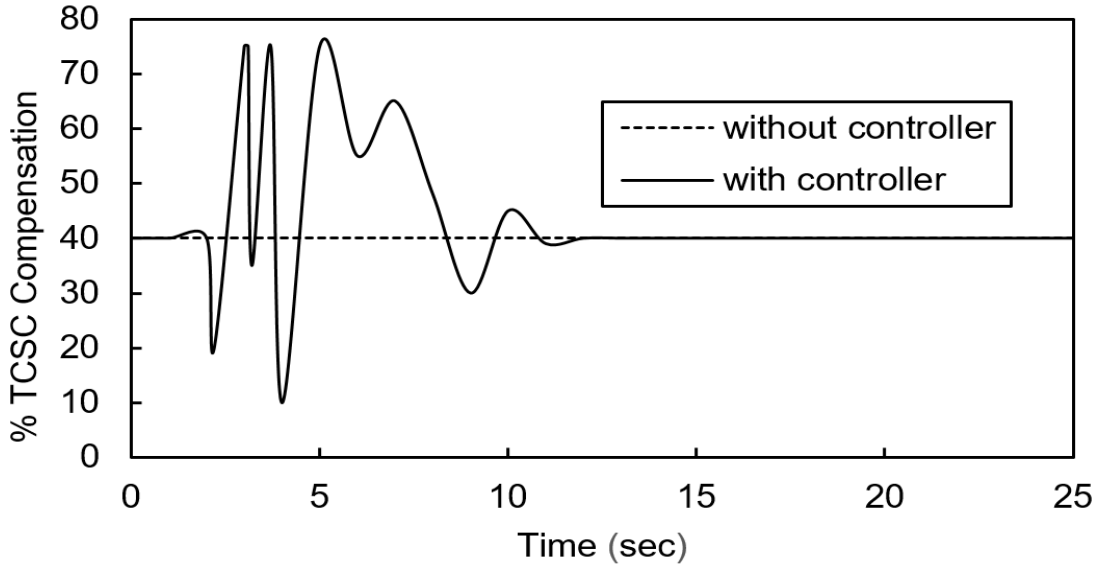

Figure 4.8 Dynamic response of TCSC WADC during line fault at bus 20 (% TCSC Compensation)

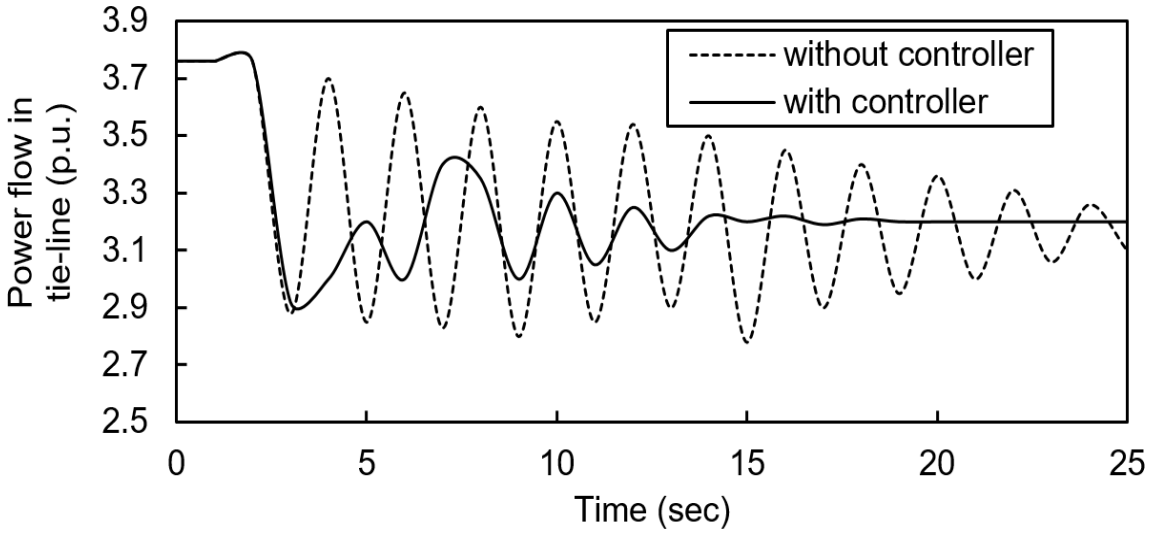

Figure 4.9 Dynamic response of TCSC WADC for load shedding at bus 15

4.4 Case Study II: Modified New York - New England (NY-NETS) Test System

The modified New York – New England test system consisting of 16 machines, 68 buses is as shown in Figure 4.10. It consists of five areas geographically dispersed through each other and connected through various tie-lines. Area 4 consists of machines G1-G9 and Area 5 consists of machines G10-G13. The other three neighboring areas (Area 1-Area 3) are represented by the equivalent machines G14-G16 (Area 1- G15, Area 2-G14, and Area 3-G16). The small signal analysis of the test system shows the existence of multiple inter-area mode oscillations. The resulting cumulative response of all the inter-area mode oscillations may result in instability of the test system. In such case, a single FACTS device may not be able to damp all the inter-area mode oscillations. Hence, for increasing the available transfer capacity of the network and damping of inter-area mode oscillations various FACTS devices are connected to the system. The test system consists of shunt FACTS device SVC connected at bus 51(Area 4), series FACTS device TCSC connected in the tie-line between bus 46 (Area 5) and bus 49 (Area 3) and UPFC located at bus 1 to control the power flow in the tie-line between Bus 1 (Area 5) and Bus 27(Area 4). The location of the devices is decided as in [59]. However, the HVDC link referred in ref. [59] is replaced by the UPFC. The detail information regarding the test system can be found in Appendix B [81].

As the number of FACTS devices in the test system are more, there may be chances of adverse interaction between the control actions of the FACTS devices. Such case may result in the poor performance of the designed controllers. This adverse interaction between the controllers can be avoided by designing the controller by the sequential approach. The details of the sequential approach for the coordinated design of multiple FACTS devices is explained in section 4.5.5.

Figure 4.11 gives a basic idea of wide area measurement for the test system. To acquire global signals, phasor measurement units (PMUs) are located strategically in different areas of the power system. The PMUs capture important dynamic data of the power system and transmit it to wide area controller (WAC) centers. The details of the WAM and WAC center are discussed in section 4.2.

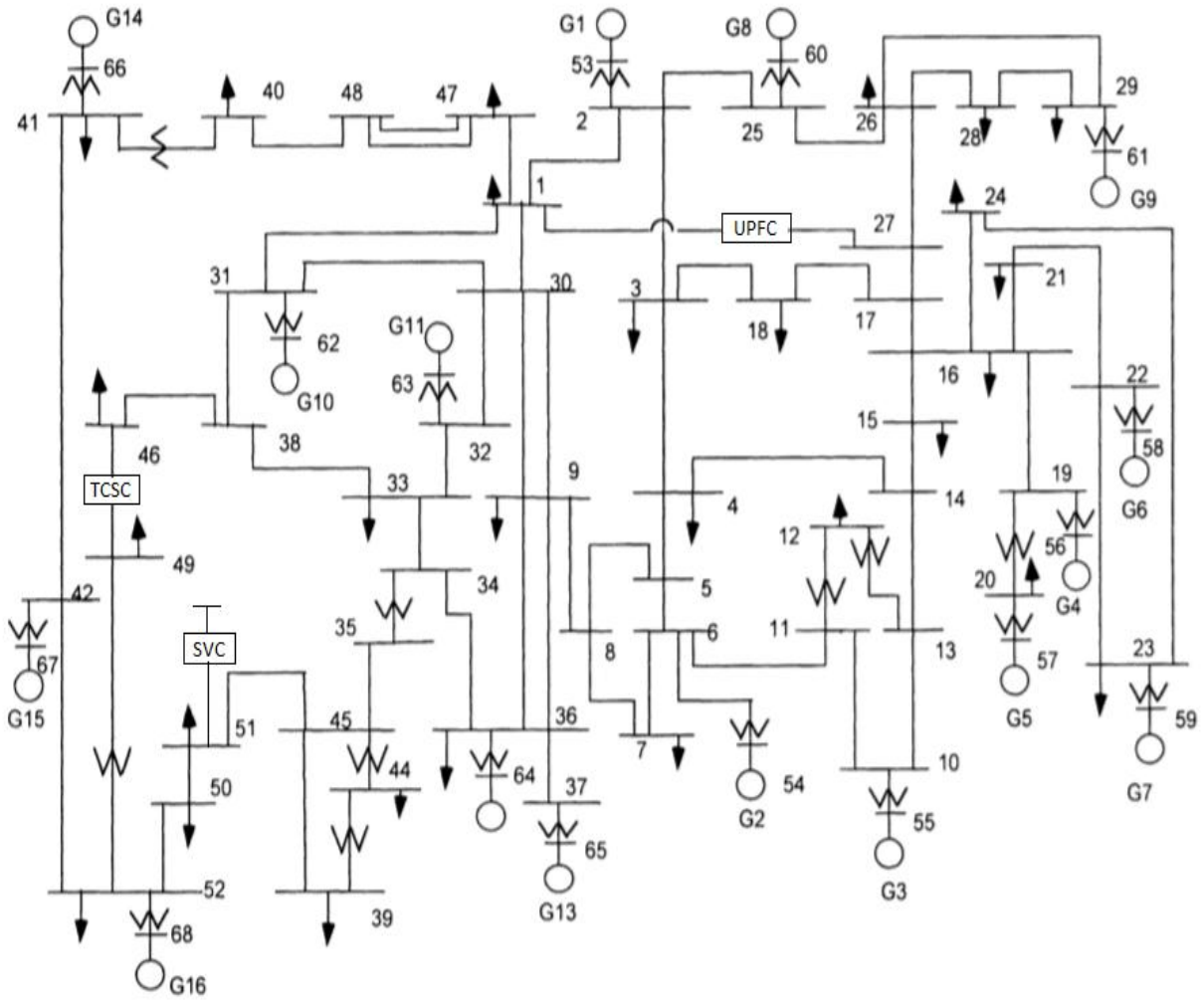

Figure 4.10 Modified NY-NETS test system

4.5 Sequential Design of Multiple WADC

The design of multiple WADC based on sequential approach includes the following steps:

4.5.1 Full Order Model and Small Signal Analysis

From the detailed modeling of all the components of the test system (i.e. generators, exciters, PSSs, FACTS devices etc.), a nonlinear model of the test system is developed which is of 211^{th} order. The modal analysis shows that this test system has 5 local modes and 3 inter-area modes oscillations which are lightly damped. The local mode oscillations are damped by PSSs. So, attention is given only to inter-area modes. The detail of the inter-area modes is as shown in Table 4.7. The mode shape of various inter-area mode oscillations are drawn for speed component of the right vector through compass chart as shown in Figure 4.12(a) - Figure 4.12 (c).

Table 4.7 clearly indicates that, in mode 1, generators of area 1, 2, 4 oscillates against generators of area 3, 5. In mode 2, generators of area 1, 3, 4 oscillates against area 2, 5. In mode 3, generators of area 1 oscillate against area 2, 3. These oscillations if not damped out, endanger the stability of the network.

Table 4.7 Critical inter-area mode oscillations of NY-NETS test system

Mode Index	Eigenvalues	*f* (Hz)	Damping ratio ζ	Mode Shape
1	-0.16 ±3.45i	0.5485	0.0475	G1-G9,G14,G15 Vs. G10-G13,G16 (Area 4,1,2 Vs Area 3,5)
2	-0.18 ± 4.10i	0.6527	0.0445	G1-G9,G15,G16 Vs. G10-G13, G14 (Area 4,1,3 Vs. Area 5,2)
3	-0.29 ± 5.08i	0.8083	0.0565	G14,G16 Vs. G15 (Area 2,3 Vs. Area 1)

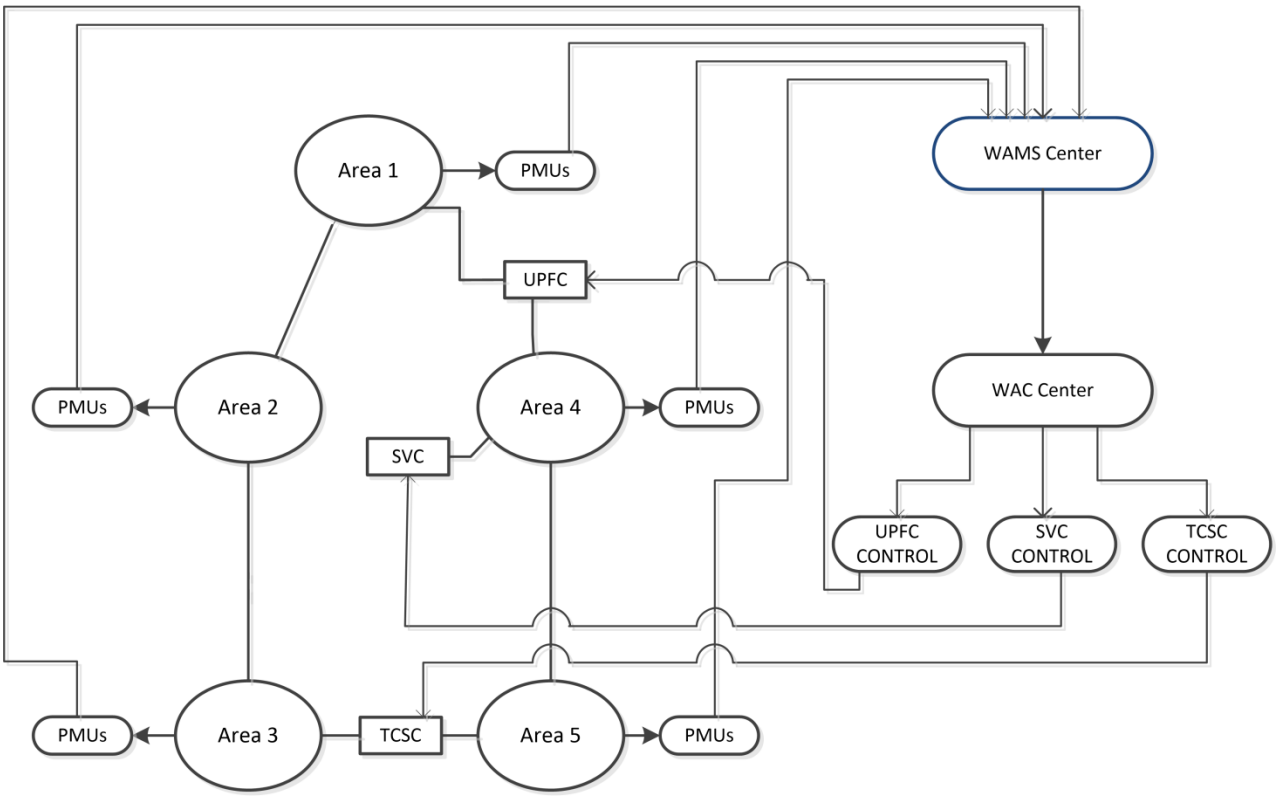

Figure 4.11 Basic structure of wide- area measurements using FACTS controllers

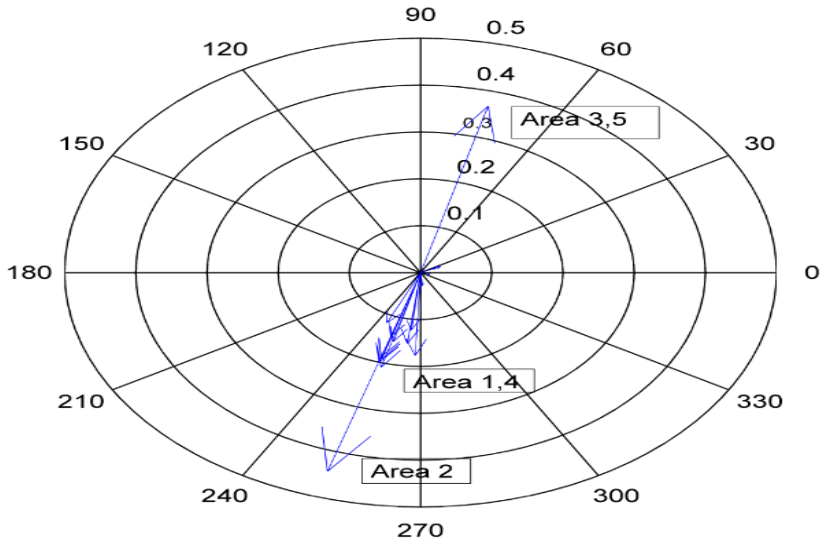

Figure 4.12 (a) Speed component of right eigenvector for mode 1

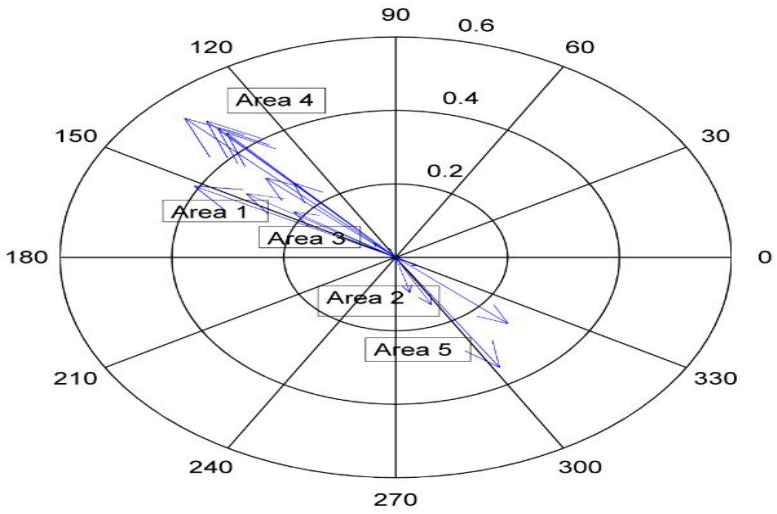

Figure 4.12 (b) Speed component of right eigenvector for mode 2

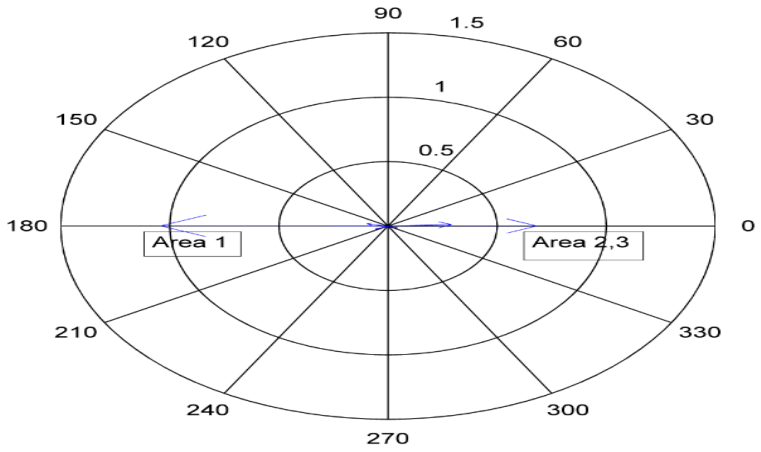

Figure 4.12 (c) Speed component of right eigenvector for mode 3

4.5.2 Selection of Suitable Global Signal

For proper damping of critical oscillations, selection of suitable control signal is equally important. Residue analysis is carried out for various modes with various FACTS devices to determine the best suitable control signals. As discussed in section 4.3.2, the line active power is considered as a control input for each concerned inter-area mode. Figure 4.13(a) - Figure 4.13(c) show the absolute values of residues of various modes of oscillations with different FACTS devices. From the Figure 4.13(a) and Figure 4.13 (b), it is clear that SVC has better damping performance for mode 1 and 2 as compared to other two FACTS devices while from Figure 4.13 (c) it is clear that UPFC has better damping performance for mode 3 than other FACTS devices.

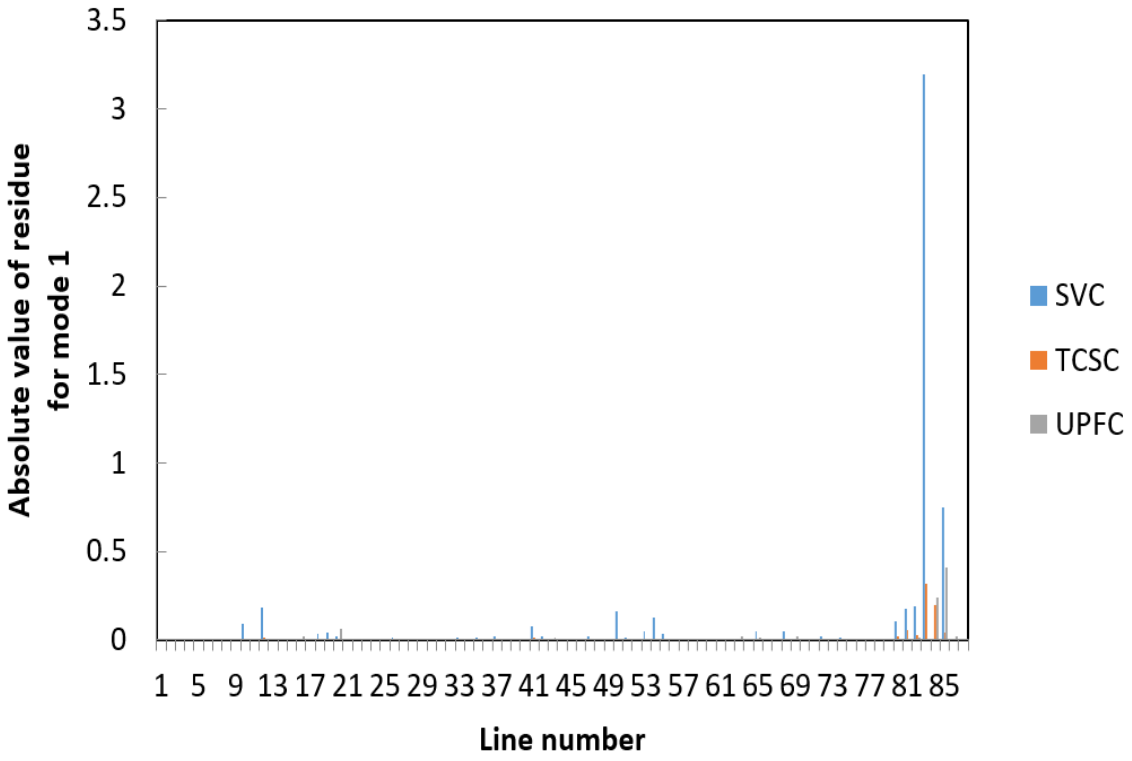

Figure 4.13 (a) Residue analysis of different FACTS controller for mode 1

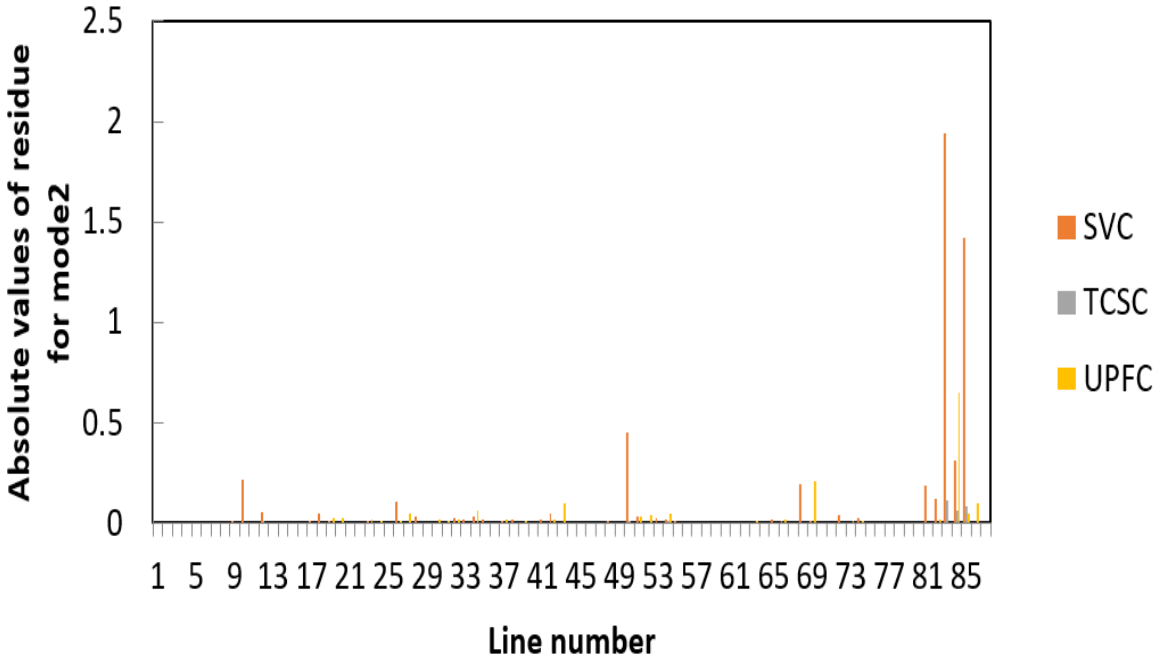

Figure 4.13 (b) Residue analysis of different FACTS controller for mode 2

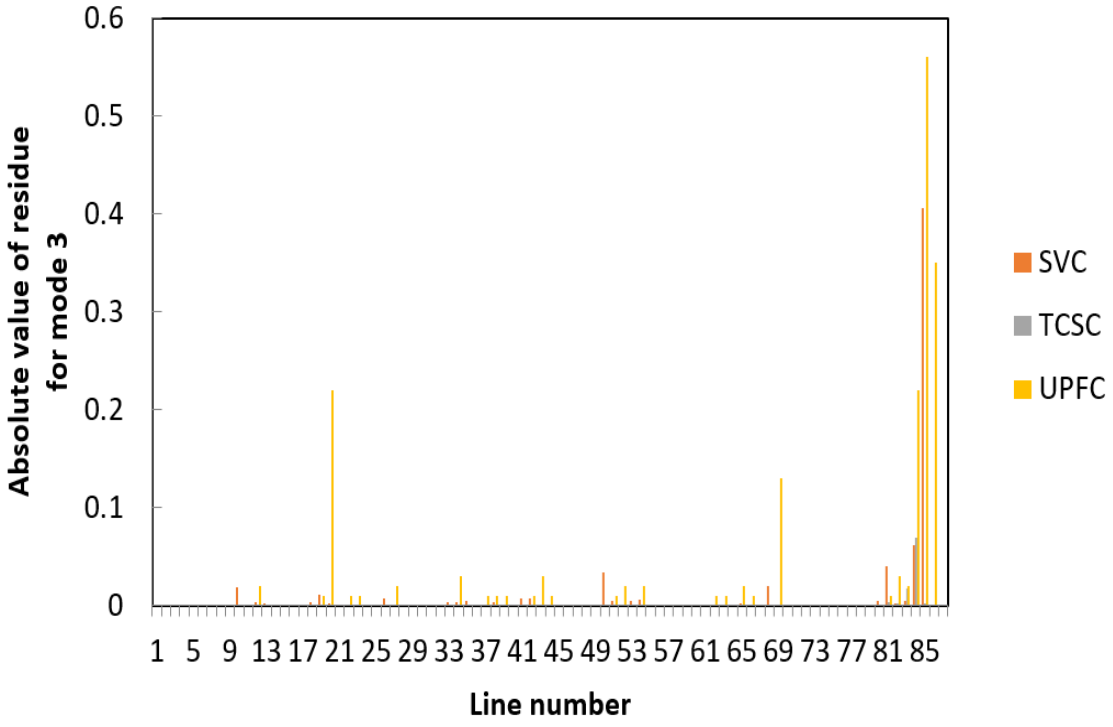

Figure 4.13 (c) Residue analysis of different FACTS controller for mode 3

Thus active power in line 83 (between bus 41-bus 66) is selected as a control signal for SVC WADC for damping mode 1 and mode 2, while active power in line 85 (between bus 42-bus 67) is selected as a control signal for UPFC WADC for damping mode 3. Although TCSC was considered as the probable device for designing WADC, absolute values of residue for all modes in case of TCSC are very less as compared to other FACTS devices. It means TCSC cannot provide effective damping to above critical modes. Hence, finally, SVC and UPFC are considered for designing the WADC.

4.5.3 Reduction of Model Order

As discussed in section 4.2.3, all the states of the linear model do not affect the inter-area modes. Therefore, it is necessary to reduce the order of the system. Schur balanced model reduction procedure is followed for reducing the order of the plant [101]. For the SVC WADC, the system model order is reduced to 12^{th} order from 211^{th}order. For the design of UPFC WAC design, the original system which is reconstructed with SVC WAC model is reduced to 12^{th} order from 225^{th} order. Figure 4.14 (a) shows the frequency response of the full order and the reduced order system in case of the SVC WADC, while Figure 4.14 (b) shows the full and the reduced order system in case of UPFC controller. It

can be seen that the reduced order system model is a close approximation of original system. It needs to be taken care that as the gain plot of both full order and reduced order system in both case are closely matching each other, so it is difficult to differentiate full order and reduced order amplitude plot in Figure 4.15 (a) and Figure 4.14 (b). Hence, both SVC WADC and UPFC WADC are suitable for the design of the robust controller.

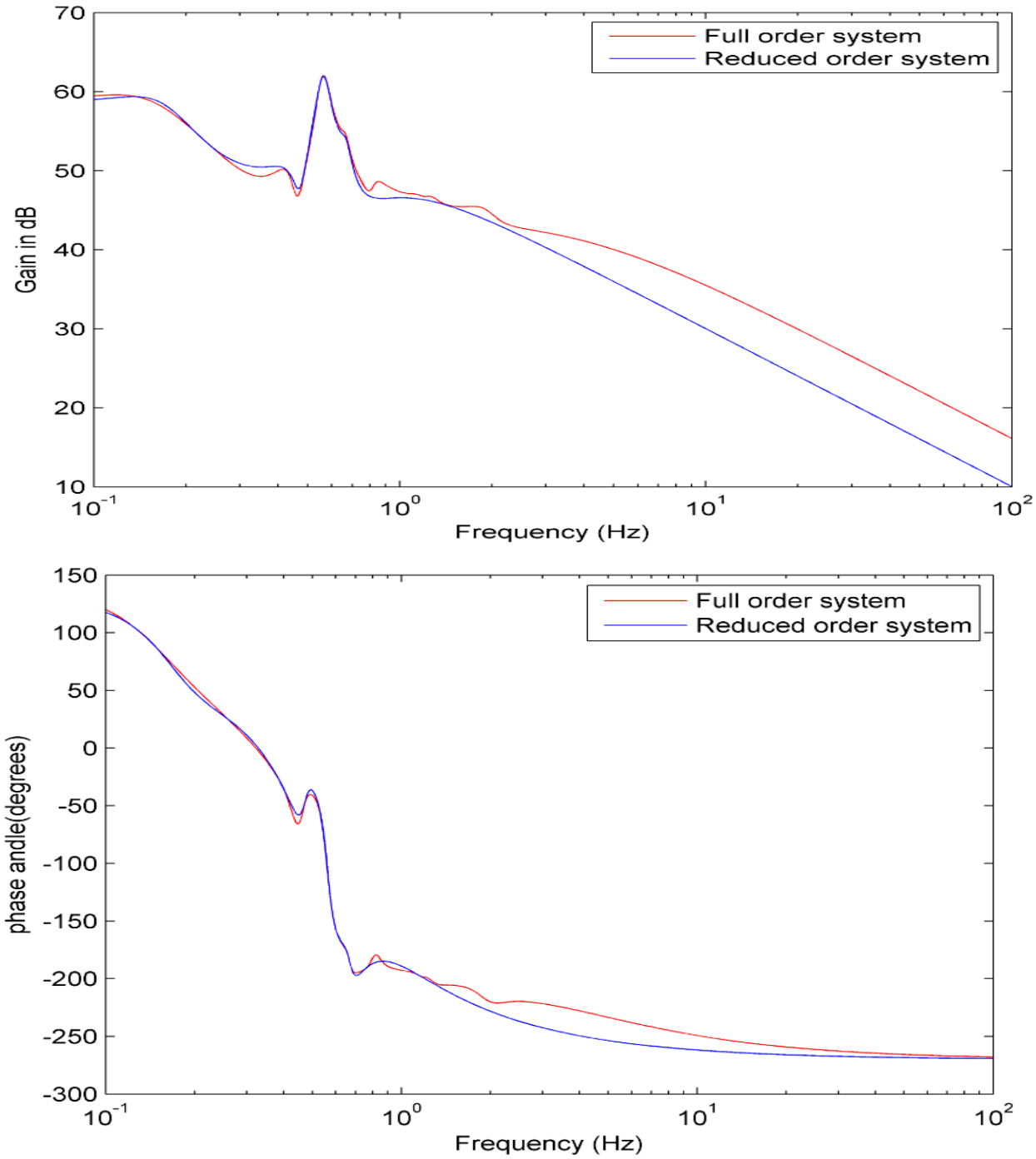

Figure 4.14 (a) Frequency response of both full and reduce order SVC WAC

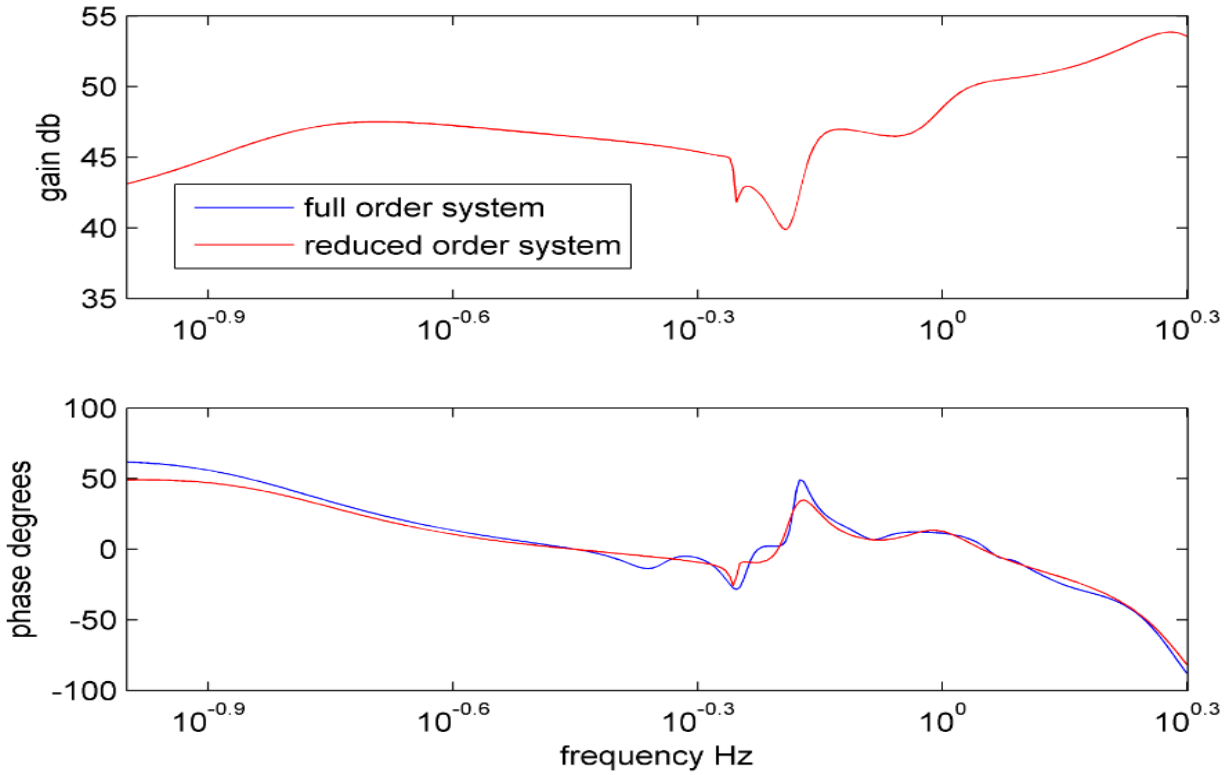

Figure 4.14 (b) Frequency response of both full and reduce order UPFC WAC

4.5.4 Proposed Load Models

The designed controllers must be tested for proposed load models which are discussed in section 4.3.4 as per Table 4.2.

4.5.5 Controller Synthesis

In case of multi-area, multi-machine test system, a number of inter-area mode oscillations are more than one. A single FACTS device cannot damp out all the inter-area mode oscillations. Hence, multiple FACTS devices are needed to damp all the inter-area mode oscillations [59]. However, while employing multiple FACTS devices, there may be chances of interaction among the control actions taken by the individual device. Such interaction may adversely affect the ability of the individual FACTS device in damping the concern inter-area mode oscillation. To avoid such interaction among the FACTS devices, the sequential design approach for proper coordination among various FACTS devices is used [59,102,103,104]. Multi-objective mixed H_2/H_∞ synthesis combined with a sequential approach for designing the WADC ensures robustness of the designed WADC. The steps to be followed for such design are mentioned below (Although some steps are the

repetition of the procedure we carried out, for better understanding they are mentioned here):

Step 1: Form the linearized model of the test system and carry out small signal stability analysis of the test system (refer section 4.3.1).

Step 2: Based on the controllability/observability index and residue analysis, select the suitable global signals as an input signal to each control device (refer section 4.3.2).

Step 3: This step involves the application of the sequential approach. From the linearized plant model achieved in step 1 and global input signal obtained for the controllers from the step 2, carry out multi-objective mixed H_2/H_∞ controller synthesis as per section 4.3.5 for first WAC design. The closed-loop system model is then formed for the original plant model and first WADC obtained. This closed-loop system model of the original plant and first WAC will act as open loop plant model for the second WAC. Similarly, when the second WAC is obtained, it can be used to form the open loop plant model for third WAC and so on. For each controller design, the multi-objective mixed H_2/H_∞ controller synthesis is performed for the updated open-loop plant with the FACTS device.

Step 5: Evaluate the performance of the designed controller for robustness as mentioned in section 4.3.5 and carry out nonlinear time domain simulations to prove further robustness as mentioned in section 4.3.6.

As discussed in section 4.3.5, before designing the controller, proper weights as low-pass and high-pass filters are to be selected. The selected weights for both SVC WADC and UPFC WADC are as follows:

$$W_1(s) = 10/(s+10) \quad (4.4)$$

$$W_2(s) = s/(s^2+s+50) \quad (4.5)$$

$$W_3(s) = 1 \quad (4.6)$$

The pole placement angle θ is set at 84º to ensure minimum 10% damping ratio. By combining the weights with the reduced order plant, the controller design is carried out in LMI framework with pole placement for SVC WADC. The closed loop system of original plant and SVC WADC act as open loop plant for UPFC WADC (The selection of either SVC first or UPFC first is at random). However, the order of the controllers obtained is

relatively high and it is difficult to implement practically. So, the order of the controllers is further reduced. The finally obtained SVC WADC is of 12^{th} order and UPFC WADC is also of 12^{th} order. The transfer functions of both SVC WADC and UPFC WADC are shown in Appendix B6.

4.5.6 Robustness Evaluation of the Controller

The small signal stability analysis is carried out to evaluate the robust performance of the designed wide area controllers. The procedure discussed in the earlier sections was applied to design SVC WAC and UPFC WAC. The reduced order SVC WAC and UPFC WAC are described in Appendix B6. The improvement in the damping ratios and oscillation frequencies of critical modes for constant impedance load (base case) by the designed SVC WADC, UPFC WADC and by sequential approach WADC are as indicated in Table 4.8. Table 4.8 clearly indicates the improvement in the damping ratio with both wide area controllers. It is clear that, for both mode 1 and 2, SVC WAC gives better performance in terms of damping. For mode 3, UPFC WAC is more effective than SVC WAC. The sequential approach results in further improvement for damping of inter-area modes as compared to two individual WADCs. The response of the coordinated wide-area controller for various load models proposed in Table 4.2 is accessed and the results for the same is as shown in Table 4.9. Table 4.9 clearly indicates that the designed WADC are able to provide sufficient damping in all proposed load model scenarios. However, the improvement in damping in case of proposed load model II and V are the least as compared to other load models.

Table 4.8 Closed-loop performance of different WADC

Mode Index	Open-loop		Closed-loop with SVC WADC		Closed-loop with UPFC WADC		Closed-loop with SVC & UPFC WADC	
	f(Hz)	***ζ***	***f(Hz)***	***ζ***	***f(Hz)***	***ζ***	***f(Hz)***	***ζ***
1	0.548	0.0475	0.524	0.156	0.538	0.102	0.512	0.1738
2	0.652	0.0445	0.661	0.138	0.557	0.1123	0.654	0.181
3	0.808	0.0565	0.788	0.109	0.825	0.1517	0.829	0.1898

Table 4.9 Closed-loop performance of SVC - UPFC WADC for proposed load models

Load Model	Mode 1		Mode 2		Mode 3		Type of load
	f(Hz)	*ζ*	*f(Hz)*	*ζ*	*f(Hz)*	*ζ*	
I	0.512	0.1738	0.654	0.1810	0.829	0.1898	CI
II	0.505	0.1217	0.611	0.1224	0.810	0.1192	CP
III	0.507	0.1418	0.641	0.1456	0.837	0.1589	CC
IV	0.510	0.1562	0.638	0.1501	0.826	0.1614	CI=CP+CC
V	0.520	0.1389	0.647	0.1449	0.814	0.1376	CP=CI+CC
VI	0.508	0.1417	0.642	0.1457	0.836	0.1498	CC=CI+CP
VII	0.517	0.1304	0.614	0.1322	0.818	0.1251	CI+ Dynamic

The robustness of the designed controller is also checked for various line outages. Table 4.10 shows the performance of the WADC for various tie-line outages. Significant improvement is observed in all cases of line outages.

Hence, it can be concluded that the sequential approach of designing SVS-UPFC WADC results in robust performance of the designed controller. It provides sufficient damping to inter-area modes under various contingency conditions.

4.5.7 Nonlinear Time-Domain Simulations

For validating the performance of the sequentially designed SVC-WADC FACTS controller, the nonlinear time-domain simulation was performed for various contingency conditions like line outage, line faults, and load shedding etc. on the test system.

a) Line fault: A line to ground fault is simulated at bus 45, which connects important tie-line between bus 45 and bus 51. This fault excites the inter-area oscillations. The variations in relative angle between generators G14 - G16 and G15-G16 can be observed in Figure 4.15(a) and Figure 4.15(b). It is very clear from the figures that with the designed damping controller, the oscillations are damped out within 10-12 seconds.

Table 4.10 Closed-loop performance of SVC- UPFC WADC for various tie-line outages

Line outage	Mode 1		Mode 2		Mode 3	
	f(Hz)	***ζ***	***f(Hz)***	***ζ***	***f(Hz)***	***ζ***
1-47	0.501	0.1651	0.623	0.161	0.809	0.1608
8-9	0.511	0.1525	0.611	0.152	0.801	0.1595
33-38	0.507	0.1429	0.603	0.149	0.788	0.1478

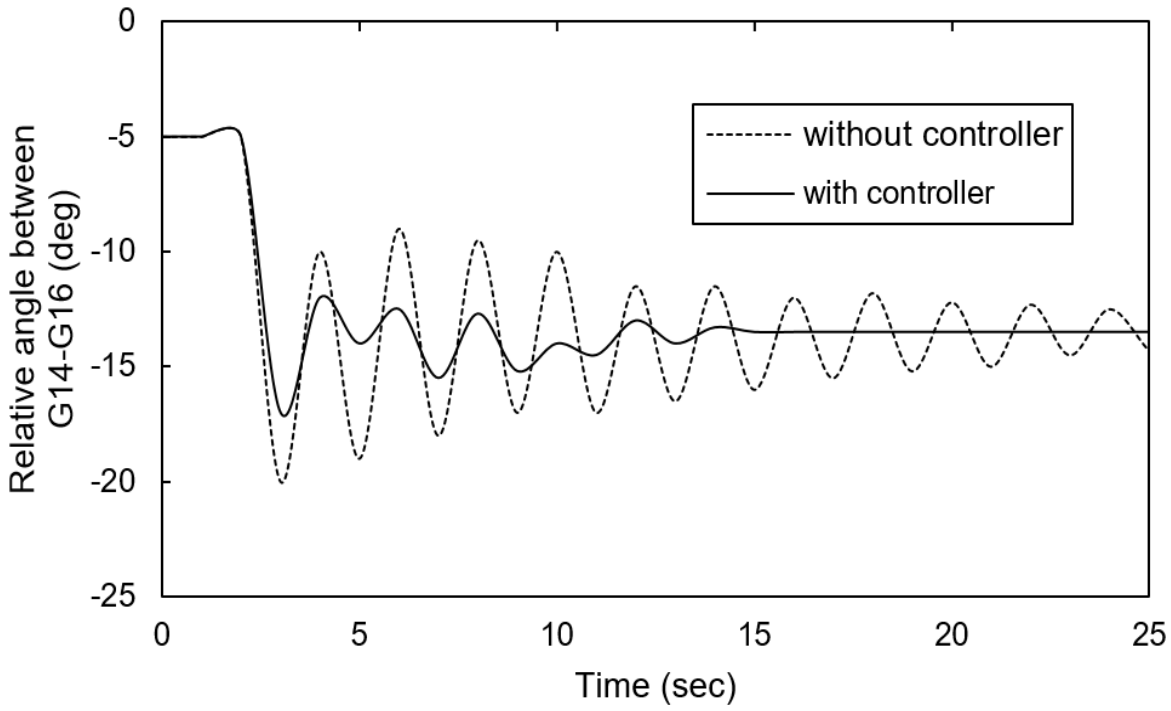

Figure 4.15(a) Dynamic response of SVC-UPFC WADC during the line fault at bus 45 (Relative angle between G14-G16)

Further Figure 4.16 (a) and Figure 4.16(b) indicated the individual responses of SVC WAC and UPFC WAC to the fault. From these responses, it is clear that both WACs are capable to damp the oscillations within the stipulated time.

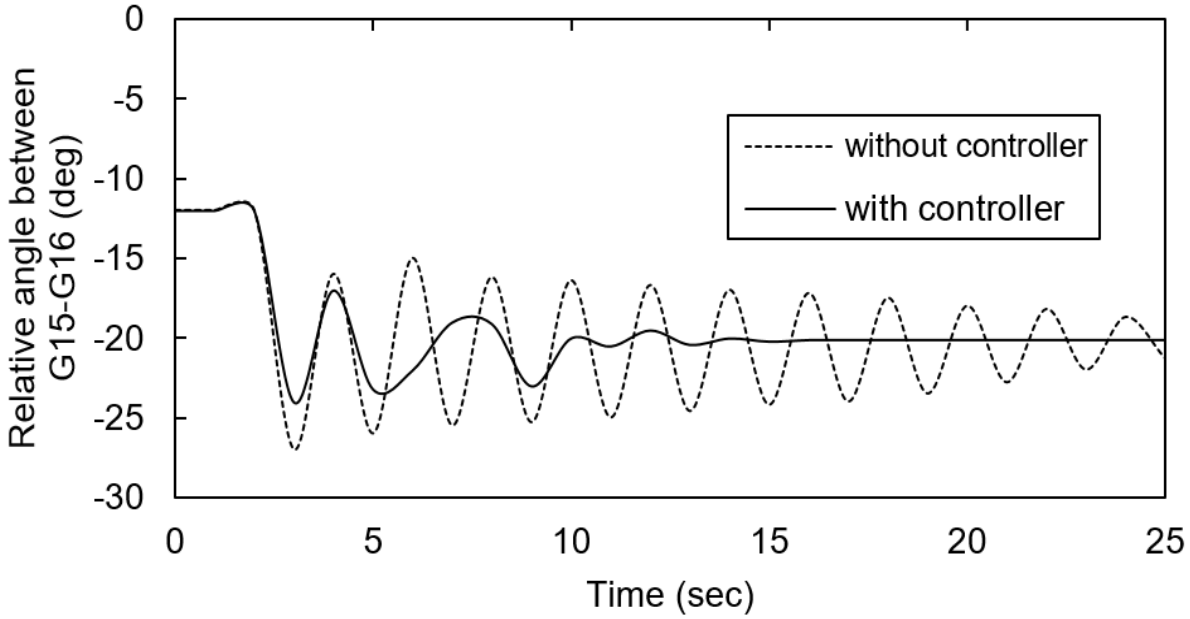

Figure 4.15(b) Dynamic response of SVC-UPFC WADC during the line fault at bus 45 (Relative angle between G15-G16)

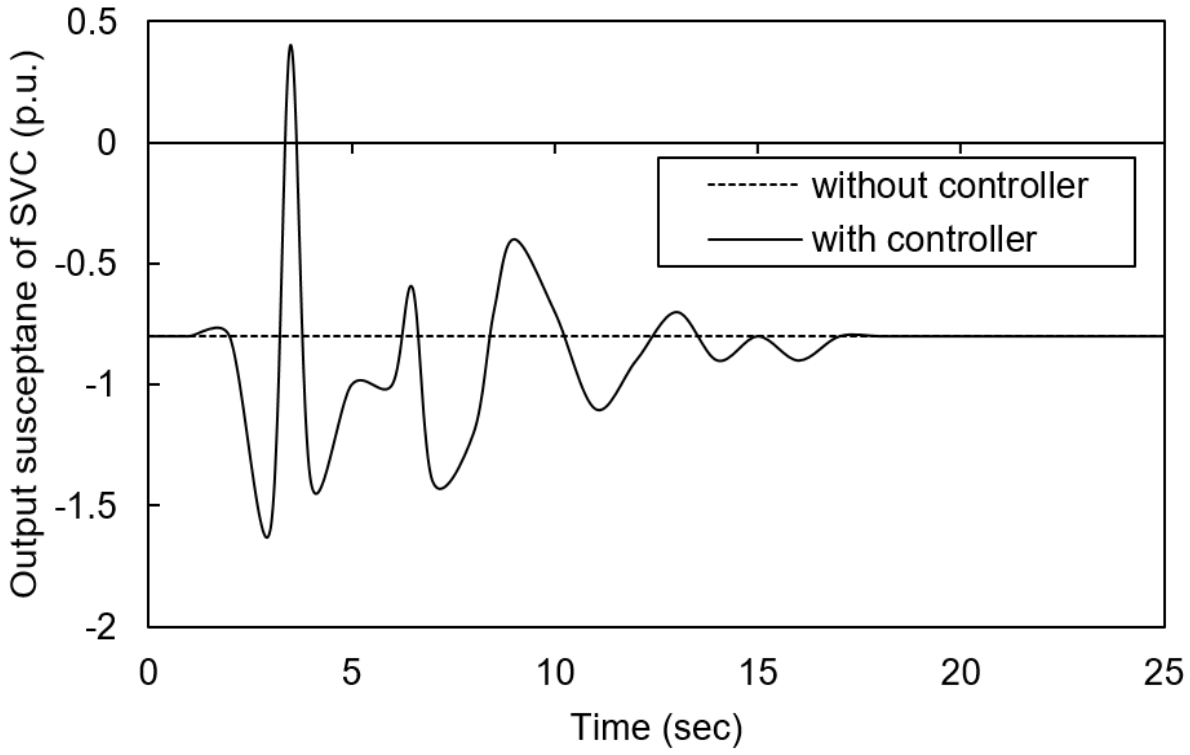

Figure 4.16 (a) Dynamic response of SVC WADC during line fault at bus 45 (Output susceptance of SVC)

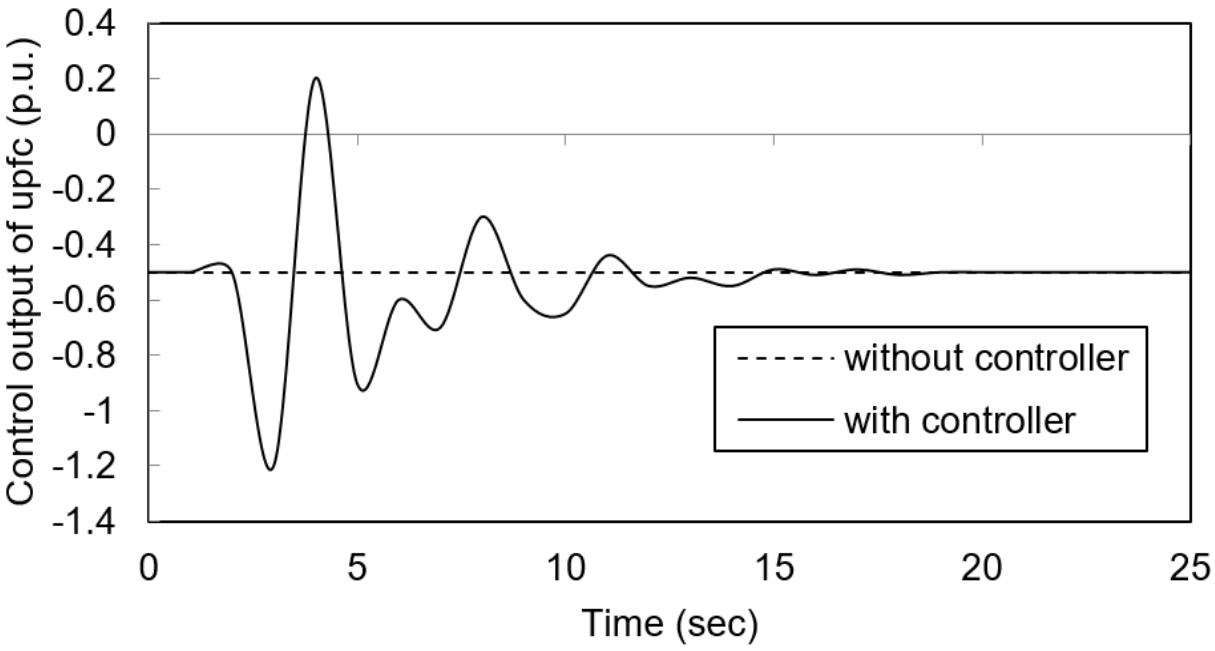

Figure 4.16 (b) Dynamic response of UPFC WADC during line fault at bus 45 (Control output of UPFC)

b) Line outage: In this case, an important tie line connecting bus 42 and bus 52 (area1 and area 3) has an outage of 1.0 sec. The response of the test system was observed with and without the WAC controllers and are as shown in Figure 4.17(a) and Figure 4.17 (b). The oscillations in the relative angle between the generators die down rapidly. Also, this outage will affect the power flow in other important tie lines. Figure 4.18 (a) and Figure 4.18 (b) shows the power flow in other important tie lines (the line between bus 37-bus 65 and line between bus 52- bus 68) with and without WADCs. It can be observed that oscillations in the line power are damped successfully with the designed controller.

c) Load shedding: In this case, the shedding of the load on bus 49 is carried for 1 sec to study the robustness of the designed controller. The resulting dynamic response of relative angle between G14 and G16 (area 2 and area 3) is represented in Figure 4.19(a). The variation in power flow in important tie-line between bus 41 and bus 66 is represented in Figure 4.19(b). All the responses indicate that the proposed WACs can play an effective role in damping inter-area oscillations and exhibit robust performance under this contingency.

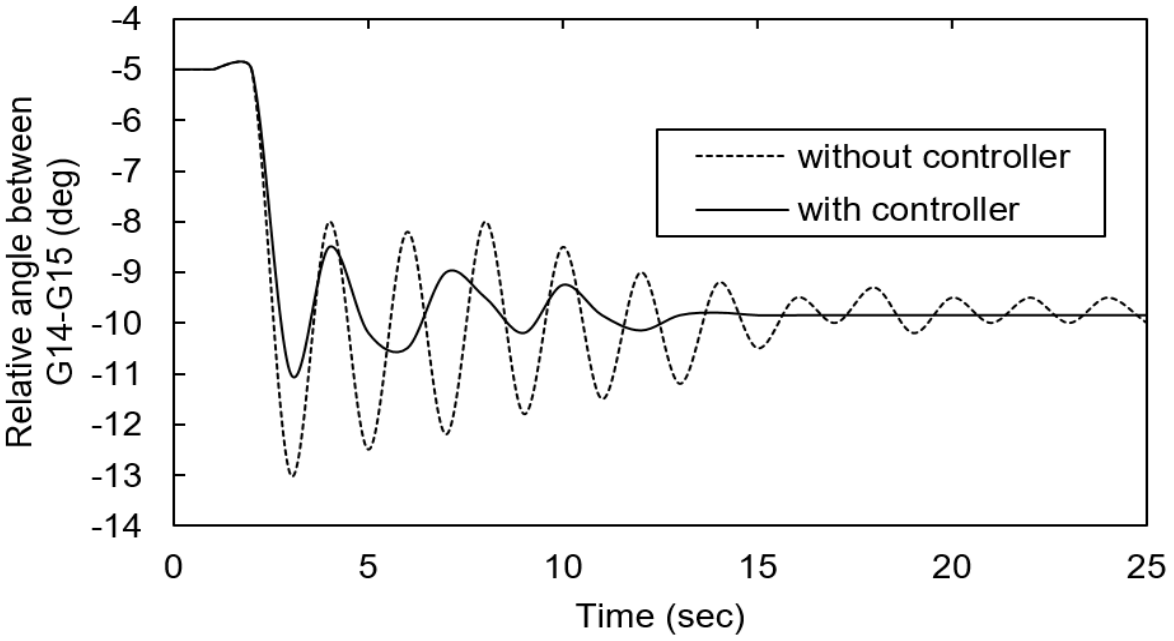

Figure 4.17(a) Dynamic response of SVC-UPFC WADC during an outage of the tie-line between bus 42-bus 52 (Relative angle between G14-G16)

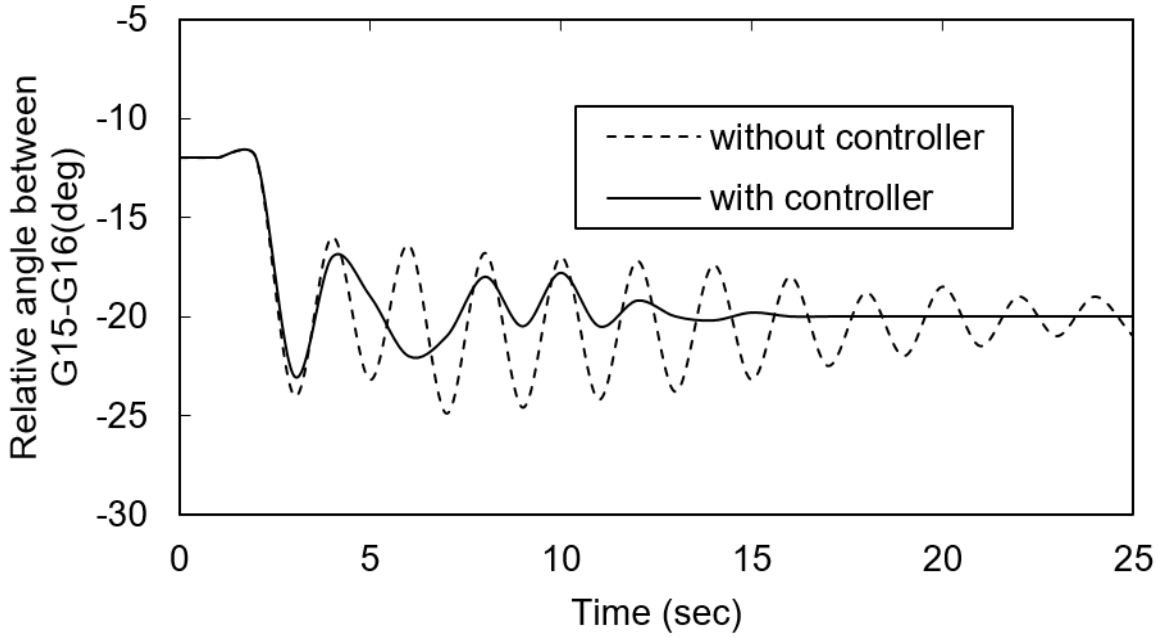

Figure 4.17(b) Dynamic response of SVC-UPFC WADC during an outage of the tie-line between bus 42-bus 52 (Relative angle between G15-G16)

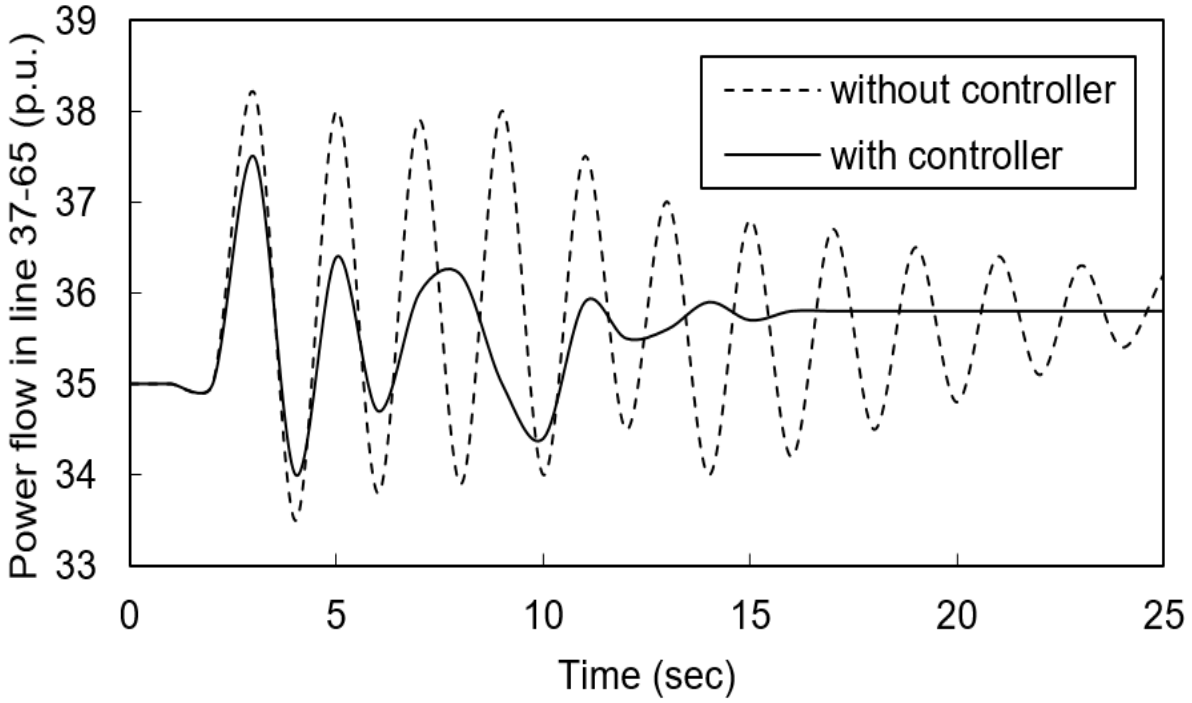

Figure 4.18 (a) Dynamic response of SVC-UPFC WADC during line outage of the tie-line (42-52) (Power flow in the tie-line connecting bus 37- bus 65)

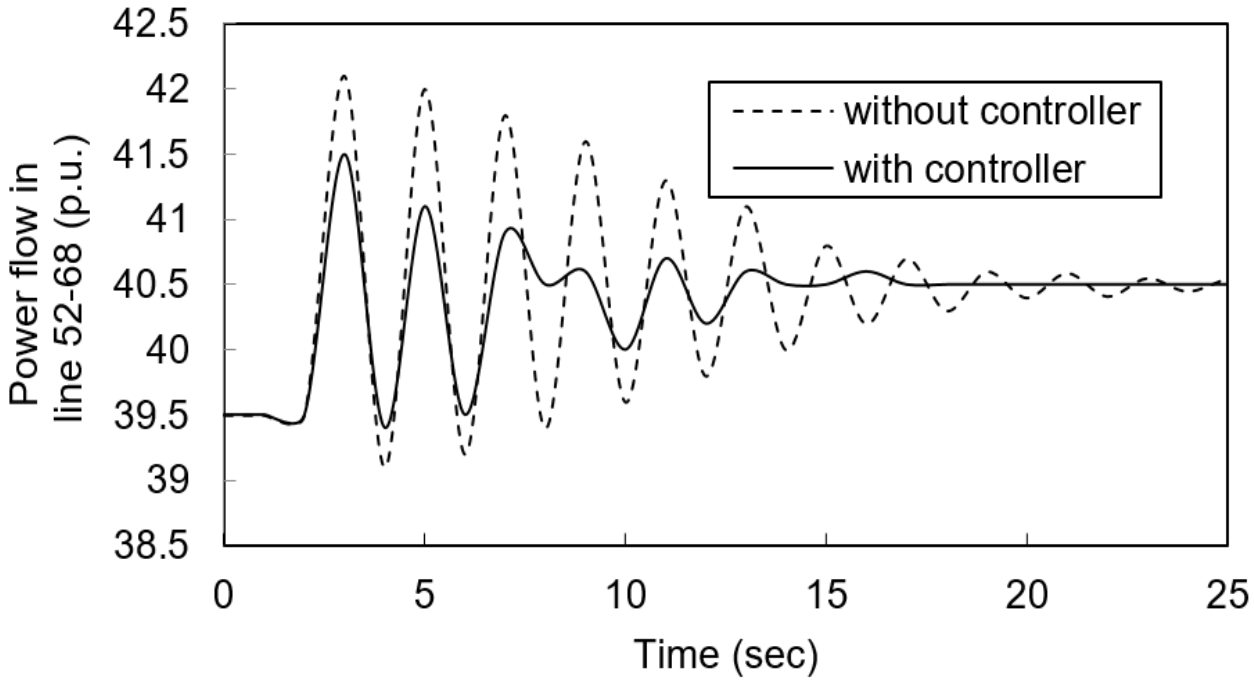

Figure 4.18 (b) Dynamic response of SVC-UPFC WADC during line outage of the tie-line (42-52) (Power flow in the tie-line connecting bus 52- bus 68)

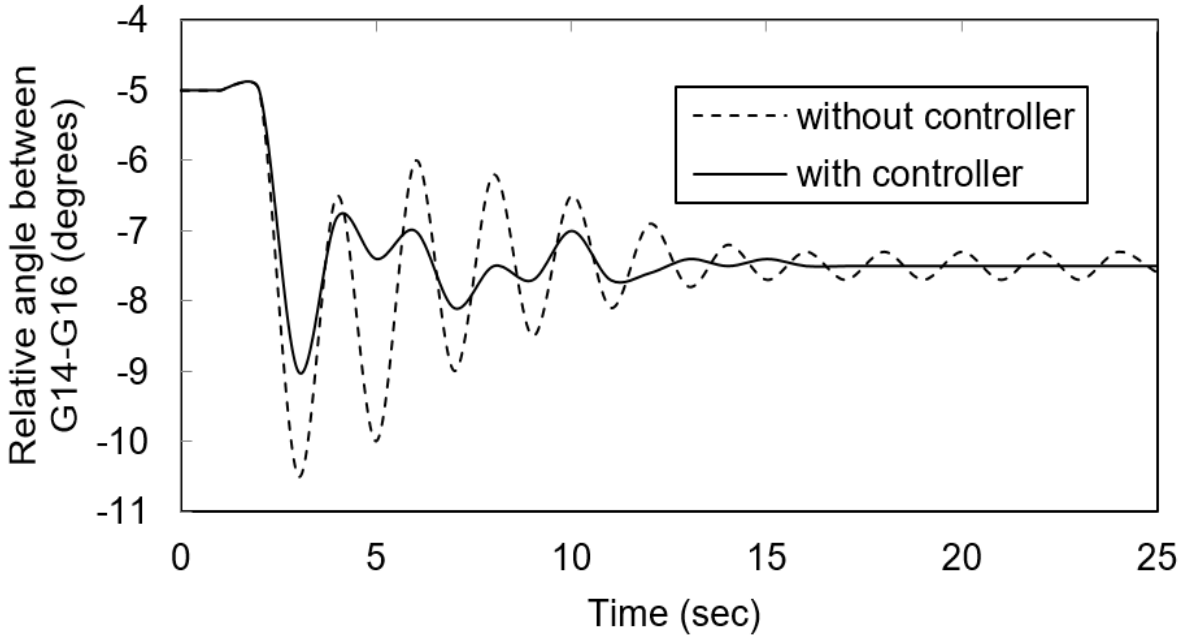

Figure 4.19(a) Dynamic response of SVC-UPFC WADC during load shedding at bus 49 (Relative angle between G14-G16)

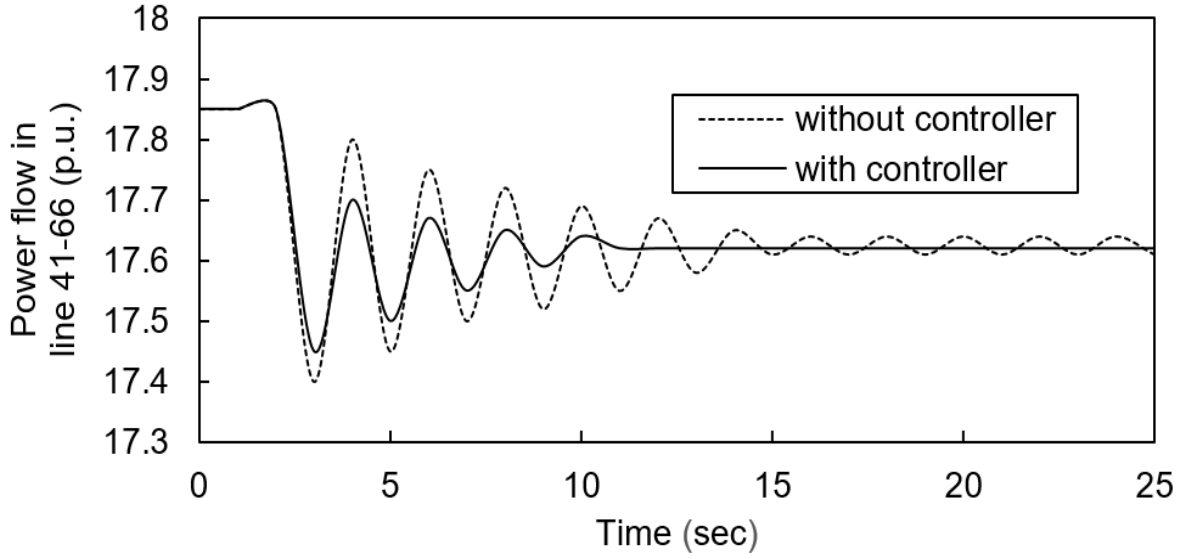

Figure 4.19(b) Dynamic response of SVC-UPFC WADC during load shedding on bus 49 (Power flow in tie-line connecting bus 41-bus 66)

Thus, the designed SVS-UPFC was tested for different operating conditions appear in power system as well as various contingencies like line faults, line outages and load shedding etc. The performance of the designed WADC was found to be robust for such

conditions. The oscillations produced by such contingency conditions were damped within 12-15 seconds. In almost all cases, the controller reduces the settling time and the first peak after initiation of disturbances.

4.6 Summary

In this chapter two case studies for the design of robust WADC based on mixed H_2/H_∞ output feedback control with pole placement in LMI framework are carried out. The first WADC was designed for two area four machine test system with TCSC while the second controller was designed for modified New-York New England test system with SVC and UPFC. The sequential design approach is applied to the design of SVC-UPFC WADC. The designed controller is found to be robust for varying operating conditions arising in power system and various contingency conditions like line faults, line outages and load shedding etc.

CHAPTER 5 CASE STUDY ON H_∞ LOOP SHAPING USING LMI

5.1 Introduction

As discussed in section 3.6, the mixed sensitivity based LMI approach suffers from two major drawbacks: The selection of proper weights is a difficult task and the dynamic properties of the plant model are not taken into consideration while specifying the performance criteria. However, these drawbacks can be overcome by H_∞ loop shaping using LMI [42, 43]. The H_∞ loop shaping method uses the weighting functions to shape the open loop matrix rather than the closed loop functions S, KS and T. It focuses on maximizing the robustness to co-prime factor uncertainty rather than multiplicative or additive uncertainty. This results in a very attractive design procedure which yields controller with strong robustness properties [105]. The H_∞ loop shaping offers following advantages [98,106]:

- No γ- iteration- the optimal solution of the H_∞ loop shaping controller can be found without the recourse of the γ- iteration which makes it attractive.
- By maximizing robustness to normalized coprime factor uncertainty, it provides robustness to unstable perturbations and uncertainty in the location of lightly damped resonant poles.
- No pole-zero cancellations which are very common in H_∞ design.
- The conflicts in the selection of weights in case of S and KS is not easy and some trade-off is required around the desired loop bandwidth frequency. In case of H_∞ loop shaping, this problem does not arise, as shaping the open loop matrix simultaneously shapes the S and KS and thus eliminating the possibility of choosing conflicting weights.
- Provides balanced robustness and performance properties at the plant input and output.
- Guaranteed simultaneous gain and phase margins.

Due to above-mentioned advantages, in this chapter, LMI approach to H_∞ loop shaping technique is applied to the design of WADC for 10-machine 39-bus modified New

England test system. The designed WADC is tested for various contingency conditions to ensure the robustness.

5.2 The 10-Machine 39-Bus Modified New England Test System

Figure 5.1 shows 10-machine 39-bus modified New England test system. The test system is modified to include a FACTS device. Reference [107] suggested an optimal location of series FACTS device between bus 16 and bus 21. Hence, UPFC is connected at bus 16 for control of power flow in the line connecting bus16- bus 21.The power flow in the line connecting bus16-bus 21 is 330 MW. The other detail regarding the generators, exciter, PSSs and system parameters are given in Appendix C [81]. To acquire the important system parameters, PMUs are located at the important buses in the test system.

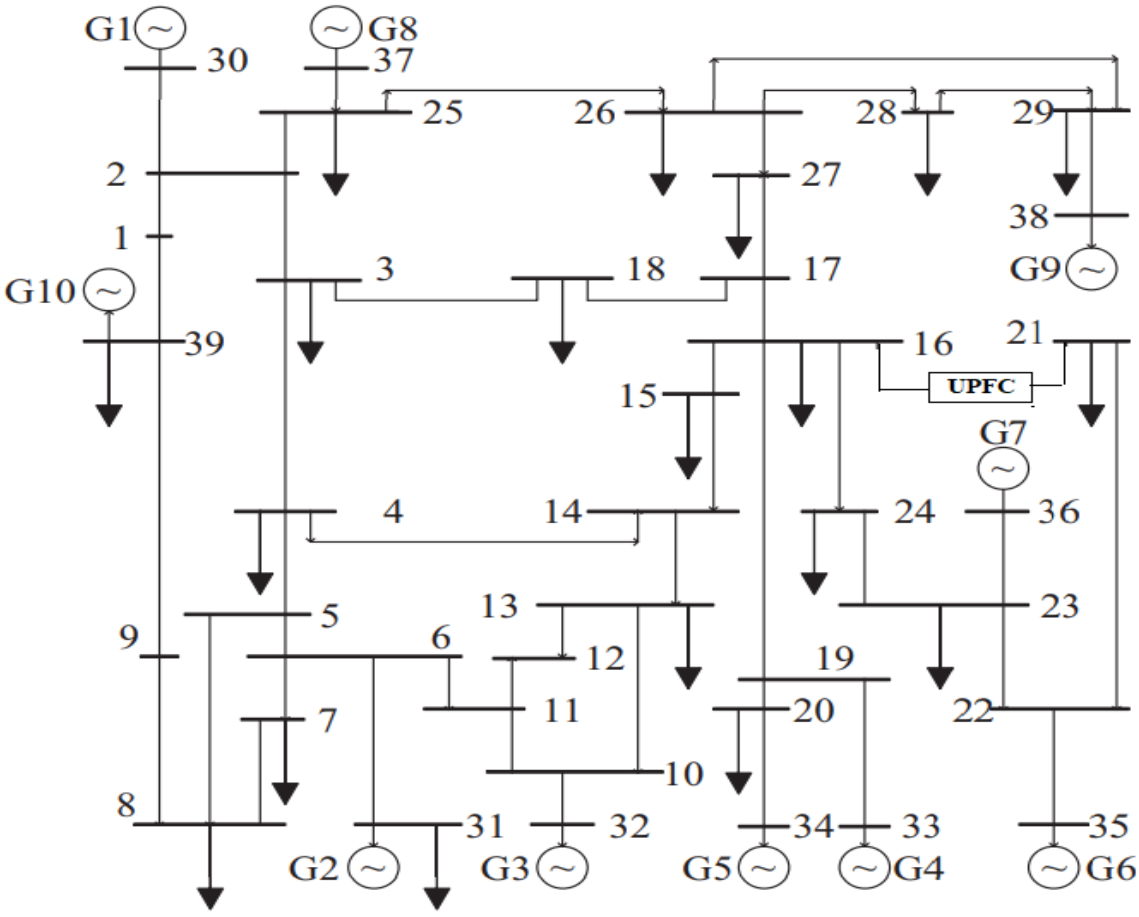

Figure 5.1 10-machine 39-bus modified New England test system

5.3 Design of H_∞ Loop Shaping Technique based UPFC WADC

The design of H_∞ loop shaping technique based UPFC WADC includes the following steps:

5.3.1 Full Order Model and Small Signal Analysis

As discussed in section 3.2, nonlinear model of all components of the test system is formed and the nonlinear model is found to be of 76^{th} order. Modal analysis is carried out in order to find out inter-area mode oscillations and local mode oscillations present in the system. The modal analysis shows that this system has two lightly damped inter-area mode oscillations and four lightly damped local mode oscillations. The local mode oscillations are properly damped with the PSSs. The details of the inter-area mode are as shown in Table 5.1. The mode shape of the inter-area mode oscillation is drawn for speed component of the right vector through compass chart as shown in Figure 5.2 (a)-(b).

Table 5.1 Critical inter-area mode oscillations of the modified NE test system

Mode Index	Eigenvalue	*f* (Hz)	Damping ratio ζ	Mode Shape
1	-0.363 ± 4.235i	0.674	0.0855	G10 Vs. All other
2	-0.052 ± 5.112i	0.813	0.01	G1 Vs. G6,G7

The compass chart clearly shows that, in mode 1, Generator G10 oscillates against all other generators while in mode 2, Generator 1 oscillates against Generators G6, G7. The motive for designing the WADC is to improve damping ratio of these modes.

5.3.2 Selection of Suitable Global Signal

As discussed in section 4.3.2, active power in the line is selected as an input signal to the controller. To decide the signal with the highest residue, residue analysis is carried out for active power flow in various lines with respect to the inter-area modes. The absolute values of residues of various lines for concerned inter-area mode are as shown in Figure 5.3(a)-(b). Residue analysis clearly shows that, for mode 1, active power in line number

12 (connecting bus 6- bus 7) has the highest residue for inter-area mode 1. So, it is selected as an input signal. Also, for mode 2, the residue of the line 12 is slightly higher than that of the residue of line 45. Hence, for both mode, active power flow in line 12 connecting bus 6 – bus 7 is selected as an input signal for the controller.

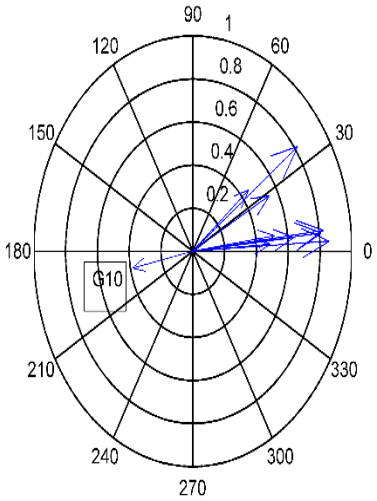

Figure 5.2 (a) Speed component of right eigenvector for mode 1

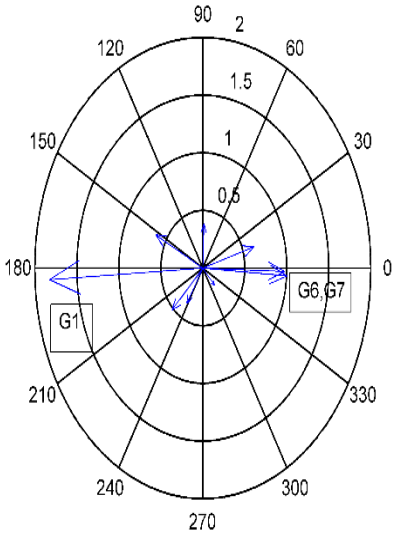

Figure 5.2 (b) Speed component of right eigenvector for mode 2

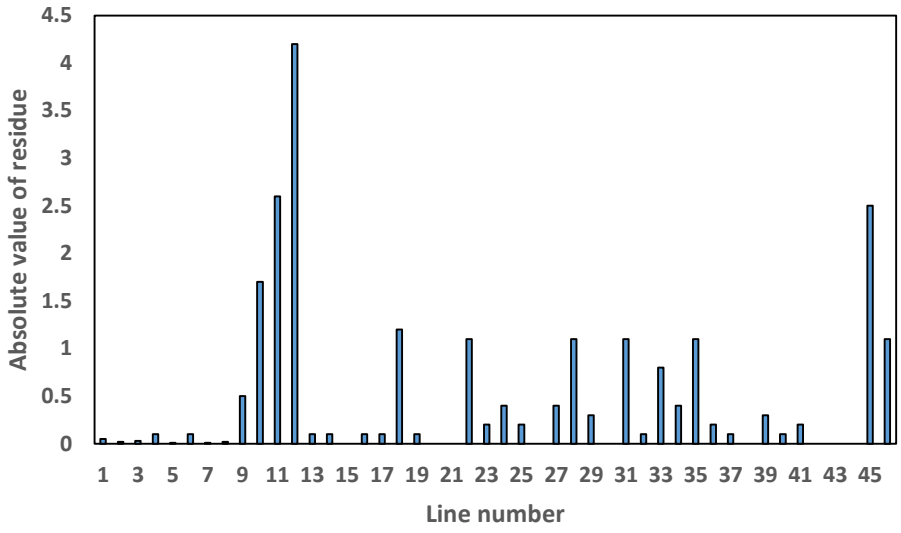

Figure 5.3 (a) Residue analysis for inter-area mode 1

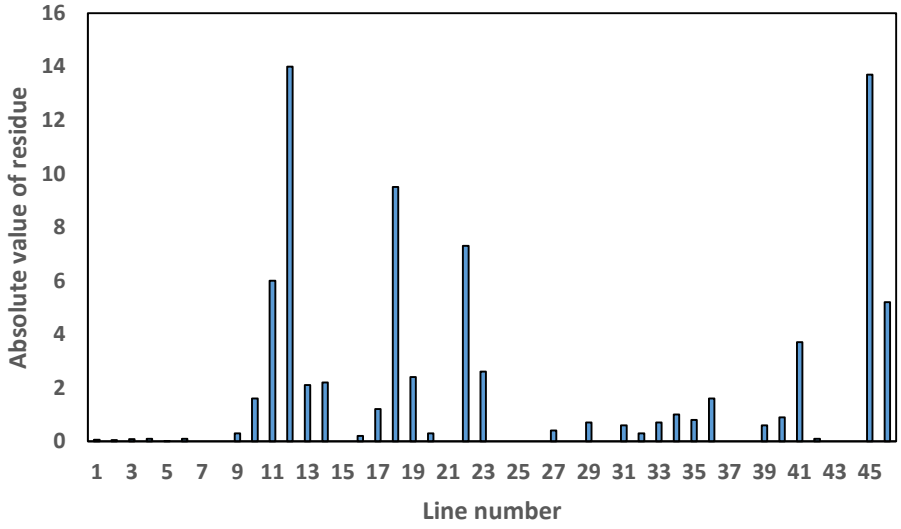

Figure 5.3 (b) Residue analysis for inter-area mode 2

5.3.3 Model Order Reduction

The next step in the design of UPFC WADC is to reduce the order of the test system. The order of the original linear model is 76^{th}. By balanced model reduction, this order is reduced to 6^{th} order. Figure 5.4 shows the frequency responses of the full-order model and reduced-order model. In the interest frequency range (< 1 Hz for inter-area modes), the frequency response of both full and reduced order model are closely matching. In fact, in the gain plot, it is difficult to differentiate between full and reduced order model. Hence, the reliability of the reduced order model is validated.

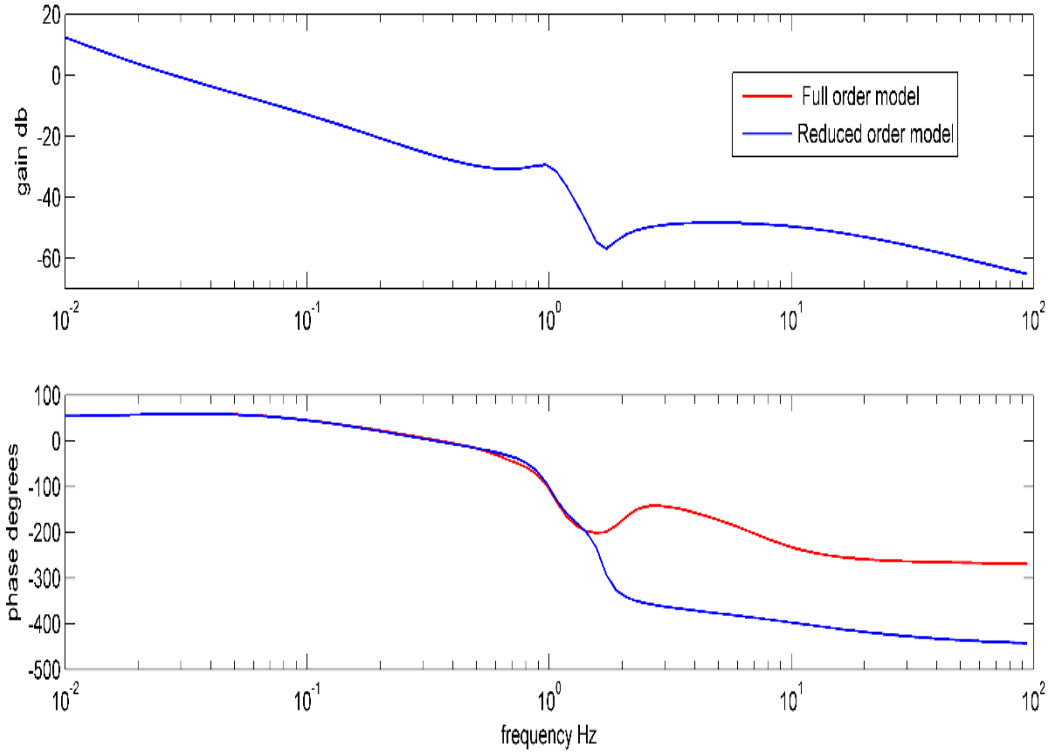

Figure 5.4 Frequency response of full order and reduced order model

5.3.4 Selection of Weights

Prior to solving the H_∞ problem, the open loop plant must be shaped as discussed in section 3.6.1. A pre-compensator is applied to open loop plant to introduce an integral action in the low-frequency region and also to reduce the overall gain of the plant in order to match the desired performance requirements. The pre-compensator weight selected for the plant is

$$W_1(s) = 10/(s+50) \quad (5.1)$$

The post-compensator is used to improve the conditioning of the plant. The post-compensator selected for the plant is

$$W_2(s) = 1/(s+50) \quad (5.2)$$

The frequency response of the original reduced order plant and shaped plant are as shown in Figure 5.5.

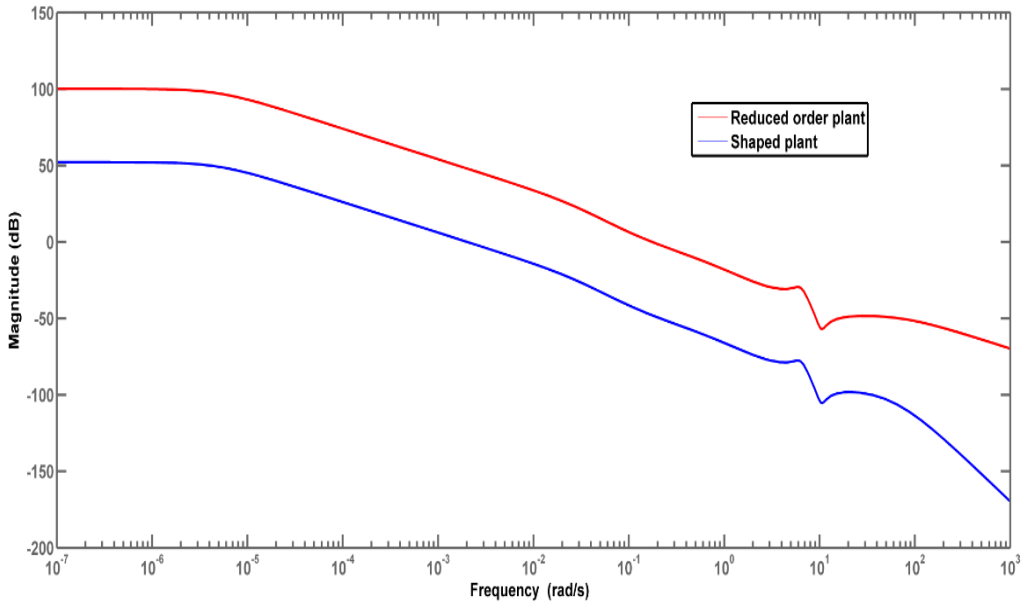

Figure 5.5 Frequency response of reduced order original plant and shaped plant

5.3.5 Controller Synthesis

After shaping the plant, the A, B, C, and D matrices of the shaped plant are used to form the generalized plant P. The controller is synthesized using the *hinfmix* function available in the LMI toolbox [100]. For ensuring the minimum damping ratio of 10%, the inner angle of the conic sector is set at 82º. The design converged to an optimum H_∞ performance index γ_{opt} of 3.892. The UPFC controller transfer function is given in the Appendix C7.

5.3.6 Robustness Evaluation of the Controller

The closed loop performance of the designed UPFC WADC for constant impedance load is as shown in Table 5.2.

Table 5.2 Closed-loop performance of the UPFC WADC

Mode Index	Open-loop		Closed-loop with UPFC WADC	
	f(Hz)	***ζ***	***f(Hz)***	***ζ***
1	0.674	0.0855	0.696	0.2012
2	0.813	0.01	0.798	0.1503

It is clear from the table that there is sufficient improvement in the damping ratio of the

inter-area modes. The performance of the designed controller is also assessed for the various load models suggested in Table 4.2. The results are shown in Table 5.3.

To check the robustness of the designed UPFC WADC, the power flow in the nearby important tie-line connecting bus 22- bus 21 is changed and the performance of the designed controller is observed for the changes. The nominal power flow in the line connecting bus 22- bus 21 is 607 MW. The results are shown in Table 5.4.

Table 5.3 Performance of UPFC WADC for proposed load models

Load Model	Mode 1		Mode 2		Type of load
	f(Hz)	*ζ*	*f(Hz)*	*ζ*	
I	0.696	0.2012	0.813	0.1503	CI
II	0.652	0.1156	0.767	0.1019	CP
III	0.688	0.1817	0.802	01467	CC
IV	0.687	0.1604	0.803	0.1140	CI=CP+CC
V	0.684	0.1412	0.791	0.1375	CP=CI+CC
VI	0.687	0.1816	0.801	0.1468	CC=CI+CP
VII	0.678	0.1619	0.798	0.1302	CI+ Dynamic

Table 5.4 Performance of UPFC WADC for variation in tie-line power flow

Power flow in the line connecting bus 22- bus 21 (MW)	Mode 1		Mode 2	
	f(Hz)	*ζ*	*f(Hz)*	*ζ*
400	0.737	0.3513	0.878	0.3245
500	0.712	0.2824	0.852	0.2516
600	0.698	0.2018	0.814	0.1513
700	0.658	0.1513	0.783	0.1134

The effect of various important line outage on the performance of the UPFC WADC is also observed. The response of the controller is as shown in Table 5.5.

Table 5.5 Performance of UPFC WADC for various line outages

Line outage	Mode 1		Mode 2	
	f(Hz)	*ζ*	*f(Hz)*	*ζ*
14-15	0.681	0.1810	0.798	0.1412
17-18	0.676	0.1610	0.785	0.1329
10-13	0.690	0.1987	0.805	0.1482

Hence, it can be concluded that the H_∞ loop shaping using LMI approach for designing the UPFC WADC results in robust performance of the designed controller. It provides sufficient damping to inter-area modes under various contingency conditions. In all cases, minimum damping of 10% is ensured. However, the improvement in damping ratio in case of load model II and load model V is less as compared to the cases of other load models.

5.3.7 Nonlinear Time-Domain Simulations

For validating the performance of the loop shaping technique based UPFCSVC-WADC FACTS controller, the nonlinear time-domain simulation was performed for various contingency conditions like line outage, line faults, and load shedding etc. on the test system.

a) Line fault: A line to ground fault is simulated near bus 15, which connects important line carrying 287 MW power from bus 16 to bus 15. This fault excites the inter-area oscillations and also affects the power flows in various lines. The variation in power flow due to this contingency in an important line between bus 16- bus 17 is shown in Figure 5.6. The relative angle between G5-G7 due to this contingency is as shown in Figure 5.7. It is very clear from the figures that with the designed damping controller, the oscillations are damped out within 10-12 seconds. Further Figure 5.8 shows the individual response of UPFC WADC to the fault. From these responses, it is clear that both WACs are capable to damp the oscillations within the stipulated time.
b) Line outage: In this case, an important tie line connecting bus 6 and bus 11 has an outage of 1.0 sec. The response of the test system was observed with and without

the WAC controllers and are as shown in Figure 5.9. The oscillations in the relative angle between the generators die down rapidly.

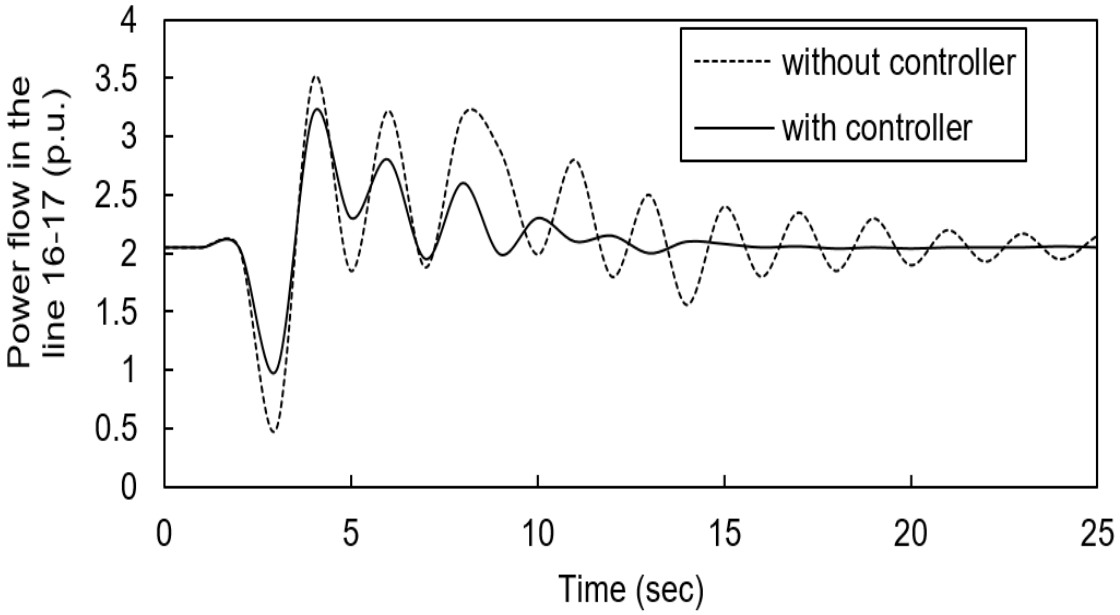

Figure 5.6 Dynamic response of UPFC WADC during the line fault at bus 15 (Power flow in line 16-17)

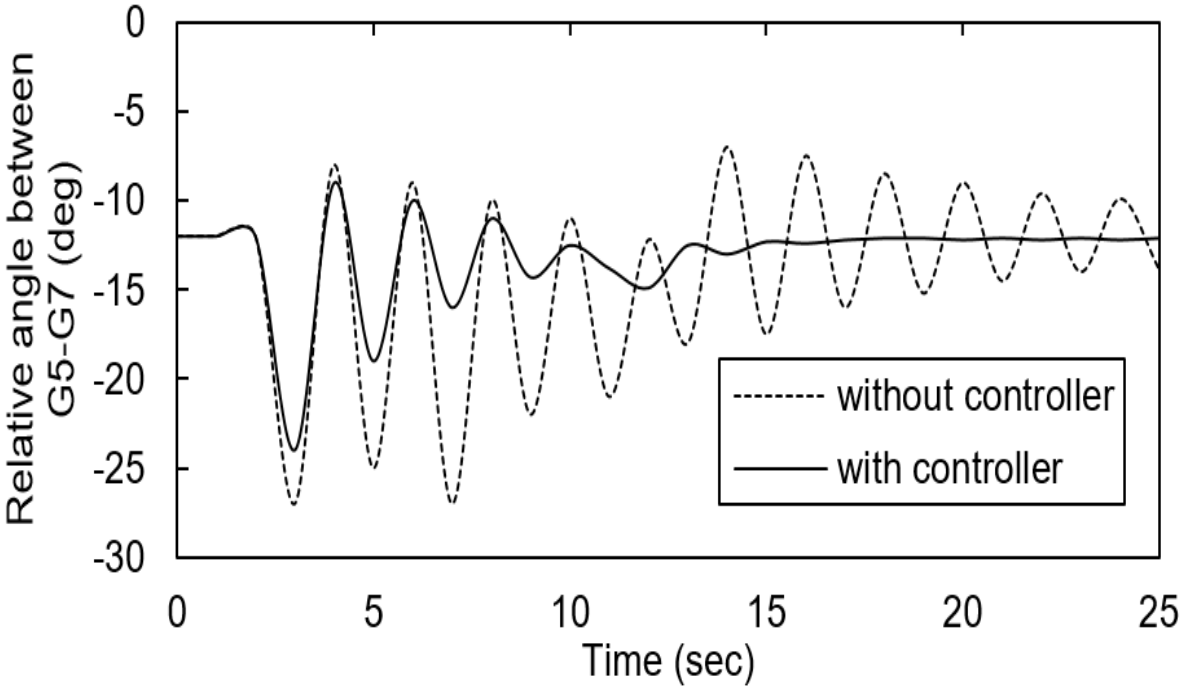

Figure 5.7 Dynamic response of UPFC WADC during the line fault at bus 15 (Relative angle between G5-G7)

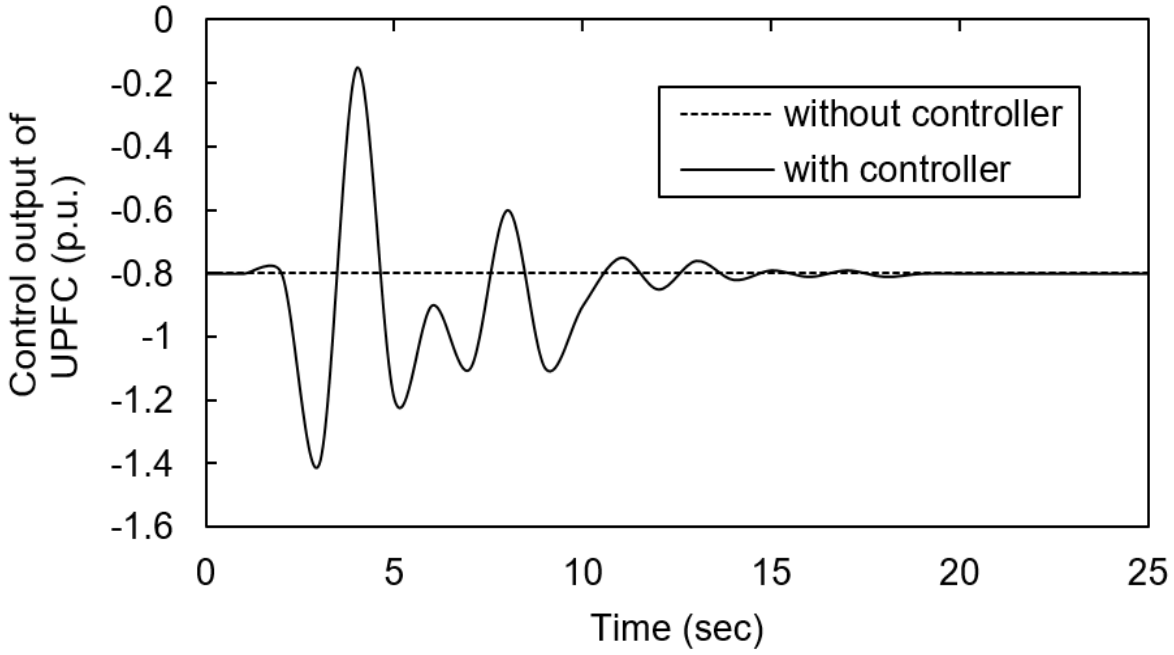

Figure 5.8 Dynamic response of UPFC WADC during line fault at bus 15 (Control output of UPFC)

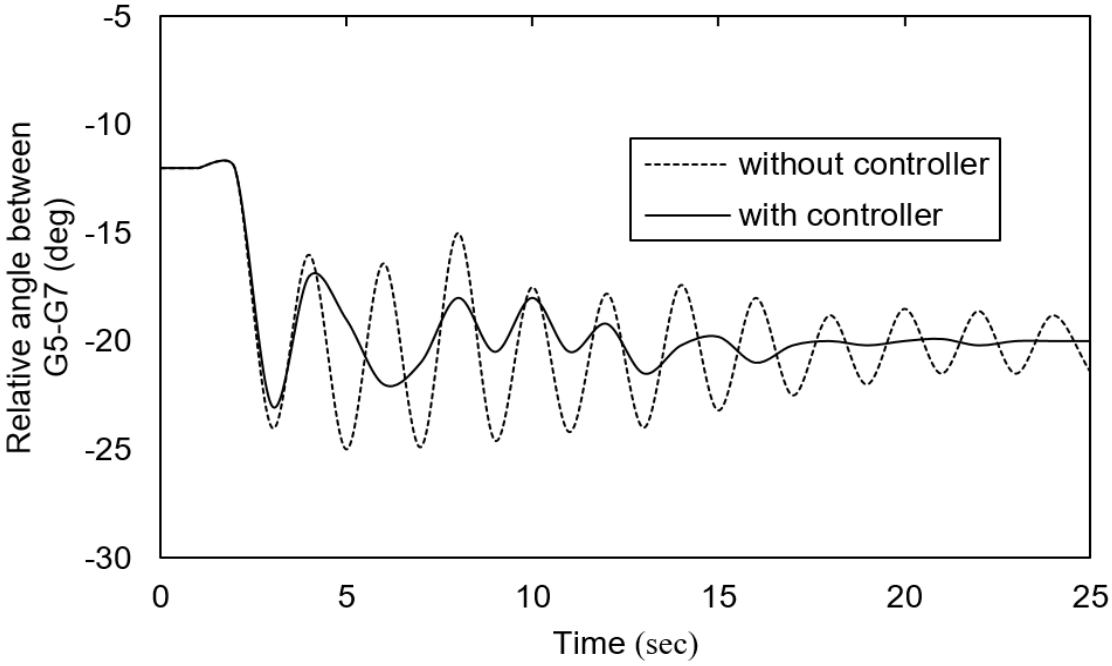

Figure 5.9 Dynamic response of UPFC WADC during a line outage (Relative angle between G5-G7)

Also, this outage will affect the power flow in other important tie lines. Figure 5.10 shows the power flow in another important tie line between bus 6-bus 7 with and without WADCs. It can be observed that oscillations in the line power are damped successfully with a designed controller.

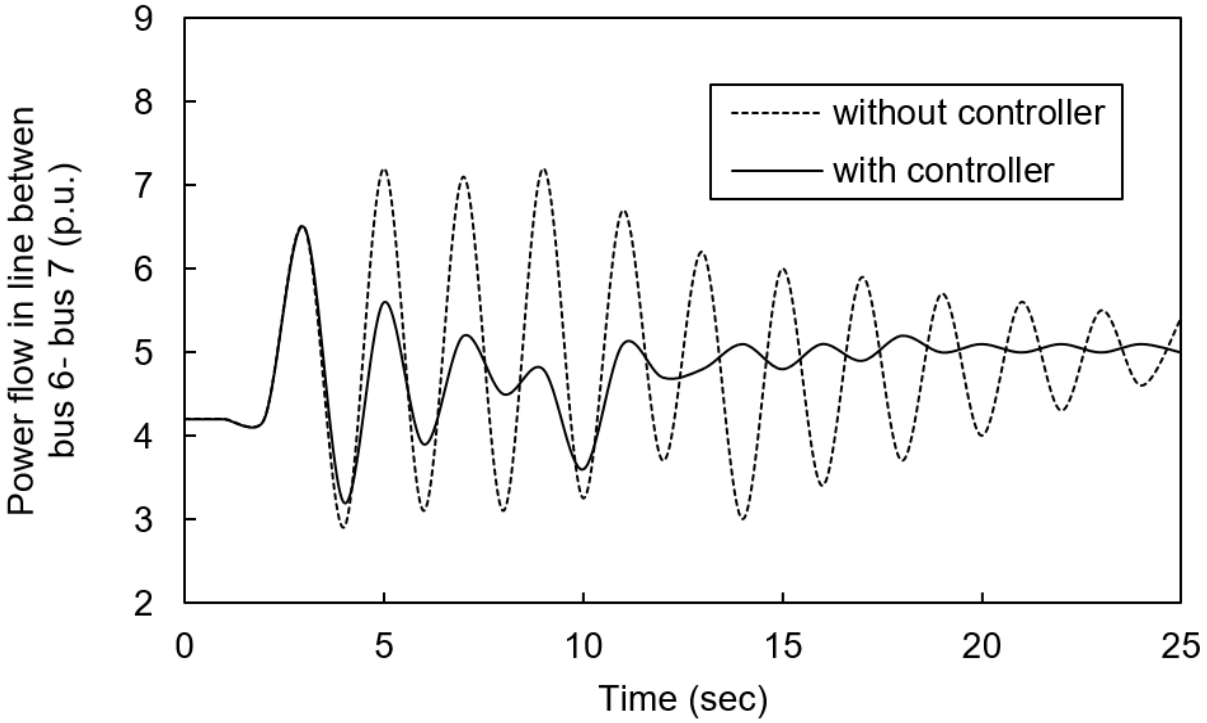

Figure 5.10 Dynamic response of UPFC WADC during a line outage (Power flow in the line between bus 6 – bus 7)

c) Load shedding: In this case, load shedding is applied on bus 15 for 1 sec to study the robustness of the designed controller. The resulting dynamic response of relative angle between G5 and G7 is represented in Figure 5.11. The variation in power flow in important tie-line between bus 16 and bus 17 is represented in Figure 5.12. All the responses indicate that the designed WADC can play an effective role in damping inter-area oscillations and exhibits robust performance under-discussed contingency.

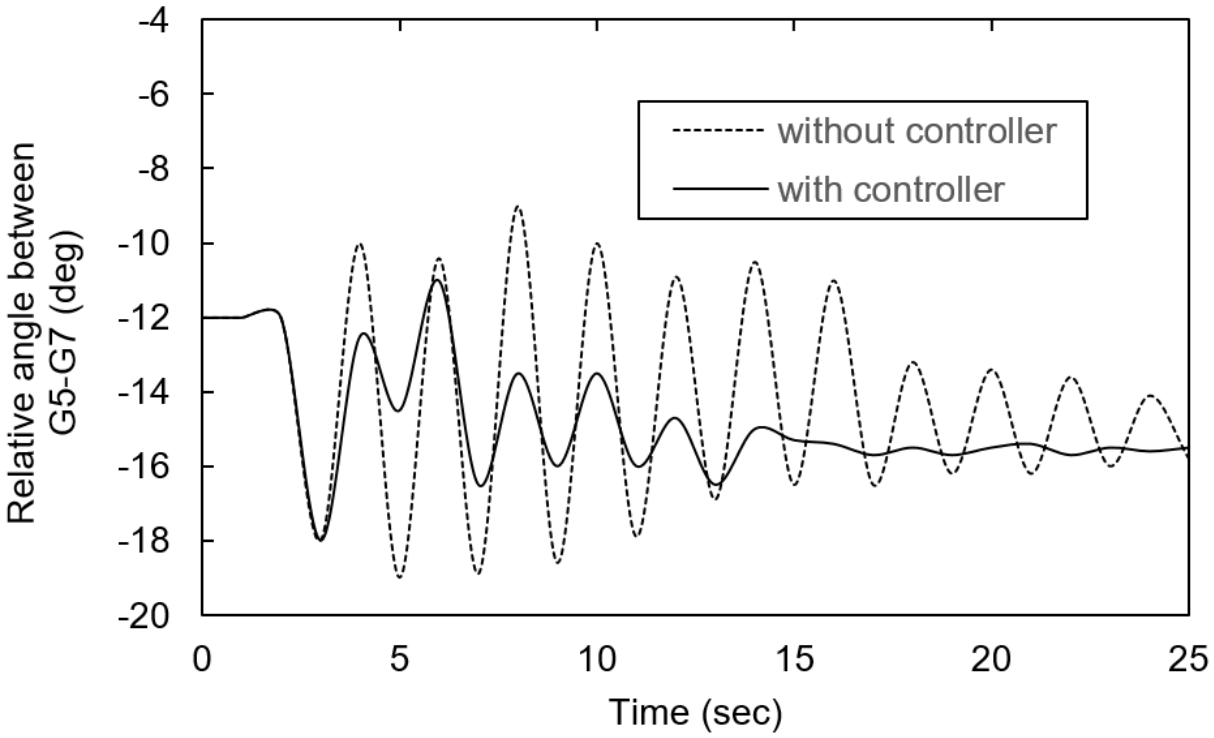

Figure 5.11 Dynamic response of UPFC WADC during load shedding (Relative angle between G5-G7)

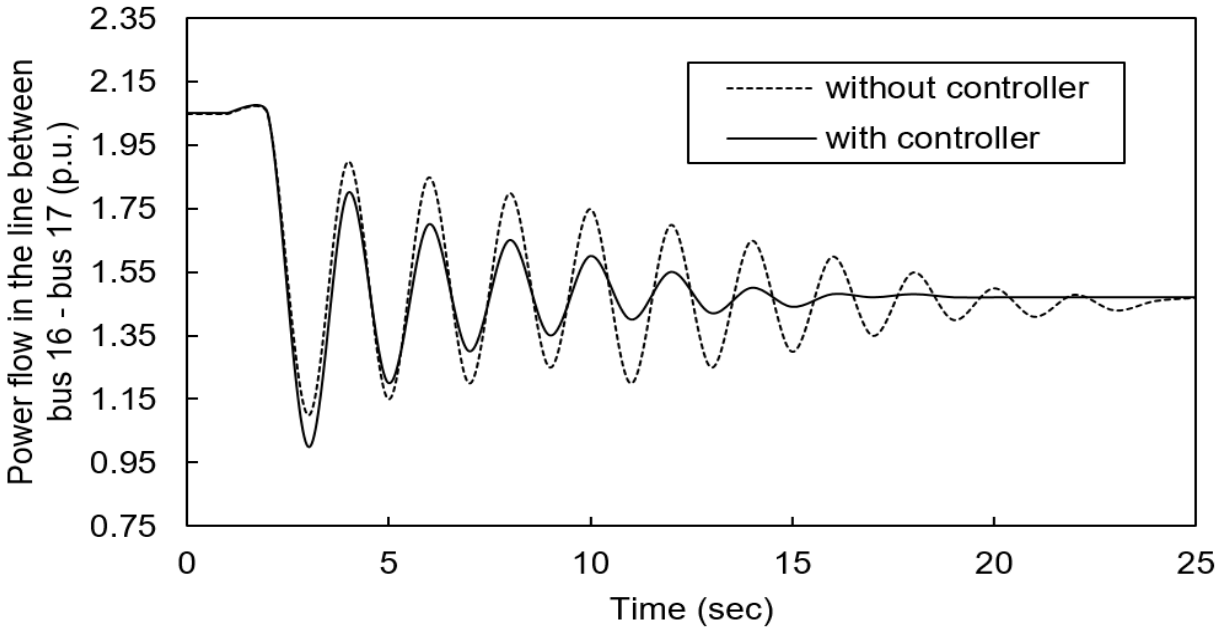

Figure 5.12 Dynamic response of UPFC WADC during load shedding (Power flow in the line between bus 16 – bus 17)

Thus, the designed UPFC WADC was tested for different operating conditions appear in power system as well as various contingencies like line faults, line outages and load shedding etc. The performance of the designed WADC was found to be robust for such conditions. The oscillations produced by such contingency conditions were damped within 12-15 seconds.

5.4 Summary

This chapter discusses the design of WADC based on H_∞ loop shaping technique using LMI. The drawbacks of the conventional mixed sensitivity based approach can be overcome with this technique by proper shaping the open loop plant with pre and post compensators. The LMI framework also ensures the pole placement objective. The controller is synthesized for 10-machine, 39-bus modified New England test system employing UPFC for damping the inter-area mode oscillations. The designed controller is found to be robust for varying operating conditions arising in power system and various contingency conditions like line faults, line outages and load shedding etc.

CHAPTER 6 CONCLUSION AND FUTURE SCOPE

6.1 Conclusion

In the present scenarios of the power system, the transmission networks are highly stressed due to a rapid increase in the demand for electricity, economic aspects of the deregulated electricity markets and the intermittent nature of the renewable energy sources. Hence, proper reinforcement of the transmission networks is the need of the hour. Although it is a challenging task for the long-term stability of the power systems, this task is inevitable. Due to large capital cost and difficulties in acquiring new right of way, building new transmission network is a very difficult task. Power electronics based FACTS devices are proved to be more cost-effective in reinforcing the present transmission network. Further, these devices also offer greater flexibility and controllability in control of power system parameters and hence, helps in improving the power system stability. This thesis mainly concentrated on the stability aspects of the power system and presented the design of robust damping controller for enhancing the small signal stability of the power systems. The work carried out in the thesis can be concluded in the following aspects:

- The nonlinear model of the power system including all the devices like generator, exciter, PSS, and FACTS device was prepared. This nonlinear model is linearized around a nominal operating point for understanding the dynamic behavior of the power system. Some important parameters like eigenvalues, damping ratio, mode shape etc. are derived from the linearized model. These parameters help in identifying the inter-area mode oscillations with poor damping ratio and its mode shape i.e. which generators are oscillating against each other. The linearized model is represented in Linear Time Invariant (LTI) state space equations which are then used for the design of the robust damping controller.
- Residue analysis is carried out to decide the best suitable global signals for the controller. The global signals are acquired with the help of wide area measurements. Active power flow in the line was selected as stabilizing signal with

respect to the critical inter-area mode oscillations as it is free from other spurious signals.

- The H_∞ control design based on mixed sensitivity approach using LMI and H_∞ loop shaping control techniques were used to design the robust controllers.
- Various load composition models which resemble actual load composition model on power system are considered and the designed WADC are tested for all proposed models to ensure adequate damping in worst case load composition scenarios. However, to derive exact load composition model is very difficult due to dynamic nature of the power system loads, a fair attempt is made here to create practical power system conditions.
- The designed controllers are found to be satisfactory in damping the inter-area modes. However, the damping ratio improvement in case of constant power load and constant power dominated load composition models were found to be less as compared to other load composition models. However, in these conditions also the damping provided by the designed WADCs are more than the specified limits in the literature (minimum 10%).
- The robustness of the controller is checked through various operating conditions and the performance of the controllers was found to be satisfactory.
- Nonlinear time domain simulations were carried out to consider the various contingent conditions that may arise in actual power system like line outages, line faults, and load shedding. The controllers were robust enough to damp the oscillations produced by such contingency conditions.

6.2 Future Scope

The work presented in the thesis can be continued for future research studies in the following aspects:

- Practical implementation: For proper utilization of the FACTS devices, the controllers proposed in the thesis must be implemented practically. Hence, one of the future aspects is the practical implementation of the proposed controllers in actual power systems.

- Time delay: In Chapter 4 and chapter 5, the global input signal to the controller are acquired through phasor measurement units based wide area measurements. However, from the acquisition of the signal to its final implementation as input to the controller, various time delays are involved in this process. This time delay may result in the reduced effectiveness of the designed controller and in some cases, the system may destabilize due to it [108,109]. Future work may include practical issues like time delays, digital environments.
- Coordination with protection system and other control systems: In this thesis, attention is not given to interactions between the designed controller and existing protections of the power systems. In future, more attention must be given in this area.
- Controller tuning: The controller designed on robust linear technique may not give a desired robust performance when implemented in the actual nonlinear system due to loss of some important dynamic properties while reducing the model order. In future, a systematic approach for tuning the parameters can be proposed so that the controller designed on linear techniques, may perform satisfactorily when tested in practical nonlinear environments.

BIBLIOGRAPHY

[1] N.G. Hingorani and L. Gyugyi, “Understanding FACTS”, *IEEE Press*, 1st edition, New York, 2000.

[2] P. Kundur, “Power system stability and control”, *McGraw- Hill*, 1st edition, New York, 1994.

[3] G. Rogers, “Power system structure and oscillations”, *IEEE Computer Appl. Power*, vol. 12(2), pp. 14-21, April 1999.

[4] M. Klein, G. Rogers, S. Moorty and P. Kundur, “Analytical investigation of factor influencing power system stabilizers performance”, *IEEE Trans. Energy Conversion*, vol.7, pp. 382-390, 1992.

[5] J.V. Milanovic and I.A. Hiskens, “Effect of load dynamics on power system damping”, *IEEE Trans. power sys.* , vol.10 (2), pp. 1022-1028, May 1995.

[6] I.A. Hiskens and J.V. Milanovic, “Locating dynamic loads which significantly influence damping,” *IEEE Trans. power Syst.*, vol. 12(1), pp. 255-261, February 1997.

[7] K. Prasertwong, N. Mithulnanthan, and D. Thakur, “Understanding low-frequency oscillations in power system”, *Int. J Electrical Eng. Edu.*, pp. 248-262, 2010.

[8] P. L. Dandeno, A.N. Karas, K.R. McClymont and W. Watson, “Effect of high-speed rectifier excitation system on generator stability limits”, *IEEE Trans. Power Appar. Syst.*, vol. PAS-87, pp.190-201, 1968.

[9] F.R. Schleif, H.D. Hunkins, G.E.Martin and E.E. Hattan, “Excitation control to improve power line stability”, *IEEE Trans. Power Appar. Syst.*, pp. 1426-

1434, 1968.

[10] G. Berube, L. Hajagos and R. Beaulieu, “Practical utility experience with power system stabilizers”, *IEEE PES working group presentation on power system stabilizers*, 1999.

[11] F.W. Keay and W.H. South, “Design of power system stabilizers sensing frequency deviation”, *IEEE Trans. Power Appar. Syst.*, vol. PAS-90, pp. 707-713, 1971.

[12] W. Watson and G. Manchur, “Experience with supplementary damping signals for generator static excitation system”, *IEEE Trans. Power Appar. Syst.*, vol. PAS-92, pp. 199-203, 1973.

[13] E.V. Larsen and D.A. Swann, “Applying power system stabilizers Part I-General concepts”, *IEEE Trans. Power Appar. Syst.*, vol. PAS-100, pp. 3017-3024, 1981.

[14] P. Kundur, M.Klein, G.J.Rogers and M.S. Zywno, “Application of power system stabilizers for enhancement of overall power system stability”, *IEEE Trans. Power Syst.*, vol. 4, pp. 614-626, 1989.

[15] M. Klein, G.J. Rogers, S. Moorty and P. Kundur, “Analytical investigation of factors influencing power system stabilizers performance”, *IEEE Trans. Energy Conv.*, vol. 7, pp.382-390, 1982.

[16] M. Parsa and J. Toyoda, “Implementation of a hybrid power system stabilizer”, *IEEE Trans. Power Syst.*, vol. 4, pp. 1463-1469, 1989.

[17] Y. Zhang, O.P. Malik and G.P. Chen, “Artificial neural network based power system stabilizers in multi-machine power system environments”, *IEEE Trans. Energy Conv.*, vol. 10, pp.147-155, 1995.

[18] H. Quinot, H. Bourles, and T. Margotin, “Robust coordinated AVR+PSS for damping large-scale power systems”, *IEEE Trans. Power Syst.*, vol. 14, pp. 1446-1451, 1999.

[19] R. Mohan Mathur and R.L. Varma, “Thyristor based FACTS controller for electrical transmission system”, *Wiley-IEEE press*, 1st edition, New York, 2002.

[20] R. L. Lee, M. J. Beshir, A. T. Finley, D. R. Hayes, J. C. Hsu, H. R. Peterson, “ Application of static VAr compensators for the dynamic performance of the Mead Adelanto and Mead-Phoenix transmission projects”, *IEEE Trans. Power Deliv.*, vol. 10, pp. 459-466, 1995.

[21] C. Gama, “Brazilian North-South Interconnection control-application and operating experience with a TCSC”, *IEEE Power Engineering Society Summer Meeting*, vol. 2, pp. 1103-1108 1999.

[22] R. J. Abraham, D. Das, A. Patra, “ Effect of TCPS on oscillations in tie power and area frequencies in interconnected hydrothermal power station”, *IET Gen. Trans. Distr.*, 1(4), pp. 632-639, 2007

[23] A. M. Simoes, D. C. Savelli, P. C. Pellanda, N. Martins, and P. Apkaria, “ Robust Design of a TCSC Oscillation Damping Controller in a Weak 500-kV Interconnection Considering Multiple Power Flow Scenarios and External Disturbances”, *IEEE Trans. Power Syst.*, vol. 24, pp. 226-236, 2009.

[24] L. Tain-Syh, H. Yuan-Yih, G. Tzong-Yih, L. Jiann-Tyng, and H. Chiung-Yi, “ Application of thyristor-controlled series compensators to enhance oscillatory stability and transmission capability of a longitudinal power system”, *IEEE Trans. Power Syst.*, vol. 14, pp. 179-185, 1999.

[25] M. Aboul-Ela, A. Sallam, J. McCalley, and A. Fouad, “Damping controller design for power system oscillations using global signals”, *IEEE Trans.*

Power Syst., vol. 11, pp. 767–773, May 1996.

[26] M. Klein, L.X. Le, G.J. Rogers, S. Farrokhpay, and N.J. Balu, “H∞ damping controller design in large power systems”, *IEEE Trans. Power Syst.*, vol.10, No.1, pp. 158-166, Feb.1995.

[27] R. A. Ramos, L. F. C. Alberto, and N. G. Bretas, “ A New Methodology for the Coordinated Design of Robust Decentralized Power System Damping Controllers”,

IEEE Trans. Power Syst., vol. 19, no.1, pp. 444-454, February 2004.

[28] Z. Chuanjiang, M. Khammash, V. Vittal, and Q. Wenzheng, “ Robust power system stabilizer design using *H*∞ loop shaping approach”, *IEEE Trans. Power Syst.*, vol. 18, no.2, pp. 810-818, May 2003.

[29] W.A. Mittelstadt, PE. Krause, P.N. Overholt, J.F. Hauer, R.E. Wilson, D.T. Rizy, “The DOE Wide-area Measurement System (WAMS) Project - Demonstration of Dynamic Information Technology for Future Power System”, Fault and Disturbance Analysis & Precise Measurements in Power Systems, Arlington, VA, November 1995.

[30] A. G. Phadke, “ Synchronized phasor measurements - a historical overview”,

IEEE/PES Trans.Distri. Conf. Exhib., pp. 416-479, 2002.

[31] I. Kamwa, J. Beland, G. Trudel, R. Grondin, C. Lafond, and D. McNabb, “ Wide-Area Monitoring and Control at Hydro-Québec: Past, Present, and Future”, *IEEE PES Summer Meeting*, pp.1-12, 18-22 June 2006.

[32] I. Kamwa, A. Heniche, G. Trudel, M. Dobrescu, R. Grondin and D. Lefebvre, “ Assessing the technical value of FACTS-based wide-area damping control loops”, *IEEE/PES General Meeting*, vol. 2, pp.1734 –1743, 12-16 June 2005.

[33] I.R. Petersen and R. Tempo, “Robust control of uncertain systems: Classical results and recent developments”, *Automatica 50*, pp. 1315-1335, 2014.

[34] G. Zames, “Feedback and optimal sensitivity: Model reference transformations, multiplicative seminorms and approximate inverses”, *IEEE Trans. Automatic Control*, vol.26, pp. 301-320, 1981.

[35] H. Kwakernaak, “Robust control and H_∞ - optimization”, *Tutorial paper. Automatica,* vol. 29, pp. 255-273, 3// 1993.

[36] J. C. Doyle, K. Glover, P. P. Khargonekar and B. A. Francis, “ State-space solutions to standard H_2 and H_∞ control problems”, *IEEE Trans. Auto. Control,* vol. 34, pp. 831-847, 1989.

[37] G. N. Taranto, J. K. Shiau, J. H. Chow and H. A. Othman, “Robust decentralized design for multiple FACTS damping controllers”, *IEE Proceedings: Gen., Trans. and Distr.,* vol. 144, pp. 61-67, 1997.

[38] C. Scherer, “The Riccati inequality and state-space H_∞ - optimal control”, *Univ.Wnrzburg*, Germany*,* 1990.

[39] C. Y. Chung, C. T. Tse, A. K. David and A. B. Rad, “ A new H_∞ based PSS design using numerator - denominator perturbation representation”, *Electric Power Syst. Research*, vol. 52, pp. 37-42, 10/1/ 1999.

[40] B. Chaudhuri and B.C. Pal, “Robust damping of multiple swing modes employing global stabilizing signal with a TCSC”, *IEEE Trans. Power Syst.,* vol. 19, no.1, pp. 499-506, 2004.

[41] M. M. Farsangi, Y. H. Song, and M. Tan, “Multi-objective design of damping controllers of FACTS devices via mixed H_2 / H_∞ with regional pole placement”, *Int. J Elect. Power & Energy Syst.,* vol. 25, pp. 339-346, 2003.

[42] D. McFarlane and K. Glover, “A loop-shaping design procedure using H_∞ synthesis”, *IEEE Trans. Auto. Control,* vol. 37, pp. 759-769, 1992.

[43] Z. Chuanjiang, M. Khammash, V. Vittal, and Q. Wenzheng, “Robust power system stabilizer design using H_∞ loop shaping approach”, *IEEE Trans. Power Syst.,* vol. 18, pp. 810-818, 2003.

[44] I. Kamwa, R. Grondin, Y. Hebert, “ Wide-area measurement based stabilizing control of large power systems—A decentralized/ hierarchical approach”, *IEEE Trans. Power Syst.*, vol. 16, no. 1, pp. 136–153, Feb. 2001.

[45] J. Chow, J. Sanchez-Gasca, H. Ren, and S. Wang, “Power system damping controller design using multiple input signals”, *IEEE Control system magazine*, vol. 20, pp. 82–90, Aug. 2000.

[46] J. Quintero and V. Venkatasubramanian, “A Real-Time Wide-Area Control Framework for Mitigating Small-Signal Instability in Large Electric Power Systems”, In Proceedings of the 38th Annual Hawaii International Conference on System Sciences, 03-06 Jan. 2005.

[47] P. Rao and I. Sen, “Robust pole placement stabilizer design using linear matrix inequality”, *IEEE Trans. Power Syst.*, vol. 15, pp. 313-319, 2000.

[48] M. Ishimaru, R. Yokoyama, G. Shirai and T. Niimura, “Robust thyristor controlled series capacitor controller design based on linear matrix inequality for a multi-machine power system”, *Int. J. electrical power and energy syst.*, 24(2002), pp. 621-629.

[49] B. Kalyankumar, S.N.Singh, and S.C. Srivastava, “Placement of FACTS controller using modal controllability indices to damp out power system oscillations”, *IET proceedings on Gen., Trans. and Distr.*, vol.1, pp.209-217, 2007.

[50] B. Kalyankumar, S.N.Singh, and S.C. Srivastava, “Optimal control strategy using pseudo-decentralization for coordination of power system stabilizer and FACTS in a multi-machine system”, *Int. Energy Journal special issue FACTS applications and stability and dynamics*, pp. 1-13, 2005.

[51] B.K.S. Roy, A.K. Sinha, A. K. Pradhan, “ An optimal PMU placement technique for power system observability”, *Int. J Electric Power Energy Syst.*, 42(1), pp. 71-77, 2012

[52] R.K. Varma, R.P. Gupta, and S. Auddy, “ Damping of inter-area oscillations in power systems by static var compensator (SVC) using PMU acquired remote bus voltage angles”, *Int. J Emerging Electric power syst.*, vol.8, pp. 6-12, 2007.

[53] N. Mithulananthan, C.A. Canizares, J. Reeve and G. Rogers, “Comparison of PSS, SVC and STATCOM controllers for damping power system oscillations”, *IEEE Trans. Power Syst.*, vol. 18, pp. 786-792, 2003.

[54] R. Gupta, B. Bandopadhyay, and A. M. Kulkarni, “Robust decentralized fast sampling technique based power system stabilizers for a multi-machine power system”, *Int. J Syst. Science*, vol. 36, pp. 297-314, 2005.

[55] Y. Zhang and A. Bose, “Design of wide area damping controller for inter-area oscillations”, *IEEE Trans. Power Syst.*, vol. 23, pp. 1136-1143, 2008.

[56] R. You, M.H. Nehrir and D.A. Pierre, “Controller design for SVC and TCSC to enhance damping of power system oscillations”, *Electric Power Compo. Syst*., 35:871–884, 2007.

[57] M. Jing, T. Wang, J. Thorp, A.G. Phadke, and Z. Wang, “Application of wide area collocated control technique for damping inter-area oscillations using FACTS devices”, *Electric Power Compo. Syst*., 39, pp. 1452-1467, 2011.

[58] N. Modi, M. Lloyd, and T. K. Saha, “Wide-area signal selection for power system damping controller”, *AUPEC 2011*, Brisbane, QLD, pp. 1-6, 2011,

[59] Y. Li, C. Rehtanz, S. Ruberg, L. Luo and Y. Cao, “Wide area robust co-ordination approach of HVDC and FACTS controller for damping multiple inter-area oscillations”, *IEEE Trans. Power Deliv.*, vol. 27, pp.1096-1105, 2012.

[60] Y. Li, C. Rehtanz, S. Ruberg, L. Luo and Y. Cao, “Assessment and choice of input signals for multiple HVDC and FACTS controllers”, *IEEE Trans. Power Deliv*., vol. 27, pp.1969-1977, 2012.

[61] Vignesh V, S.C. Srivastava and Saikat Chakrabarti, “A robust decentralized wide-area controller for wind generators and FACTS controllers considering load model uncertainties”, *IEEE Transaction on smart grid*, vol. PP, pp. 1-6, 2016.

[62] A.C. Zolotas, B. Chaudhuri, I.M. Jaimoukha and P. Korba, “A study on LQG/LTR control for damping inter-area oscillations in power systems”, *IEEE Trans. Control Syst. Technology*, vol. 15, pp.151-160, 2007.

[63] B. Chaudhuri, S. Ray, and R. Majumder, “Robust low order controller design for multimodal power oscillation damping using flexible AC transmission system devices”, *IET Gen., Trans. Distr.*, vol.3, pp. 448-459, 2009.

[64] I. Kamwa, G. Trudel, and L. Gerin-lajoie, “Robust design and coordination of multiple damping controllers using nonlinear constrained optimization”, *IEEE Trans. Power Syst.*, vol. 15, pp. 1084-1092, 2000.

[65] C. Li-Jun and I. Erlich, “Simultaneously coordinated tuning of PSS and FACTS damping controller in large power system”, *IEEE Trans. Power Deliv.*, vol. 20, pp. 294-300, 2005.

[66] T. Lobos, J. Rezmer and H.J. Koglin, “Analysis of power system transients using wavelet and prony method”, *IEEE porto powertech proceedings,* vol. 4,

2001.

[67] T. Lobos, J. Rezmer, T. Sikorski, P. Schegner, “Time-frequency analysis of non-stationary signals in power system”, "*IET conference*, vol.1, pp. 68-71, 2004.

[68] IEEE standard 421.5-1992, “IEEE recommended practice for excitation system models for power system stability studies”, The institute of electrical and electronics engineers, Piscataway, NJ, USA.

[69] P.M. Anderson and A.A. Faued, “Power system control and stability”, *IEEE press*, 1st edition, 1994.

[70 C. Concordia and S. Ihara, “Load representation in power system stability studies”, *IEEE Trans. Power Appr. Syst.*, vol. PAS-101, No.4, pp. 969-76, April 1982.

[71] IEEE task force on load representation for dynamic performance, “Load representation for dynamic performance analysis”, *IEEE Trans. Power Syst.*, Vol. 8, No.2, pp. 472-82, May 1993.

[72] IEEE FACTS working group 15.05.15. FACTS Application, 1995.

[73] Power system toolbox, version 3, Cherry tree scientific software, 2000-2008.

[74] Perez-Arriaga I.J., G.C. Verghese and F.C. Schweppe, “Selective modal analysis with applications to electric power system”, Part I: Heuristic introduction. IEEE T-PAS, vol. 101, pp. 3117-3125, 1982.

[75] B. Porter and R. Crossley, “Modal control- Theory and applications”, *Taylor & Francis*, 1972.

[76] M. Tarokh, “Measures for controllability, observability and other modes”,

IEEE Trans. Auto. Control, vol. 37, pp. 1268-1273, 1992.

[77] R.Y. Chiang and M.G. Safonov, "Robust Control toolbox", *The Math Works Inc.*, 1988.

[78] A.M.A. Hamdan and A.M. Elabdalla, "Geometric measures of modal controllability and observability of power system models", *Electric power system research*, vol. 15, pp. 147-155, 1988.

[79] J.J. Sinchez-Gasca and J.H. Chow, "Power system reduction to simplify the design of damping controllers for inter-area oscillations", *IEEE Trans. Power Syst.*, vol. 11, pp. 1342-1349, 1996.

[80] D Kumar, J P Tiwari, and S K Nagar, "Reduction of large-scale system by extended balanced truncation approach", *Int. J Engg. Science Techno*., 3(4), 2011.

[81] G. Rogers, "Power system oscillations", Norwell, MA: Kluwer, 2000.

[82] G. Zames, "Feedback and optimal sensitivity: Model reference and transformation, multiplicative semi norms and approximate inverses", *IEEE Trans. Auto. Control*, vol. AC 26, pp. 301-320, 1981.

[83] K. Glover, "Robust stabilization of linear multivariable system: Relation to approximation", *Int. J Control*, vol. 43, pp. 741-766, 1986.

[84] S. Chen and O.P. Malik, "H_∞ optimization based power system stabilizer design", *IEE Proc. Gen. Trans. Distr.*, vol. 142, pp. 179-184, 1995.

[85] S.S. Ahmed, L. Chena and A. Petroianu, "Design of sub optimal H_∞ excitation controller", *IEEE Trans. Power Syst.,* vol. 11, 1996.

[86] N C Sahoo, B K Panigrahi, P K Dash and G Panda, "Application of multivariable feedback linearization scheme for STATCOM control", *Elect*

Power system research, 62(2), pp. 81-91, 2002.

[87] Vijay Vittal, M. Khammash, C. Zhu and W. Qiu, “Robust control of large power systems”, Project report, PSERC publication 02-43, 2002.

[88] J.C. Doyle and G. Stein, “Multivariable feedback design: Concept for classical/modern synthesis”, *IEEE Trans. Auto. Control*, vol. AC 26, pp. 4-16, 1981.

[89] C. Scherer, P. Gahinet and M. Chilali, “ Multi-objective output-feedback control via LMI optimization”, *IEEE Trans. Auto. Control*, vol. 42, pp. 896–911, 1997.

[90] J. Sefton and K. Glover, “ Pole/zero cancellations in the general H_∞ problem with reference to a two-block design, *Systems and control letters*, vol. 14, pp. 295–306, 1990.

[91] P. Gahinet and P. Apkarian, “A linear matrix inequality approach to H_∞ control”, *Int. J. Robust and Nonlinear Control*, vol. 4, pp. 421–448, 1994.

[92] S. Boyd, L. EI Ghaoui, E.Feron, and V. Balakrishnan, “ Linear Matrix Inequalities in System and Control Theory”, vol. 15 of Studies in Applied Mathematics, SIAM, Philadelphia, PA, June 1994.

[93] C. Scherer, P. Gahinet and M. Chilali, “$H\infty$ design with pole placement constraints: an LMI approach”, *IEEE Trans. Auto. Control*, vol. 41, (3), pp. 358–367, 1996.

[94] R.A. Ramos, L.F.C. Alberto and N.G. Bretas, “LMI-based controller design with feedback linearization: application to power systems”, *IEE Proc.-Control Theory Appl.*, vol. 150, no. 5, September 2003.

[95] P Gahinet, “Explicit Controller Formulas for LMI-based H∞ Synthesis”, *Proc.*

Amer. Contr. Conf., 1994, pp. 2396–2400.

[96] M.M. Farsangi, Y.H. Song, W.L. Fang and X.F. Wang, " Robust facts control design using H∞ loop-shaping method", *IEE Proceedings on Gen. Trans. Distr.*, vol. 149(3), pp. 352-357,2002.

[97] K. Glover and D. McFarlane, "Robust stabilization of normalized coprime factor plant descriptions with H,-bounded uncertainty", *IEEE Trans. Auto. Control*, vol. 34(8), pp. 821-830, 1989.

[98] S. Skogestad and I. Postlethwaite, "Multivariable Feedback Control: Analysis and Design", *New York: Wiley*, 2000.

[99] N. Martins and L. Lima, "Determination of suitable locations for power system stabilizers and static var compensators for damping electromechanical oscillations in large power systems", *IEEE Trans. Power Syst.*, vol. 5, pp. 1455–1469, Nov. 1990.

[100] P. Gahinet, A. Nemirovski, A. Laub and M. Chilali, "LMI Control toolbox for use with Matlab", Natick, MA: MathWorks Inc., 1995.

[101] M.G. Safonov and R.Y. Chiang, "A Schur method for balanced load model reduction", *IEEE Trans. Auto. Control*, Vol. AC-34, No.7, pp. 729-33, 1989.

[102] M.S. Chiu and Y. Arkun, "A methodology for the sequential design of robust decentralized control systems", *Automatica*, 28(5), pp. 997-1001, 1992.

[103] M. Hovd and S. Skogestad, "Sequential design of decentralized controller", *Automatica*, vol.30 (10), pp. 1601-1607, 1994.

[104] T.C. Yang, "Applying a sequential loop-closure method to power system stabilizer design", Control Engg. Pract, vol. 4 (10), pp. 1371-1380, 1996.

[105] R. Majumder, B. Chaudhuri, H. El-Zobaidi, B.C. Pal and I.M. Jaimoukha, "LMI approach to normalized H_∞ loop shaping design of power system damping controller, *IEE Proc.- Gen. Transm. Distrib.*, vol. 152, No. 6, pp.

952-960, 2005.

[106] M.C. Turner and D.G. Bates, “Mathematical methods for robust and nonlinear control”, Lecture notes in control and information sciences, Springer, 2007.

[107] N. Magaji, M.W. Mustufa and Z. bint Muda, “Optimal location of variable impedance devices for damping power system oscillations”, *2nd International Conference on Computer and Automation Engineering (ICCAE)*, vol. 5, pp. 97-101, Singapore, 2010.

[108] A. F. Snyder, “Delay-input wide-area stability control with synchronized phasor measurements”, in proc. *IEEE PES Summer Meeting*, vol. 2, pp. 1009–1014, 2000.

[109] W. Hongxia, K. S. Tsakalis, and G. T. Heydt, “Evaluation of Time Delay Effects to Wide-Area Power System Stabilizer Design”, *IEEE Trans. Power Syst*., vol. 19, no. 4, pp 1935-1941, Nov. 2004.

APPENDIX A

Two Area Four Machines System Parameters:

Two area test system consists of four thermal generators each rated at 900 MVA. Area 1 (comprises of G1, G2) and Area 2 (comprises of G3, G4) are connected through a tie-line in which TCSC is installed. The details of the system are as follows:

A1: Generator Parameters

	G1	G2	G3	G4
Rated MVA	900	900	900	900
x_l	0.20	0.20	0.20	0.20
r_a	0	0	0	0
x_d	1.80	1.80	1.80	1.80
x'_d	0.30	0.30	0.30	0.30
x"_d	0.25	0.25	0.25	0.25
T'_do	8.00	8.00	8.00	8.00
T"_do	0.03	0.03	0.03	0.03
x_q	1.70	1.70	1.70	1.70
x'_q	0.55	0.55	0.55	0.55
x"_q	0.24	0.24	0.24	0.24
T'_qo	0.4	0.4	0.4	0.4
T"_qo	0.05	0.05	0.05	0.05
H	6.5	6.5	6.5	6.5

A2: Static Exciters

Type: ST1A

	G1	G2	G3	G4
K_A	210	210	210	210
T_A	0.05	0.05	0.05	0.05

A3: Power System Stabilizers (PSSs) (speed input)

	G1	G3
K_{PSS}	10	10
T_W	10	10
T_1	0.05	0.05
T_2	0.02	0.02
T_3	0.08	0.08
T_4	0.015	0.015

A4: Transmission Line Parameters

Line Index	From bus	To bus	Resistance (p.u.)	Reactance (p.u.)	Line charging (p.u.)
1	1	10	0	0.0167	0
2	2	20	0	0.0167	0
3	3	4	0	0.005	0
4	3	20	0.001	0.010	0.0175
5	3	101	0.011	0.11	0.1925
6	10	20	0.0025	0.025	0.0437
7	11	110	0	0.0167	0
8	12	120	0	0.0167	0
9	13	14	0	0.01	0
10	13	15	0	0.01	0
11	13	102	0.011	0.11	0.1925
12	101	102	0	-0.088*	0
13	13	120	0.001	0.01	0.0175
14	110	120	0.0025	0.025	0.0437

* 40% series compensation with TCSC

A5: Generation Parameters

Generator index	Active power (MW)	Reactive power (MVAr)
G1	680	110
G2	720	66.8
G3	720	166.7
G4	720	181.3

A6: Load Parameters

Bus index	Active load (MW)	Reactive load (MVAr)
4	976	100
14	767	100
15	1000	100

A7: TCSC WAD Controller matrices for two area four machine test system

The Controller matrices for the mixed sensitivity formulation LMI framework based TCSC WAD Controller are given as:

	192.046	-349.11	-16.87	-109.9	-34.12	12.79	9.52	71.53	80.22
	24318.1	-28550	-1481.6	-10146	-3094.7	1091.14	892.399	6520.80	7584.60
	-15972	19013.3	983.07	6729.52	2053.16	-725.21	-591.6	-4325.3	-5028.4
	49967.4	-59250	-3069	-21005	-6411.5	2262.9	1847.21	13506	15693.6
Ak =	-137804	163749.	8472.23	58007.2	17690.8	-6249.0	-5099	-37273	-43340
	-271869	323580	16744.2	114578	34955.6	-12354	-10073	-73651	-85602
	123939	-147399	-7626.96	-52204	-15925.4	5628	4566.3	33549	39003
	-717007	853749	44221.9	302321	92275.9	-32556	-26589	-194431	-225832
	-1.9E+08	2.27E+08	11763327	80495818	24561315	-8676656	-7077590	-5.2E+07	-6E+07

Bk =	-10.562	-141.15	112.793	-335.35	955.247	1927.64	-870.24	5102.44	1349933.1

T

Ck =	-484.853	533.2639	27.99913	193.6129	58.85236	-20.5226	-17.0726	-124.117	-145.348

Dk =	0

APPENDIX B

Modified 16 Machines, 68 buses New York - New England test system parameters:

B1: Generator Parameters

	MVA	xl	ra	x_d	x'_d	x"_d	T'_do	T"_do	x_q	x'_q	x"_q	T'_qo	T"_qo	H
G1	2200	0.013	0	1.8	0.558	0.45	10.2	0.05	1.242	0.504	0.45	1.5	0.035	2.33
G2	800	0.004	0	1.8	0.425	0.305	6.56	0.05	1.72	0.366	0.305	1.5	0.035	4.95
G3	800	0.03	0	1.8	0.383	0.324	5.7	0.05	1.71	0.36	0.324	1.5	0.035	4.96
G4	800	0.03	0	1.8	0.299	0.24	5.69	0.05	1.772	0.274	0.24	1.5	0.035	4.16
G5	700	0.027	0	1.8	0.36	0.272	5.4	0.05	1.69	0.327	0.272	0.44	0.035	4.76
G6	900	0.022	0	1.8	0.352	0.283	7.3	0.05	1.707	0.318	0.283	0.4	0.035	4.91
G7	800	0.032	0	1.8	0.298	0.244	5.66	0.05	1.781	0.274	0.244	1.5	0.035	4.32
G8	800	0.028	0	1.8	0.353	0.279	6.7	0.05	1.737	0.31	0.279	0.41	0.035	3.92
G9	1000	0.03	0	1.8	0.487	0.384	4.79	0.05	1.752	0.427	0.384	1.96	0.035	4.03
G10	1200	0.02	0	1.8	0.486	0.426	9.37	0.05	1.224	0.479	0.426	1.5	0.035	2.91
G11	1600	0.01	0	1.8	0.253	0.168	4.1	0.05	1.729	0.21	0.168	1.5	0.035	2
G12	1900	0.022	0	1.8	0.552	0.445	7.4	0.05	1.693	0.499	0.445	1.5	0.035	5.18
G13	12000	0.003	0	1.8	0.334	0.243	5.9	0.05	1.739	0.304	0.243	1.5	0.035	4.07
G14	10000	0.002	0	1.8	0.285	0.23	4.1	0.05	1.73	0.25	0.23	1.5	0.035	1.73
G15	10000	0.002	0	1.8	0.285	0.23	4.1	0.05	1.73	0.25	0.23	1.5	0.035	1.73
G16	11000	0.004	0	1.8	0.358	0.278	7.8	0.05	1.688	0.303	0.278	1.5	0.035	4.45

B2: Exciters

All the exciters are of type AC4A [68] and voltage regulator gain K_A= 100, voltage regulator time constant T_A =0.01 sec for all the exciters.

B3: Power System Stabilizers (Speed input type)

	G2	G8	G9	G12
K_{PSS}	10	5	5	11
T_W	10	10	10	10
T_1	0.08	0.05	0.08	0.1
T_2	0.02	0.02	0.02	0.02
T_3	0.08	0.08	0.05	0.1
T_4	0.02	0.015	0.01	0.02

B4: Transmission Line Parameters

From bus	To bus	Resistance (p.u)	Reactance (p.u)	Line charging (p.u)	Tap ration
1	2	0.007	0.0822	0.3493	0
1	30	0.0008	0.0074	0.48	0
2	3	0.0013	0.0151	0.2572	0
2	25	0.007	0.0086	0.146	0
2	53	0	0.0181	0	1.025
3	4	0.0013	0.0213	0.2214	0
3	18	0.0011	0.0133	0.2138	0
4	5	0.0008	0.0128	0.1342	0
4	14	0.0008	0.0129	0.1382	0
5	6	0.0002	0.0026	0.0434	0
5	8	0.0008	0.0112	0.1476	0
6	7	0.0006	0.0092	0.113	0
6	11	0.0007	0.0082	0.1389	0
6	54	0	0.025	0	1.07
7	8	0.0004	0.0046	0.078	0
8	9	0.0023	0.0363	0.3804	0
9	30	0.0019	0.0183	0.29	0
10	11	0.0004	0.0043	0.0729	0
10	13	0.0004	0.0043	0.0729	0
10	55	0	0.02	0	1.07
12	11	0.0016	0.0435	0	1.06
12	13	0.0016	0.0435	0	1.06
13	14	0.0009	0.0101	0.1723	0
14	15	0.0018	0.0217	0.366	0
15	16	0.0009	0.0094	0.171	0
16	17	0.0007	0.0089	0.1342	0
16	19	0.0016	0.0195	0.304	0
16	21	0.0008	0.0135	0.2548	0
16	24	0.0003	0.0059	0.068	0
17	18	0.0007	0.0082	0.1319	0
17	27	0.0013	0.0173	0.3216	0
19	20	0.0007	0.0138	0	1.06

Continue….

19	56	0.0007	0.0142	0	1.07
20	57	0.0009	0.018	0	1.009
21	22	0.0008	0.014	0.2565	0
22	23	0.0006	0.0096	0.1846	0
22	58	0	0.0143	0	1.025
23	24	0.0022	0.035	0.361	0
23	59	0.0005	0.0272	0	0
25	26	0.0032	0.0323	0.531	0
25	60	0.0006	0.0232	0	1.025
26	27	0.0014	0.0147	0.2396	0
26	28	0.0043	0.0474	0.7802	0
26	29	0.0057	0.0625	1.029	0
28	29	0.0014	0.0151	0.249	0
29	61	0.0008	0.0156	0	1.025
9	30	0.0019	0.0183	0.29	0
9	36	0.0022	0.0196	0.34	0
9	36	0.0022	0.0196	0.34	0
36	37	0.0005	0.0045	0.32	0
34	36	0.0033	0.0111	1.45	0
35	34	0.0001	0.0074	0	0.946
33	34	0.0011	0.0157	0.202	0
32	33	0.0008	0.0099	0.168	0
30	31	0.0013	0.0187	0.333	0
30	32	0.0024	0.0288	0.488	0
1	31	0.0016	0.0163	0.25	0
31	38	0.0011	0.0147	0.247	0
33	38	0.0036	0.0444	0.693	0
38	46	0.0022	0.0284	0.43	0
46	49	0.0018	0.0274	0.27	0
1	47	0.0013	0.0188	1.31	0
47	48	0.0025	0.0268	0.4	0
47	48	0.0025	0.0268	0.4	0
48	40	0.002	0.022	1.28	0
35	45	0.0007	0.0175	1.39	0
37	43	0.0005	0.0276	0	0
43	44	0.0001	0.0011	0	0
44	45	0.0025	0.073	0	0
39	44	0	0.0411	0	0
39	45	0	0.0839	0	0
45	51	0.0004	0.0105	0.72	0
50	52	0.0012	0.0288	2.06	0
50	51	0.0009	0.0221	1.62	0

Continue…

49	52	0.0076	0.1141	1.16	0
52	42	0.004	0.06	2.25	0
42	41	0.004	0.06	2.25	0
41	40	0.006	0.084	3.15	0
31	62	0	0.026	0	1.04
32	63	0	0.013	0	1.04
36	64	0	0.0075	0	1.04
37	65	0	0.0033	0	1.04
41	66	0	0.0015	0	1
42	67	0	0.0015	0	1
52	68	0	0.003	0	1
1	27	0.032	0.32	0.41	1

B5: Load Parameters

Bus Index	P_L (p.u.)	Q_L (p.u.)
1	2.527	11856
3	3.22	0.02
4	5.00	1.840
7	2.34	0.84
8	5.22	1.77
9	1.04	1.25
12	0.09	0.88
15	3.20	1.53
16	3.29	0.32
18	1.58	0.3
20	6.80	1.03
21	1.74	1.15

Bus Index	P_L (p.u.)	Q_L (p.u.)
23	1.48	0.85
24	3.09	-0.92
25	2.24	0.47
26	1.39	0.17
27	2.81	0.76
28	2.06	0.28
29	2.84	0.27
33	1.12	0.0
36	1.02	-0.19
37	60.0	3.00
39	2.67	0.126
40	0.656	0.235

Bus Index	P_L (p.u.)	Q_L (p.u.)
41	10.0	2.50
42	11.5	2.50
44	2.675	0.126
45	2.08	0.21
46	1.507	0.285
47	2.031	0.325
48	2.412	0.022
49	1.64	0.29
50	2.00	-1.47
51	4.37	-1.22
52	24.70	1.23

B6: SVC WADC and UPFC WADC Transfer Functions

The reduced order SVC and UPFC wide area controllers can be represented as following transfer function:

$$K_{SVC}(s) = \frac{N_{SVC}(s)}{D_{SVC}(s)}$$

$$\begin{aligned} N_{SVC}(s) = & -4.88*10^5 s^{11} - 4.98*10^7 s^{10} - 5.83*10^8 s^9 - 4.06*10^9 s^8 - 1.897*10^{10} s^7 \\ & - 7.092*10^{10} s^6 - 1.78410^{11} s^5 - 3.633*10^{11} s^4 - 4.928*10^{11} s^3 - 2.82*10^{11} s^2 \\ & - 2.028*10^{11} s + 9.8414*10^{10} \end{aligned}$$

$$\begin{aligned} D_{SVC}(s) = & s^{12} + 3.872*10^5 s^{11} + 3.064*10^9 s^{10} + 1.836*10^{11} s^9 + 8.497*10^{11} s^8 + 8.3785*10^{12} s^7 \\ & + 2.3723*10^{13} s^6 + 1.163*10^{14} s^5 + 2.1122*10^{14} s^4 + 5.421*10^{14} s^3 + 5.989*10^{14} s2 \\ & + 6.4989*10^{14} s + 1.169*10^{14} \end{aligned}$$

$$K_{UPFC}(s) = \frac{N_{UPFC}(s)}{D_{UPFC}(s)}$$

$$\begin{aligned} N_{UPFC}(s) = & 1.064*10^4 s^{11} - 1.0910*10^5 s^{10} - 1.5863*10^6 s^9 - 1.4565*10^7 s^8 - 6.9626*10^7 s^7 \\ & - 2.9313*10^8 s^6 - 7.711*10^8 s^5 - 1.7426*10^9 s^4 - 2.5497*10^9 s^3 - 2.031*10^9 s^2 \\ & - 1.3071*10^9 s + 6.044*10^7 \end{aligned}$$

$$\begin{aligned} D_{UPFC}(s) = & s^{12} + 1.5884*10^4 s^{11} - 1.5233*10^7 s^{10} + 5.2124*10^8 s^9 + 1.3381*10^9 s^8 \\ & + 2.1966*10^{10} s^7 + 4.0521*10^{10} s^6 + 2.6262*10^{11} s^5 + 3.2324*10^{11} s^3 \\ & + 1.0937*10^{12} s^2 + 1.4702*10^{12} s + 2.6272*10^{11} \end{aligned}$$

APPENDIX C

10-machines 39-bus modified New England Test System

C1. Generator Parameters

	MVA	xl	ra	x_d	x'_d	x"_d	T'_do	T"_do	x_q	x'_q	x"_q	T'_qo	T"_qo	H
G1	1000	0.13	0	1	0.31	0.31	10.2	0	0.69	0.69	0.69	0	0	4.2
G2	1000	0.35	0	2.95	0.7	0.7	6.56	0	2.82	1.7	1.7	1.5	0	3.03
G3	1000	0.3	0	2.5	0.53	0.53	5.7	0	2.37	0.88	0.88	1.5	0	3.58
G4	1000	0.295	0	2.62	0.44	0.44	5.69	0	2.58	1.66	1.66	1.5	0	2.86
G5	1000	0.54	0	6.7	1.32	1.32	5.4	0	6.2	1.66	1.66	0.44	0	2.6
G6	1000	0.224	0	2.54	0.5	0.5	7.3	0	2.41	0.81	0.81	0.4	0	3.48
G7	1000	0.322	0	2.9	0.49	0.49	5.66	0	2.8	1.86	1.86	1.5	0	2.64
G8	1000	0.28	0	2.9	0.57	0.57	6.7	0	2.8	0.91	0.91	0.41	0	2.43
G9	1000	0.298	0	2.106	0.57	0.57	4.79	0	2.05	0.59	0.59	1.96	0	3.45
G10	1000	0.03	0	0.2	0.06	0.06	7	0	0.19	0.08	0.08	0.7	0	50

C2: Exciters

All the exciters are of type AC4A [68] and voltage regulator gain K_A= 200, voltage regulator time constant T_A =0.015 sec for all the exciters.

C3: Power System Stabilizers (Speed input type)

	G3	G5	G8	G9
K_{PSS}	10	10	10	10
T_W	10	10	10	10
T_1	0.08	0.08	0.08	0.08
T_2	0.02	0.02	0.02	0.02
T_3	0.08	0.08	0.08	0.05
T_4	0.02	0.02	0.02	0.02

C4: Transmission Line Parameters

Line Data					Transformer Tap	
From Bus	To Bus	R	X	B	Magnitude	Angle
1	2	0.0035	0.0411	0.6987	-	-
1	39	0.001	0.025	0.75	-	-
2	3	0.0013	0.0151	0.2572	-	-
2	25	0.007	0.0086	0.146	-	-
3	4	0.0013	0.0213	0.2214	-	-
3	18	0.0011	0.0133	0.2138	-	-
4	5	0.0008	0.0128	0.1342	-	-
4	14	0.0008	0.0129	0.1382	-	-
5	6	0.0002	0.0026	0.0434	-	-
5	8	0.0008	0.0112	0.1476	-	-
6	7	0.0006	0.0092	0.113	-	-
6	11	0.0007	0.0082	0.1389	-	-
7	8	0.0004	0.0046	0.078	-	-
8	9	0.0023	0.0363	0.3804	-	-
9	39	0.001	0.025	1.2	-	-
10	11	0.0004	0.0043	0.0729	-	-
10	13	0.0004	0.0043	0.0729	-	-
13	14	0.0009	0.0101	0.1723	-	-
14	15	0.0018	0.0217	0.366	-	-
15	16	0.0009	0.0094	0.171	-	-
16	17	0.0007	0.0089	0.1342	-	-
16	19	0.0016	0.0195	0.304	-	-
16	21	0.0008	0.0135	0.2548	-	-
16	24	0.0003	0.0059	0.068	-	-
17	18	0.0007	0.0082	0.1319	-	-
17	27	0.0013	0.0173	0.3216	-	-
21	22	0.0008	0.014	0.2565	-	-
22	23	0.0006	0.0096	0.1846	-	-
23	24	0.0022	0.035	0.361	-	-
25	26	0.0032	0.0323	0.513	-	-
26	27	0.0014	0.0147	0.2396	-	-
26	28	0.0043	0.0474	0.7802	-	-
26	29	0.0057	0.0625	1.029	-	-
28	29	0.0014	0.0151	0.249	-	-
12	11	0.0016	0.0435	0	1.006	0
12	13	0.0016	0.0435	0	1.006	0
6	31	0	0.025	0	1.07	0
10	32	0	0.02	0	1.07	0
19	33	0.0007	0.0142	0	1.07	0
20	34	0.0009	0.018	0	1.009	0
22	35	0	0.0143	0	1.025	0
23	36	0.0005	0.0272	0	1	0
25	37	0.0006	0.0232	0	1.025	0
2	30	0	0.0181	0	1.025	0
29	38	0.0008	0.0156	0	1.025	0
19	20	0.0007	0.0138	0	1.06	0

C5: Generation Data

Bus	Type	Voltage	Load		Generator		
		[PU]	MW	MVar	MW	MVar	Unit No.
1	PQ	-	0	0	0	0	
2	PQ	-	0	0	0	0	
3	PQ	-	322	2.4	0	0	
4	PQ	-	500	184	0	0	
5	PQ	-	0	0	0	0	
6	PQ	-	0	0	0	0	
7	PQ	-	233.8	84	0	0	
8	PQ	-	522	176	0	0	
9	PQ	-	0	0	0	0	
10	PQ	-	0	0	0	0	
11	PQ	-	0	0	0	0	
12	PQ	-	7.5	88	0	0	
13	PQ	-	0	0	0	0	
14	PQ	-	0	0	0	0	
15	PQ	-	320	153	0	0	
16	PQ	-	329	32.3	0	0	
17	PQ	-	0	0	0	0	
18	PQ	-	158	30	0	0	
19	PQ	-	0	0	0	0	
20	PQ	-	628	103	0	0	
21	PQ	-	274	115	0	0	
22	PQ	-	0	0	0	0	
23	PQ	-	247.5	84.6	0	0	
24	PQ	-	308.6	-92	0	0	
25	PQ	-	224	47.2	0	0	
26	PQ	-	139	17	0	0	
27	PQ	-	281	75.5	0	0	
28	PQ	-	206	27.6	0	0	
29	PQ	-	283.5	26.9	0	0	
30	PV	1.0475	0	0	250	-	Gen10
31	PV	0.982	9.2	4.6	-	-	Gen2
32	PV	0.9831	0	0	650	-	Gen3
33	PV	0.9972	0	0	632	-	Gen4
34	PV	1.0123	0	0	508	-	Gen5
35	PV	1.0493	0	0	650	-	Gen6
36	PV	1.0635	0	0	560	-	Gen7
37	PV	1.0278	0	0	540	-	Gen8
38	PV	1.0265	0	0	830	-	Gen9
39	PV	1.03	1104	250	1000	-	Gen1

C6: Load Parameters

Bus	Load	
	P [PU]	Q [pu]
1	0.000	0.000
2	0.000	0.000
3	3.220	0.024
4	5.000	1.840
5	0.000	0.000
6	0.000	0.000
7	2.338	0.840
8	5.220	1.760
9	0.000	0.000
10	0.000	0.000
11	0.000	0.000
12	0.075	0.880
13	0.000	0.000
14	0.000	0.000
15	3.200	1.530
16	3.290	0.323
17	0.000	0.000
18	1.580	0.300
19	0.000	0.000
20	6.280	1.030
21	2.740	1.150
22	0.000	0.000
23	2.475	0.846
24	3.086	-0.920
25	2.240	0.472
26	1.390	0.170
27	2.810	0.755
28	2.060	0.276
29	2.835	0.269
31	0.092	0.046
39	11.040	2.500

C7: UPFC Transfer Functions

The UPFC wide area controllers can be represented as following transfer function:

$$K_{UPFC}(s) = \frac{N_{UPFC}(s)}{D_{UPFC}(s)}$$

$$N_{UPFC}(s) = 3.486*10^{8}s^{7} + 4.464*10^{10}s^{6} + 1.47*10^{12}s^{5} + 5.962*10^{12}s^{4} + 5.883*10^{13}s^{3} + 5.849*10^{12}s^{2} + 1.735*10^{12}s + 8.48*10^{6}$$

$$D_{UPFC}(s) = s^{8} + 4.165*10^{4}s^{7} + 9.812*10^{8}s^{6} + 1.026.2124*10^{11}s^{5} + 3.076*10^{12}s^{4} + 2.817*10^{13}s^{3} + 4.564*10^{14}s^{2} + 1.984*10^{15}s + 1.915*10^{14}$$

LIST OF PUBLICATIONS

Conference publications:

[1] Bhavin J Shah, G N Pillai and Pramod Agarwal, “Power Oscillation Damping in Multi-Machine Power System Using PSSs Considering Various Load Models”, Nov. 2013 Nirma University IEEE International Conference on Engineering (NUiCONE).

[2] Bhavin J Shah, G N Pillai, and Pramod Agarwal, “H_∞ Loop shaping technique based robust control design of SVC controller for power oscillations damping considering global signal”, Nov. 2015 5th Nirma University IEEE International Conference on Engineering (NUiCONE).

[3] Bhavin J Shah, G N Pillai, and Pramod Agarwal, “Robust TCSC controller for POD considering global signal and load composition uncertainties”, 2015 Annual IEEE India Conference (INDICON), Dec. 2015.

Journal publications:

[1] Bhavin J Shah, G N Pillai, and Pramod Agarwal, “An LMI approach with pole placement objective for the design of robust SSSC controller for damping inter-area mode oscillation considering global signal”, International Journal of Engineering & Technology, UAE (SCOPUS Indexed) (Accepted for publication).

[2] Bhavin J Shah, G N Pillai and Pramod Agarwal, “Inter-area mode power oscillation damping by coordinated control of robust FACTS controller considering global signal and load model uncertainties”, Journal of Electrical Engineering and Technology (under review).

[3] Bhavin J Shah, G N Pillai, and Pramod Agarwal, “Damping of inter-area mode oscillations in multi-machine power system using robust control technique based FACTS controller considering various load composition models”, Sadhana Academic Proceeding in Engineering Sciences (under review).